SGP-TR-31

ANALYSIS OF HEAT TRANSFER AND ENERGY RECOVERY IN FRACTURED GEOTHERMAL RESERVOIRS

by

R. Iregui
A. Hunsbedt
P. Kruger
A. L. London

Stanford Geothermal Program
Stanford University

June 1978

ACKNOWLEDGMENT

The work described in this report was sponsored by the National Science Foundation Grant No. NSF-AER-72-3490, and later by the Department of Energy Contract No. LBL-167-3500. Their support is gratefully acknowledged.

TABLE OF CONTENTS

LIST OF ILLUSTRATIONS

FIGURE

page

LIST OF TABLES

LIST OF SYMBOLS

English Letter Symbols

Symbol	Description	Units
A	Surface area of rock	in^2
A_s	Surface area of equal volume sphere	in^2
a	Rock length	ft
b	Rock breadth	ft
C	Rock thermal capacitance	Btu/°F
C_1 C_2	Coefficients for a lineal regression	-
c	Specific heat	Btu/lb-°F
c	Rock thickness	ft
d_s	Equivalent sphere diameter	ft
E_A	Actual energy injected	Btu
E_i	Total energy injected	Btu
E_P	Total energy produced	Btu
H	Reservoir level	ft
h	Convective heat transfer coefficient	Btu/hr-ft-°F
i	Enthalpy	Btu/lb
k	Thermal conductivity	Btu/hr-ft-°F
L	Distance between injection and production wells	ft
ℓ_{cond}	Conduction path length	ft
M'''_m	Mass of the metallic vessel per unit volume (Eq. *C.24)*	lb/ft^3
M_R	Rock mass	lb_m
m''	Mass flow or fluid per unit area of solid and crack	lb/ft^2-hr

Symbol	Description	Units
$\dot{m}_i$	Injection rate	lb/hr
$\dot{m}_p$	Production rate	lb/hr
N	Total number of rocks in the collection	-
N_L	Number of groups of different rock sizes	-
n	Sample size	-
n_i	Number of rocks of equal size	-
P	Probability	-
Q	Thermal energy	Btu
Q_{actual}	Actual thermal energy extracted	Btu
Q_e	External heat transfer parameter	Btu
Q_{max}	Maximum thermal energy that can be extracted	Btu
q	Heat transfer	Btu/hr
q'	Heat transfer per unit length	Btu/hr-ft
q''	Heat transfer per unit area	$Btu/hr-ft^2$
R	Total thermal resistance	°F/Btu/hr
R_{Bi}	Radius for Biot number	ft
$R_{e,c}$	Bulk-effective radius, **(Eq. *3.34*)**	ft
R_{Fo}	Radius for Fourier number	ft
R_i	Internal thermal resistance	°F/Btu/hr
R_o	Overall thermal resistance	°F/Btu/hr
R_s	Thermal resistance at the rock surface	°F/Btu/hr
R_s	Equivalent sphere radius (Eq. 2.2)	ft
RC	Time constant	hr
r	Distance from rock center	ft
S	Cross sectional area of reservoir	ft^2

Symbol	Description	Units
$S_{\bar{X}}$	Estimated standard deviation of the mean	-
T	Temperature	°F
t	Time	hr
t_c	Crack width	ft
t_{re}	Residence time	hr
U_o	Overall heat transfer coefficient for effective rock size	Btu/hr-ft^2-°F
UA	Overall heat transfer coefficient for heat losses from the vessel	Btu/hr-°F
u	Water velocity	ft/hr
V_{Re}	Rock volume	ft^3
V_{re}	Total reservoir volume	ft^3
v_i	Darcy velocity	ft/hr
$\bar{v}$	Arithmetic mean rock volume for total collection	ft^3
w	Sweep velocity	ft/hr
$\bar{X}$	Arithmetic mean	-

Greek Letter Symbols

α	Rock thermal diffusivity	ft^2/hr
γ	Standard deviation for exponential distribution	-
η	Number of cracks per unit length	1/ft
ξ	Time dummy variable	hr
μ	Fluid cooling rate	°F/hr
μ	Actual mean of a variable	-
μ	Fluid viscosity	lb$_f$hr/ft^2
ρ	Density	lb/ft^3

Symbol	Description	Units
σ	Standard deviation	-
$\sigma_{\bar{R}_s}$	Standard deviation of equivalent sphere radius	ft
$\sigma_{\bar{X}}$	Standard error of the mean	-
τ	Time constant (Eq. *3.10*)	hr
τ_e	Bulk-effective time constant (Eq *3.35*)	hr

Dimensionless Symbols

Symbol	Description	Equation Number
c^*	Heat capacity ratio, $\rho_r c_r / \rho_f c_f$	
c^*_{mo}	Modified heat capacity ratio ($c^* + c^*_m$)	
c^*_m	Metal to fluid heat capacity ratio	C.27
F_c	Fluid temperature drop fraction	*3.26*
F_E	Energy extracted fraction from a single rock	*3.17*
$F_{E,c}$	Local energy extracted fraction for a collection of rocks	*3.28*
$\bar{F}_{E,c}$	Reservoir rock energy extracted fraction	*3.43*
F_P	Reservoir energy fraction produced	*3.46*
$\bar{F}_c$	Reservoir mean temperature drop fraction	*3.45*
K'_{Bi}	Biot number correlation factor	*3.13*
K'_{Fo}	Fourier number correlation factor	3.12
ℓ^*	Conduction path length	*3.24*
N_{Bi}	Biot number $h R_s / k$	
N_{Fo}	Fourier number $\alpha t / R_s^2$	
N_{tu}	Number of transfer units	*3.55*
q^*	External heat transfer parameter	*3.56*
r^*	Distance from rock center, r/R	

Symbol	Description	Equation Number
r^*_s	Normalized rock radius	C.1
T^*_f	Fluid temperature	*3.54*
AT^*_m	Mean rock to fluid temperature difference	*3.20*
AT^*_{rc}	Rock center to fluid temperature difference, Figure *3-2*	
t^*	Time, t/t_{re}	*3.53*
X	Volumetric fraction	3.29b
X*	Distance from the bottom, or from injection point, X/L	
Y	Surface area fraction	
γ	Storage ratio, $\phi/c^*(1 - \phi)$	
γ_{mo}	Modified storage ratio	C.28
β	Eigenvalue	
ϕ	Porosity, ratio of volume occupied by the fluid, to the total reservoir volume	
ψ_1	Krumbein sphericity	*2.7*
ψ_1	Kuo's sphericity	*2.3*
$\psi_.$	Pseudo Kuo's sphericity	*2.6*

Subscripts

c = refers to a collection of rocks

e = effective

f = fluid

in = injection

m metal or steel

r rock

ref reference

Symbol		Description
rc	=	rock center
1	=	initial value
2	=	reference
∞	=	environment

Special Symbols

$\mathcal{L}^{-1}$	=	inverse Laplace transform
$\triangleq$	=	indicated a definition
$\Gamma( )$	=	gamma function
$\bar{\ }$	=	mean value
$\hat{\ }$	=	variable in Laplace space

1. INTRODUCTION

Large-scale development of geothermal energy resources rests on the ability to extract commercial quantities of thermal energy from natural hydrothermal reservoirs, or from hot dry rock deposits using artificial circulation cycles. The energy available in igneous resources has been estimated to be much larger than that in hydrothermal reservoirs (White and Williams, 1975). For both types of resources, means for enhancing the fraction of the available energy that can be extracted need to be developed. Since more than 70 percent of the available energy in a geothermal resource resides in the reservoir rock, the development of techniques to enhance the fraction of energy extraction from the rock itself is imperative to effectively increase the fraction of recoverable energy from geothermal reservoirs. The enhancement of thermal energy extraction from fractured geothermal reservoirs has been studied as part of the Stanford Geothermal Program (SGP) since its inception (Kruger and Ramey, 1973).

The rate of energy extraction from geothermal resources is limited by the slow heat transfer process from large impermeable rocks to the convecting fluid, and by the resistance to the flow of fluid through the formation to transport the extracted energy to the well heads. If the rock is naturally unfractured, or only lightly fractured, long conduction paths to the surface wetted by the convective fluid--usually water--decreases the rate of heat transfer to an uneconomically low level. If the heat transfer process from the hot rock is accelerated by reducing the temperature of the surrounding fluid, the rock mass close to the wetted

surface cools faster than the mass inside the rock. The non-uniform temperature profile inside the rock results in unexploited energy. The larger the rock, the larger the amount of recoverable energy that remains unexploited. Stimulation techniques, such as hydraulic fracturing, explosive fracturing, and thermal stress cracking have been proposed (Ewing, 1973). The overall effect of reducing the conduction path lengths within the rock, increasing the surface area for convection to the geothermal fluid, and increasing the permeability of the formation, combine to make the reservoir a better "heat exchanger."

Several approaches have been used to analyze the energy extraction process from the rock in a geothermal reservoir. Gringarten and Witherspoon (1973) based their analysis on an infinite series of parallel vertical fractures of uniform aperture, and separated by blocks of homogeneous and isotropic impermeable rock with a uniform spacing between fractures. Diadkin (1973) used an approximate analytical solution in which the particle size is averaged to a spherical shape of a given radius; they also investigated the variable particle size using a finite-element method (Diadkin and Pariiskii, 1975).

Experimental studies of fracture-stimulated reservoirs were performed by Hunsbedt, Kruger, and London (1975b) with two different rock collections in the Stanford Geothermal Program (SGP) Large Reservoir Model. He considered the effect of rock sizes on the energy extraction process by lumping the complete rock size distribution in three different average size groups; he also considered the effect of the shape of the rock segments by empirically

averaging their temperature transient behavior as if they were shaped like something in between a plate and a sphere. The degree of energy extraction from the rock was found to depend mainly on the relative magnitudes of the time constant of the mean rock size and the production time.

Kuo, Kruger, and Brigham (1976) studied the heat transfer from single irregular shaped rocks. He developed a shape factor correlation which allows the modeling of the heat transfer from a rock of arbitrary shape by treating it as an equivalent spherical rock, and thereby the classical spherical conduction solutions can be used.

The purpose of the present study is to determine the conditions under which the energy recovery from geothermal reservoirs is limited by heat transfer. To characterize the heat-transfer limitations independently from other limiting factors, the energy that is actually transferred from the rock to the geothermal fluid is evaluated as a fraction of the energy that would be extracted if the total rock mass was cooled to the surrounding fluid temperature. An analytical model based on observed experimental data is developed to predict the rock energy extracted fraction from a collection of rocks with given rock size and shape distributions, and under variable fluid cooling-rate conditions. The analysis is completed by formulating a model of a reservoir exploited by the cold-water sweep process to find the relationship between the energy production rate and the characteristics of the formation, such as the rock size distribution and porosity, which determines when the recoverable energy from the reservoir is limited by heat transfer.

It is intended to formulate a simple methodology which can be readily used to evaluate the importance of the various physical parameters

on the rock energy extraction process from geothermal reservoirs. Its direct application represents an important step in the geothermal field development to assess techniques for reservoir stimulation and to estimate geothermal energy reserves.

The specific objectives of the present work are:

1. To develop a model to predict the temperature transient in a single irregular shaped rock. This task involves purely conductive heat transfer considerations and is achieved in the following manner: (a) investigate the validity of the one-lump parameter method to describe the temperature transient in a spherical rock; (b) apply the shape factor correlation developed by Kuo, Kruger, and Brigham (1976) to model irregular shaped rocks; and (c) develop an analytical method to predict the temperature transient in irregular shaped rocks under variable fluid cooling-rate conditions,

2. To develop a model to evaluate the "energy extracted fraction" from a collection of rocks with given size and shape distributions. This task involves statistical analysis of the geometrical characteristics of the rocks to determine the effect of the particle size and shape distribution on the overall energy extraction from a rock system.

3. To develop a model for the cold-water sweep process based on (1) and (2) to predict the rock and fluid temperature transients as a function of the production and injection rates, the rock size and shape distributions, and other important reservoir parameters. This task involves the analysis of

the coupled temperature transient behavior of the fluid and the rock, and the development of non-dimensional parameters that determine the heat-transfer limitations on the effective energy extraction from the rock,

4. To verify experimentally objectives (1) through (3). A collection of rocks consisting of granitic rock from the Pile-driver underground nuclear explosion was used for this purpose as a representative sample of artificially fractured rock. Two in-place boiling experiments and one cold-water sweep experiment were performed to verify the models developed.

2. EXPERIMENTAL SYSTEM

2.1 Description of Experimental Apparatus

The experiments conducted in this study were performed in the Stanford Geothermal Program Large Reservoir Model constructed in 1972-73 to study the energy extraction processes in fracture-stimulated geothermal reservoirs. Detailed descriptions of the model are given by Hunsbedt, Kruger, and London (1975a and 1975b). The physical model shown in Figure 2-1 consists of three major components: (1) the reservoir, (2) the external loop, and (3) the instrumentation and recording system.

2.1.1 The Reservoir

The reservoir is a cylindrical carbon steel vessel approximately 5 feet high and 2 feet in diameter. It holds about one ton of fractured rock and water. The system can be operated at a maximum pressure of 800 psig (56 kg/cm^2) and a maximum temperature of 500°F (260°C) to simulate geothermal reservoir environments. The vessel, well insulated to reduce heat losses, has wrapped-around electric tape heaters with power controls to compensate for heat losses or model external heat transfer to the reservoir.

2.1.2 The External Loop

The external loop noted in Figure 2-1, consists of a circulation system, an injection system, and a production system. The circulation system, used to heat up the system (rock, water, and steel vessel) to initial reservoir conditions (see Figure 2-1), consists of a circulation pump, an electrical heater, and two accumulators used to pressurize the reservoir with an external supply of argon gas at high pressure. The 15 gpm (57 1/min)

centrifugal pump provides 9 feet (2.74 m) head for the water circulation through the electric heater (23 kW input) which produces a heating rate of approximately 10°F (5.56°C) in the water temperature per pass. The water from the heater circulates through the reservoir, where some of the thermal energy is transferred to the rock and the steel vessel. Water is then returned via Accumulator 1. Heat-up circulation is continued until the desired temperature and pressure conditions are achieved and temperature equilibrium of the rock/water/steel system is established. Heat-up from room temperature to about 480°F (250°C) is normally accomplished in about 10 hours.

The production system shown in Figure 2-2 consists of a flow control valve, a condenser, and a weighing tank. When the reservoir has reached equilibrium at the desired temperature, circulation is stopped and production is initiated by opening the flow control valve. Fluid production rate is controlled manually with the flow control valve. The produced fluid flows through the condenser which is cooled with tap water in the cold side. The production mass flow rate is measured by weighing the condensate as a function of time.

The injection system, which can be operated simultaneously with the production system, consists of a metering tank and a positive displacement pump delivering a maximum head and injection flow of 800 psi (57 kg/cm^2) and 1 gpm (3.785 1/min), respectively. The flow rate can be controlled continuously by adjustment of the piston displacement in the range of 0-1 gpm (0-3.785 1/min). The desired inlet temperature is achieved by prehating with the electric heater.

A feedback automatic control system is used in the circulation and injection systems to control the temperature vs time characteristics of

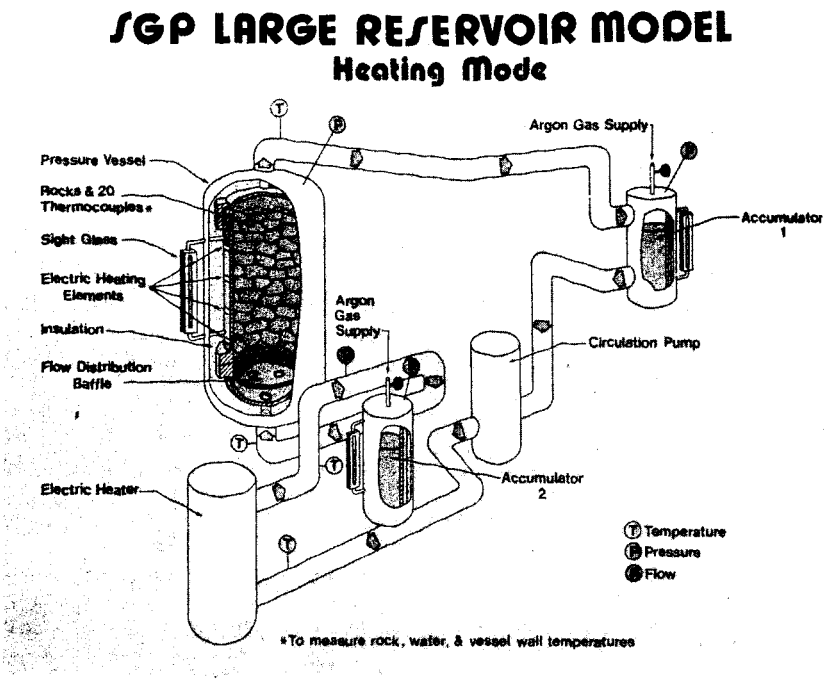

FIGURE 2-1. **Diagram of SGP** Large **Reservoir Model--heating mode operation**

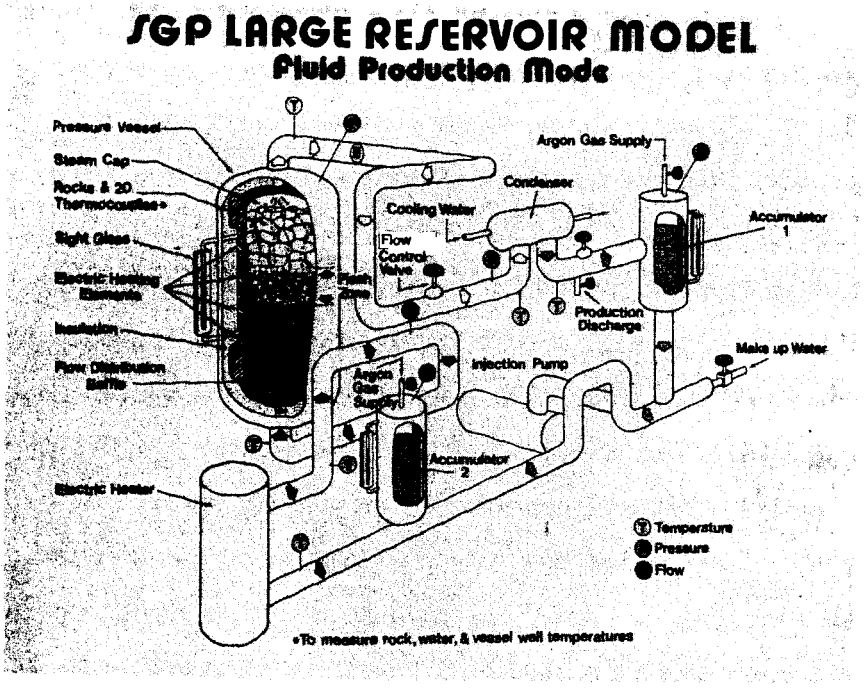

FIGURE 2-2. **Diagram of** SGP **Large Reservoir Model--fluid production mode operation**

centrifugal pump provides 9 feet (2.74 m) head for the water circulation through the electric heater (23 kW input) which produces a heating rate of approximately 10°F (5.56°C) in the water temperature per pass. The water from the heater circulates through the reservoir, where some of the thermal energy is transferred to the rock and the steel vessel. Water is then returned via Accumulator 1. Heat-up circulation is continued until the desired temperature and pressure conditions are achieved and temperature equilibrium of the rock/water/steel system is established. Heat-up from room temperature to about 480°F (250°C) is normally accomplished in about 10 hours.

The production system shown in Figure 2-2 consists of a flow control valve, a condenser, and a weighing tank. When the reservoir has reached equilibrium at the desired temperature, circulation is stopped and production is initiated by opening the flow control valve. Fluid production rate is controlled manually with the flow control valve. The produced fluid flows through the condenser which is cooled with tap water in the cold side. The production mass flow rate is measured by weighing the condensate as a function of time.

The injection system, which can be operated simultaneously with the production system, consists of a metering tank and a positive displacement pump delivering a maximum head and injection flow of 800 psi (57 kg/cm^2) and 1 gpm (3.785 l/min), respectively. The flow rate can be controlled continuously by adjustment of the piston displacement in the range of 0-1 gpm (0-3.785 l/min). The desired inlet temperature is achieved by preheating with the electric heater.

A feedback automatic control system is used with the injection system to control the temperature vs time characteristic of

the fluid at the exit of the electric heater. Heat losses in the line from the electric heater to the reservoir inlet are balanced by heating with electric tapes wrapped around the inlet pipe line.

2.1.3 Instrumentation and Recording System

Instrumentation for temperature and pressure measurements at various points in the reservoir, circulation, and injection systems are indicated in Figures 2–1 and 2–2. A more detailed process flow and instrumentation diagram for the model was given by Hunsbedt, Kruger, and London (1975b). Electric power inputs to the tape heaters on the reservoir and on the inlet line are measured as a function of time. A sight glass installed on the vessel covering about 60 percent of the reservoir height is used to observe the liquid level during production. Similarly, a level meter installed in the injection head tank is used to measure the flow rate of fluids injected. The tank that receives the condensate of the produced fluid is installed on top of a weighting balance to measure the production flow rate. An orifice meter measures the cooling water flow in the condenser.

Most temperature and pressure readings are recorded automatically using multipoint recorders. Temperature measurements can also be read directly in a digital meter. Generally, a test pressure gauge measurement is recorded to check the electronic pressure transmitter measurements.

2.2 Rock Characteristics

To perform the energy extraction experiments, the collection of rocks selected had to be well characterized. The characteristics of the rock loading were obtained in three forms: (1) Instrumented rocks geometrical

parameters; they are required to study and verify analytical models for the rock temperature transients. (2) Mean geometrical parameters and their distributions. These parameters describe the size and shape of the rocks which govern their temperature transient behavior. (3) Bulk parameters, which determine the total amount of energy that can be stored (or recovered) in the rock and the liquid. These parameters are described in the following sections.

The collection of rocks chosen to study the energy extraction process from a fracture geothermal reservoir was obtained from the rubble chimney formed by collapse of the overburden into the cavity created by the "Piledriver" nuclear explosion. The Piledriver (61-kt) nuclear explosive was detonated on June 2, 1966, at a depth of 1,500 feet (457 meters) in a formation of granodiorite. The explosion produced a cavity radius of 131.5 feet (40.1 meters) and a collapsed rubble chimney 390 feet (271 meters) high and 160 feet (49.8 meters) in width, measured in the re-entry tunnel 103 feet (31.4 meters) above the explosive. The rubble chimney is estimated to contain about: 67 million ft^3 (1.9 million m^3) of fractured rock with a zone of fractures created by the immense shock wave out to a distance of more than 1000 feet (305 meters). This rock represents a sample of a rock size distribution resulting from a high-energy fracture mechanism. The particle size distribution of the Piledriver chimney rock has been extensively studied. Figure 2-3 shows the weight fraction (or volume) distribution of two samples taken and measured directly at the explosion site, as reported by Rabb (1970), and Figure 2-4 shows the estimated frequency distribution, as estimated by assuming spherical shape particles. The sample used in the present study was obtained from the

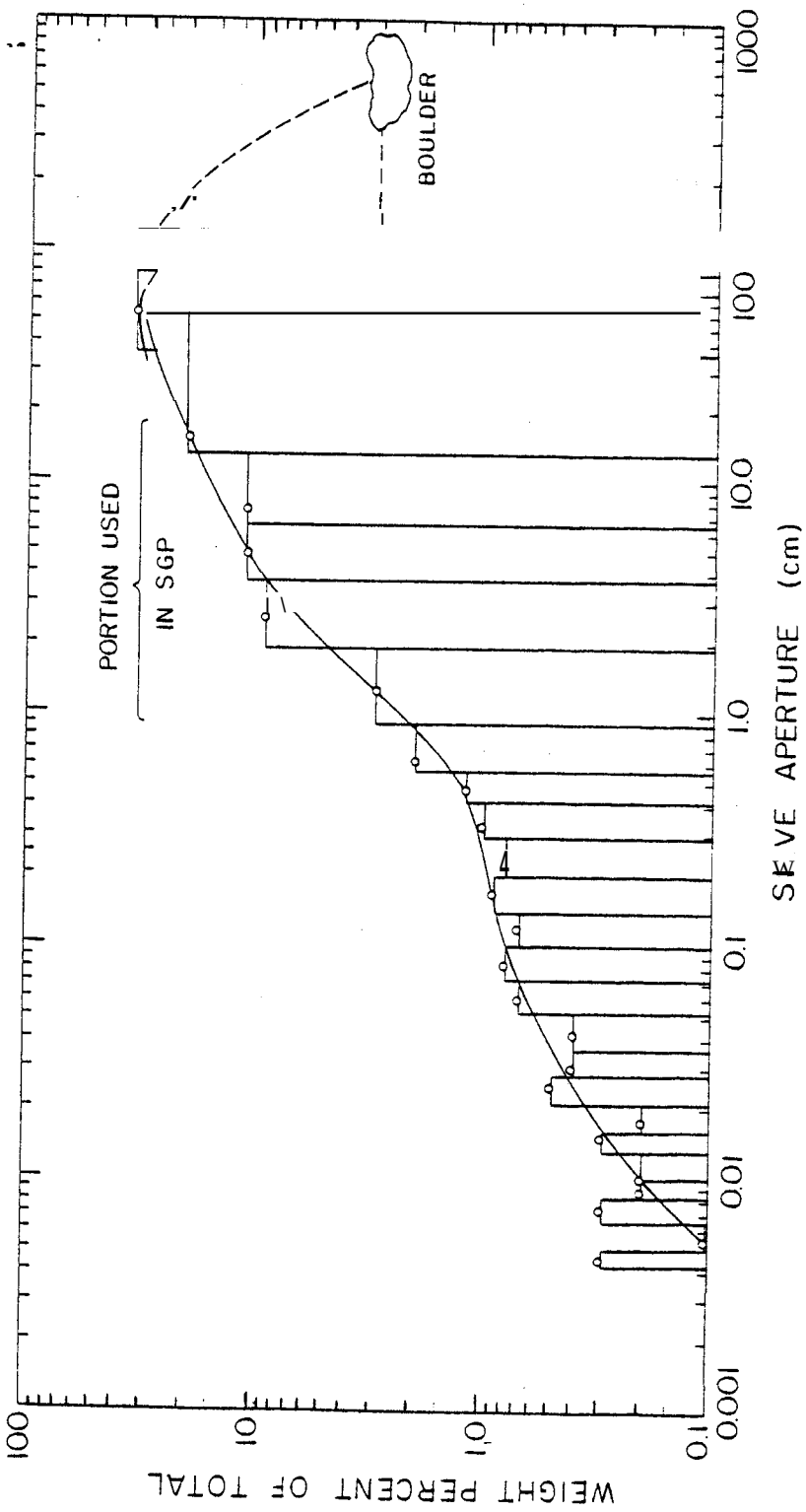

FIGURE 2-3. Piledriver rock weight fraction distribution (Rabb, 1970)

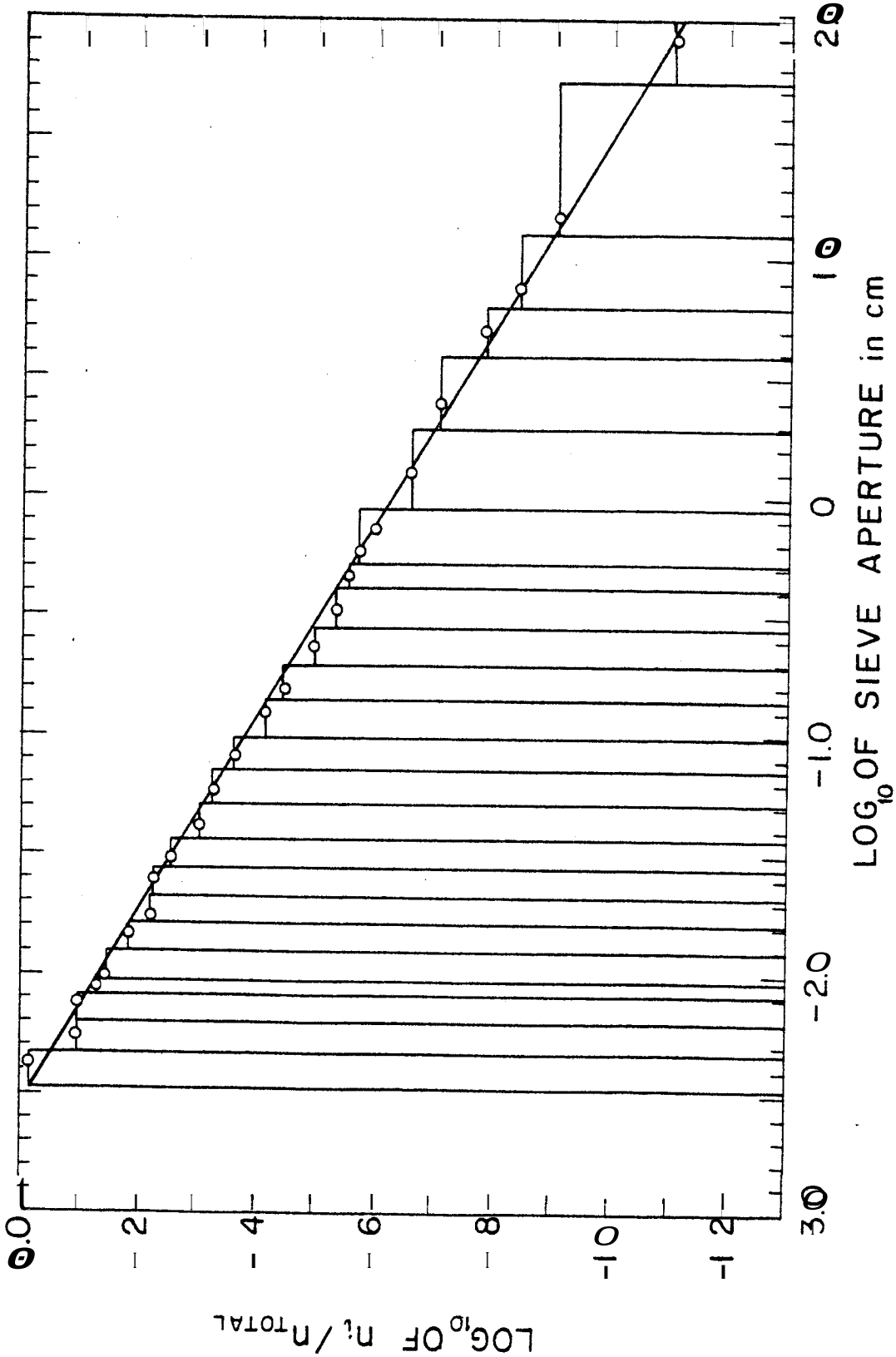

FIGURE 2-4. Piledriver rock size distribution

re-entry tunnel at a distance of about 100 feet (30.5 meters) from the chimney axis, and was transported in 30-gallon drums to Stanford University from the Nevada Test Site.

Initial tests performed with the Piledriver rock loading included radioactivity leaching tests as a function of convecting fluid temperature, and radon emanation measurements into liquid and vapor fluid as a function of temperature. The results of these tests will be reported elsewhere.

2.2.1 Definition of Geometrical Parameters

2.2.1.1 For individual rocks:

The study of the energy extraction from fractured geothermal reservoir requires the analysis of the heat transfer from irregularly shaped rocks to the surrounding fluid. Kuo, Kruger, and Brigham (1976) developed a shape factor correlation to model the heat transfer from irregularly shaped rocks using classical solutions for spherical rocks. A description of this correlation is presented in Section 3.1.3. According to his development, the effective radius of an irregularly shaped rock is given by:

$$R_e = R_s \times \psi_K \tag{2.1}$$

where the equivalent sphere radius R_s is defined as:

$$R_s \triangleq \{\text{radius of a sphere of equal volume}\} = \left(\frac{3v}{4\pi}\right)^{1/3} \tag{2.2}$$

and the sphericity ψ_K is defined as

$$\psi_K \triangleq \frac{\{\text{surface area of a sphere of equal volume}\}}{\{\text{actual surface area}\}} = \frac{A_s}{A_{actual}} \tag{2.3}$$

Thus, there are two important parameters required to obtain the

effective radius of a rock of irregular shape: (1) The volume, from which R_s and A_s are calculated, and (2) the surface area, from which the sphericity is calculated.

2.2.1.2 For a collection of rocks:

A methodology was developed in Section 3.5 of the present study to calculate the energy extraction from a collection ofrocks. The energy extraction from a collection of rocks was found to depend on the distribution of size (R_s or v) and shape (ψ_K) of individual rocks, and their volumetric fraction relative to the total volume of the collection.

The volumetric fraction of a group of rocks of equal size can be calculated from the frequency distribution of the rock volume as (see Appendix B.5 for derivation):

$$\chi_i = p(v_i) \times \frac{v_i}{\bar{v}} \qquad \text{(B. 17b)}$$

where $p(v_i)$ is the frequency or probability of finding a rock of volume v_i and is given by

$$p(v_i) = \frac{n_i}{N} \qquad (2.4)$$

Based on this methodology, it was demonstrated (Section 3.5.2) that it is possible to characterize a collection of rocks with a single parameter. This parameter, referred to as the bulk-effective radius, is the radius of a sphere that behaves thermally as the total collection of rocks. It was found to be given by (Eqs. 3.32 and 3.34):

$$R_{e,c} = \frac{\sum_{j=1}^{N_L} p(R_{s,j}) \cdot R_{s,j}^3}{\sum_{j=1}^{N_L} p(R_{s,j}) \cdot \frac{R_{s,j}^2}{\psi_{K,j}}} \qquad (2.5)$$

where $p(R_{s,j})$ is the frequency or probability of finding a rock with equivalent sphere radius $R_{s,j}$, and it can be calculated directly from the frequency distribution of the equivalent sphere radius R_s.

The measurement of the surface area of each individual rock in a collection of rocks (or a representative sample) is not practical. To solve this problem, a parameter referred to as the "pseudo Kuo's sphericity," ψ'_K, was derived. It was defined as the Kuo's sphericity of a tri-axial ellipsoid whose three axes are the dimensions of the rock as described in Figure A-1. It is given by (see Appendix A for details):

$$\psi'_K = \frac{4}{\psi_H\left(\frac{b}{c}+1\right)\left[1+\frac{(a/b)}{\sqrt{1-\left(\frac{b}{a}\right)^2}}\sin^{-1}\sqrt{1-\left(\frac{b}{a}\right)^2}\right]} \qquad (2.6)$$

where ψ_H is the Krumbein Sphericity used by Hunsbedt, Kruger, and London (1975b), which is defined as the cubic root of the ratio of the rock volume, approximated by the one of the tri-axial ellipsoid, to the volume of a circumscribing sphere:

$$\psi_H \triangleq \left(\frac{\pi abc/6}{\pi a^3/6}\right)^{1/3} = \left(\frac{bc}{a^2}\right)^{1/3} \qquad (2.7)$$

The pseudo Kuo's sphericity provides an approximate value of the Kuo's sphericity from the measurement of the three dimensions of the rocks. This is certainly much simpler than measuring the surface area of each individual rock. The validity of this approximation was demonstrated for the instrumented rocks by comparing the measured ψ_K and ψ'_K.

Thus, the main parameters required to characterize a collection of rocks are (1) volume frequency distribution, (2) equivalent sphere radius frequency distribution, and (3) distribution of Kuo's sphericity.

2.2.2 Instrumented Rocks

To study the temperature transient behavior of individual rocks, six instrumented rocks were installed at different locations of the reservoir as shown in Figure 2-5. Thermocouples were installed in the center of all of them, as illustrated in detail in Figure 2-6, and on the surface of rock number 3 to measure convection heat transfer coefficients. Care was taken in the specifications and quality of the cements used in the thermocouple installation to avoid the distortion of temperature measurements due to steam bubbles and liquid water penetrating the drilled holes. Thermocouples were also located next to each of the instrumented rocks and at other locations of the reservoir volume (see Figure 2-5) to measure the temperature transient of the surrounding fluid.

The surface area measurement technique developed by Kuo, Kruger, and Brigham (1976) was employed to determine the surface area for the instrumented rocks. The technique involves the immersion of a rock, previously cooled in dry ice, in a bath of paraffin during fixed time and temperature conditions. Under these controlled conditions, the rock is covered with a uniform and reproducible thickness of paraffin coating, which is easily removed from the rock surface because the paraffin thermo-cracks a few seconds after the rock has been extracted from the bath. The coating is weighted and the surface area is readily calculated from the thickness measurement and density information.

The volume of the six rocks was determined by measuring the volume of water displaced in a calibrated tank, and an average value of 2.64 g/cm^3 for the granite density was determined from their weight. The three dimensions of the rocks (length a, breadth b, and thickness c) were also measured to determine the value of the pseudo Kuo's sphericity.

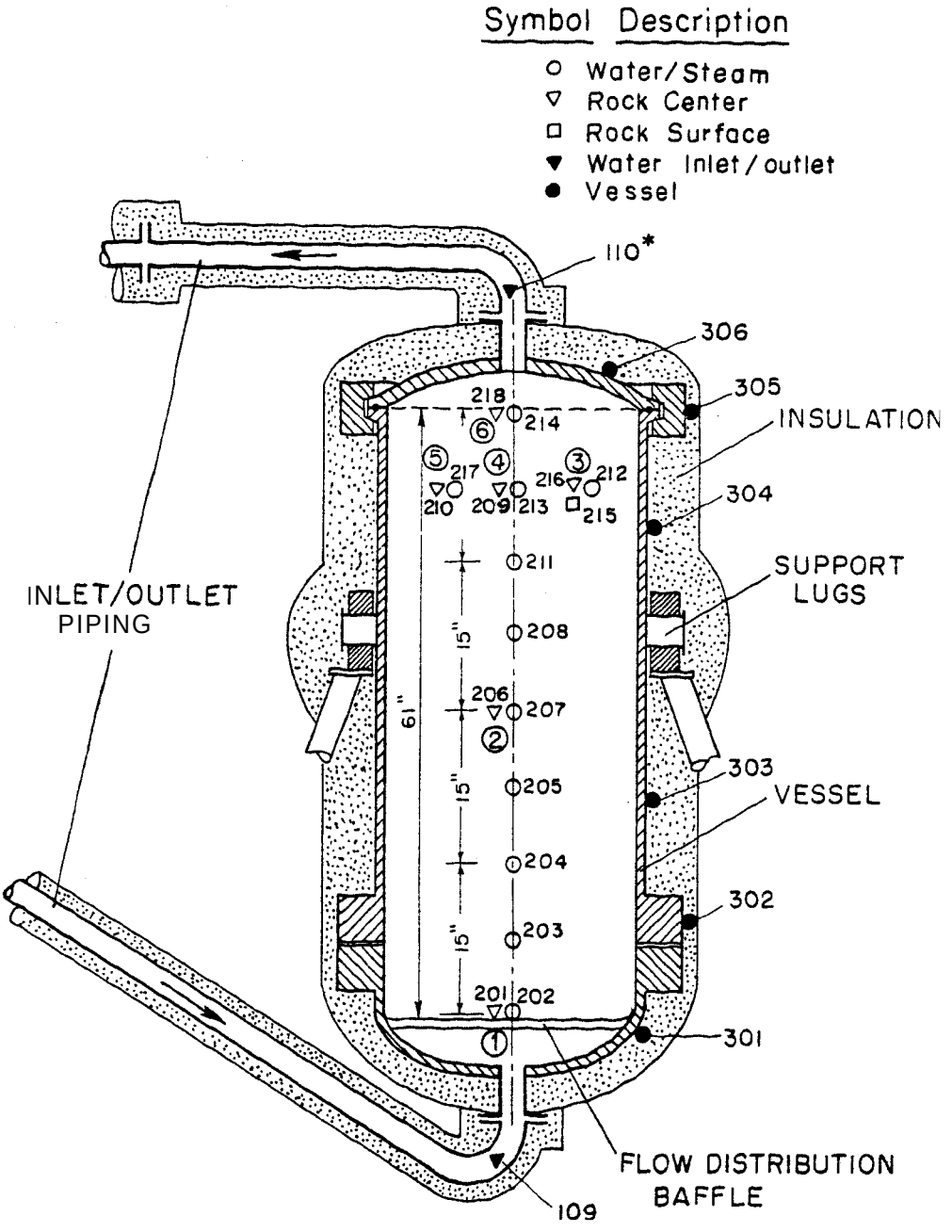

FIGURE 2-5. Reservoir thermocouple locations (Hunsbedt, Kruger, and London, 1975b).

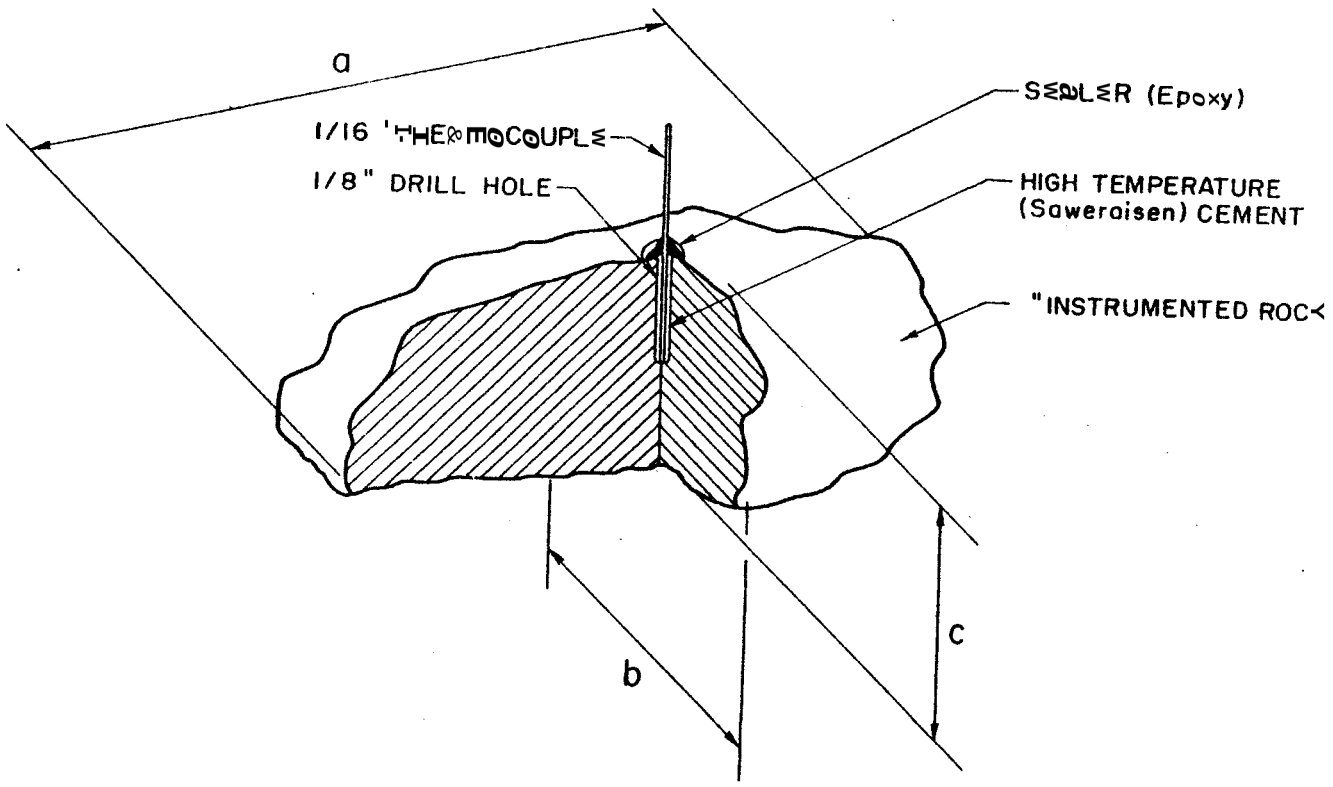

FIGURE 2-6. Details of thermocouple in an instrumented rock (Hunsbedt, Kruger, and London, 1975b).

Table 2–1 shows a summary of the important instrumented rock geometrical parameters (more detailed information of the measurements is presented in Appendix A). The main uncertainty in the surface area measurement resulted from the uncertainties involved In the paraffin coating thickness measurements. This uncertainty is larger in the bigger rocks where the uniformity of the coating was more difficult to control. However, it was found to be ±10 percent (for 95 percent confidence level) for all rocks. It can be seen in Table 2–1 that a relatively large value of the sphericity resulted for the six rocks. However, as it will be demonstrated in Section 3.5, the rate of energy extraction from a rock is proportional to the square of the sphericity which results in a significant impact of a small deviation of a rock from spherical shape.

The ratio of the Kuo's sphericity ψ_K to the pseudo Kuo's sphericity ψ'_K is also shown in Table 2–1 for the six instrumented rocks. It can be

TABLE 2–1

Summary of Instrumented Rock Geometrical Parameters

Rock Number	Actual Surface Area A (in^2)	Surface Area of Equal Volume Sphere A_s (in^2)	Kuo's phericity ψ_K dim-less)	Pseudo Kuo's phericity ψ'_K dim-less)	ψ_K/ψ'_K	Effective Radius $R_e = R_s \cdot \psi_K$ (in)
1	137.4	i26.0	0.92	0.89	1.03	2.91
2	236.3	190.5	0.8	0.9	0.89	3.11
3	76.5	72.4	0.95	0.89	1.07	2.28
4	109.2	101.7	0.93	0.9	1.03	2.65
5	260.6	228.4	0.87	0.92	0.95	3.71
6	131.8	113.4	0.85	0.95	0.89	2.55

seen from these ratios that ψ_K' was within 10 percent of ψ_K for all cases. The average value of this ratio was found to be:

$$\left(\frac{\psi_K}{\psi_K'}\right) = 0.97 \pm 0.06 \qquad (2.8)$$

for 95 percent confidence level (i.e., ± 1.96 times the standard error of the mean of the sample of 6 rocks). Therefore, it can be said with a confidence level of 95 percent that the expected value of Kuo's sphericity is 0.97 ± 0.06 times the value of the pseudo Kuo's sphericity. This empirical relationship was used to correct the value of the pseudo Kuo's sphericity for the collection of rocks as it is described in the following section.

2.2.3 Rock Size and Shape Distribution

Before loading the granitic rocks into the reservoir model, the rock size distribution of the collection was determined. Ideally, the best way to perform this measurement was to determine the size of every single rock loaded in the model. However, this was not practical and only a representative sample was measured. Standard statistical sampling techniques were used to do this.

The number of rocks required to obtain a representative sample was determined by performing an uncertainty analysis of the rock to fluid temperature difference for a range of typical rock sizes (see Appendix A for a detailed description of the method). It was found that the maximum allowable uncertainty in the rock radius for a reasonable uncertainty in the rock to fluid temperature difference was about 0.01 ft. Thus, the mean (arithmetic) value of the rock radius estimated from the sample had to be within ± 0.01 ft of the actual mean radius of the collection of

rocks. According to the central limit theorem of statistical inference, the arithmetic mean of a population tends to be normally distributed among the actual mean, almost independently of the shape of the distribution of the original population. Therefore, for a given confidence level (95 percent in this study) the standard deviation of the mean, which is inversely proportional to the sample size, had to be equal or less than a given value determined by the definition of the normal distribution (0.01 ft/1.96 for 95 percent confidence level).

A small sample was initially taken and the important parameters were measured (a, b, c, and R_s). The standard deviation was estimated for each parameter and the required number of rocks was determined according to the desired value of the standard deviation of the mean.* This calculation was checked as more rocks were measured to account for possible changes in the initial estimate of the standard deviation. The required number of rocks was found to be 360. It was assumed that if the mean value of the rock radius was within the required limits, the distribution of the rock radius (and of other parameters) was also within the allowable range of the actual distribution.

The main geometrical parameters were measured for the 360 rocks of the representative sample. Their measured mean values and standard deviations are listed in Table 2-2 as compared to the first and second rock collections utilized by Hunsbedt, Kruger, and London (1975b). The uncertainties for the parameters of the Piledriver rock are listed for a 95 percent confidence level.

*The standard deviation of the mean or just standard error is equal to the standard deviation (which can be estimated from a small sample), divided by the square root of the number of rocks in the sample.

TABLE 2-2

Mean and Standard Deviation of Main Rock Geometrical Parameters

Parameter	Gabbro		Granite		Piledriver Granite	
	Mean	Standard Deviation	Mean	Standard Deviation	Mean[a]	Standard Deviation
Length, a (cm)	3.83	1.44	10.9	7.96	6.73 ± 0.31	2.9
Breadth, b (cm)	2.82	1.08	7.41	5.07	4.32 ± 0.27	2.6
Thickness, c (cm)	1.88	0.77	4.11	2.32	2.8 ± 0.19	1.88
Mass, M_r (g)	32.6	26.5	1093	1796	245.5 ± 62	604
Equivalent sphere diameter, d_s (cm)	2.52	0.93	6.73	4.54	4.11 ± 0.06	2.56
Breadth/length ratio, b/a (dimensionless)	0.74	0.13	0.71	0.16	0.66 ± 0.15	0.15
Thickness/length ratio, c/a (dimensionless)	0.5	0.12	0.44	0.17	0.42 ± 0.14	0.14
Pseudo Kuo's sphericity, ψ'_K (dimensionless)	~0.9	-	~0.8	-	0.86 ± 0.01	0.08
Krumbein sphericity, ψ_H (dimensionless)	0.71	0.09	0.67	0.12	0.64 ± 0.01	0.11
Surface area, A (cm^2)	31.98	19.42	306.25	365	85.7 ± 12.7	123.3
Volume, v (cm^3)	11.68	9.48	419	688	93.4 ± 23.5	228.2
Bulk-effective radius, $R_{e,c}$ (cm)	-	-	-	-	4.63	-

[a] Uncertainties are expressed for 95 percent confidence level, i.e. $\pm 1.96\ \sigma_{\bar{X}}$

Note that the uncertainties are all within the desired limits of ±0.3 cm (0.01 ft). It is seen from Table 2-2 that the mean values of the equivalent sphere diameter and the pseudo Kuo's sphericity for the Piledriver granite are somewhere between the values for the first and second rock loadings used by Hunsbedt, Kruger, and London (1975b).

The rock size and shape distributions characterized by the equivalent sphere radius and the pseudo Kuo's sphericity are shown in Figures 2-7 and 2-8, respectively. The distribution of the equivalent sphere radius shown in Figure 2-7 is approximately exponential. The high frequency of small rocks can be explained if Figure 2-7 is compared to Figure 2-4. It is seen from Figure 2-4 that the frequency of small rocks at the explosion site was several orders of magnitude higher than the frequency of large rocks. Thus, it was expected that the sample brought to the laboratory has a similar size distribution.

From Figure 2-8 it is seen that the distribution of the pseudo Kuo's sphericity is approximately normal with the tail end of the high values cut at the maximum value of 1.0 imposed by the definition of Kuo's sphericity. The same type of distribution (normal) was observed for all the parameters related to the shape of the rocks, such as the Krumbein sphericity ψ_H and the ratios of the rock dimensions b/a and c/a . This characteristic was also reported by Hunsbedt, Kruger, and London (1975b). The distribution of these parameters are shown in Appendix A.

It was inferred from these distributions that the shape of the rock tends to be independent of the rock size. This was verified by assuming that the pseudo Kuo's sphericity is a linear function of the equivalent sphere radius. Inmathematical form:

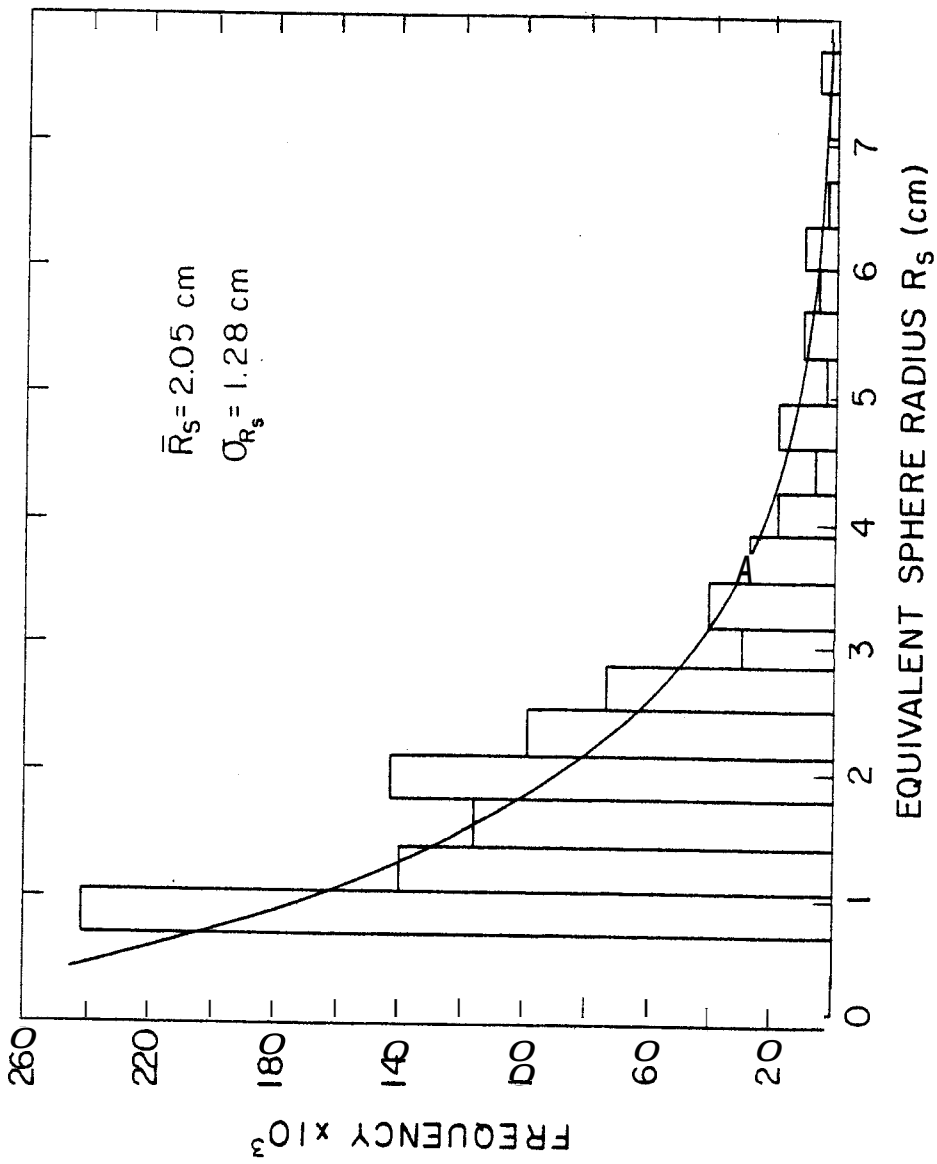

FIGURE 2-7. Frequency distribution of the equivalent sphere radius

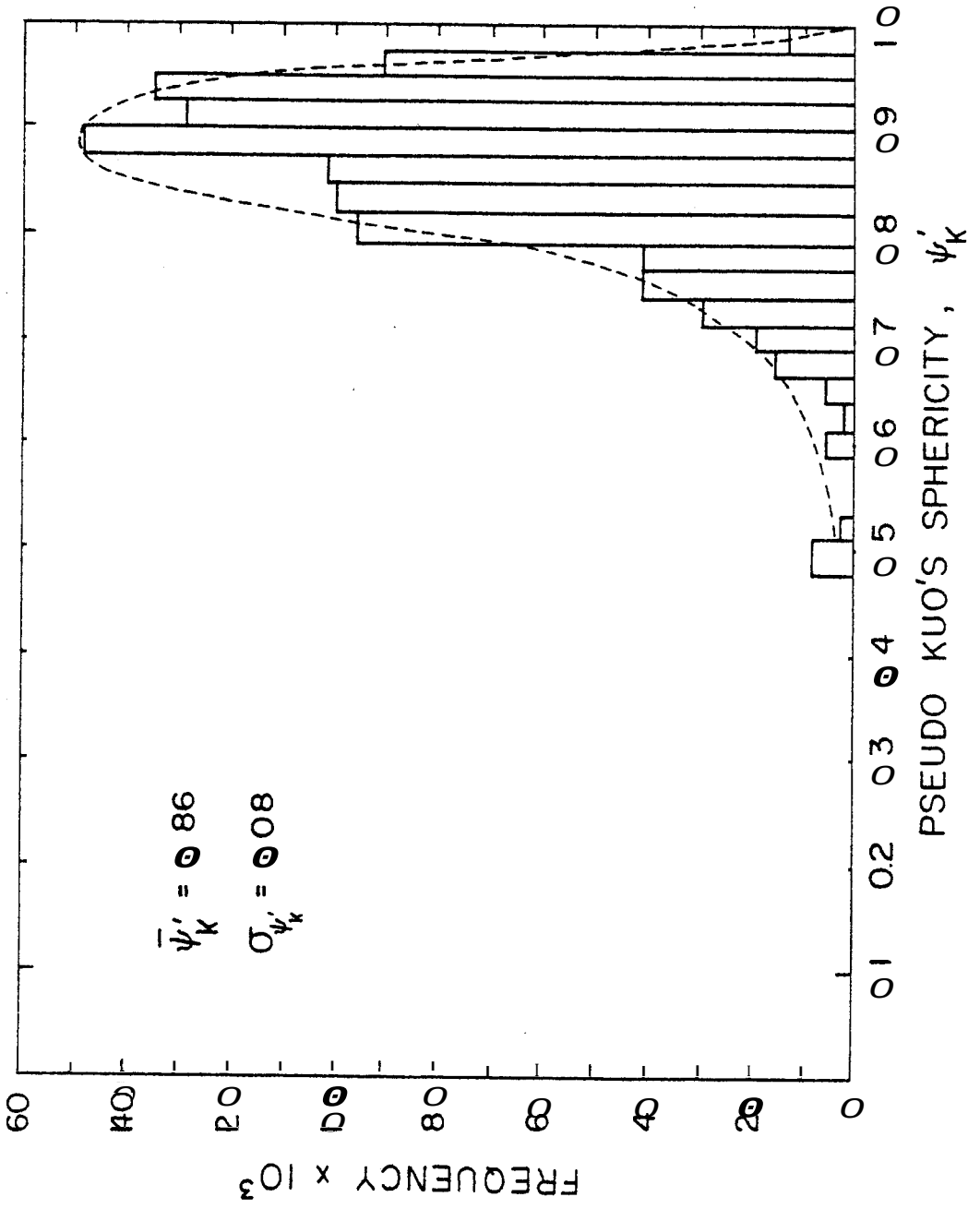

FIGURE 2-8. Frequency distribution of the pseudo Kuo's sphericity, ψ'_K

$$\psi'_K = C_1 + C2\ Rs \qquad (2.9a)$$

The dependence of the pseudo Kuo's sphericity on the equivalent sphere radius is measured by the value of the coefficient C_2. A least-squares regression analysis was performed for the 360 rocks of the measured sample to estimate the values of the coefficients C_1 and C_2. They were found to be:

$$\psi'_K = (0.838 + 0.005\ R_s) \pm 0.16 \qquad (2.9b)$$

Figure 2-9 shows the observed values of the pseudo Kuo's sphericity as a function of the equivalent sphere radius, and the predicted values using the regression equation, Eq. 2.9b. It can be seen that ψ'_K is slightly dependent on R_s. However, the value of the coefficient of determination r^2 equal to 0.0195 indicates that only 1.95 percent of the variations of ψ'_K from its mean value were explained by variations on R_s. This indicates that the relationship determined by the regression is not statistically significant. Therefore, it was concluded that for practical purposes the pseudo Kuo's sphericity is independent on the rock size, and that its mean value can be used to characterize the shape of a collection of rocks.

The mean value of the pseudo Kuo's sphericity was corrected to find the expected mean value of the Kuo's sphericity using Eq.2.8 and the mean value of ψ'_K from Figure 2.8:

$$\bar{\psi}_K = 0.97 \times 0.86 = 0.83$$

From Figure 2-7 and the mean value of the sphericity $\bar{\psi}_K$, the bulk-effective radius was readily calculated from Eq. 2.5 to be 4.63 cm. Note that if all the rocks were spheres, the bulk-effective radius would be

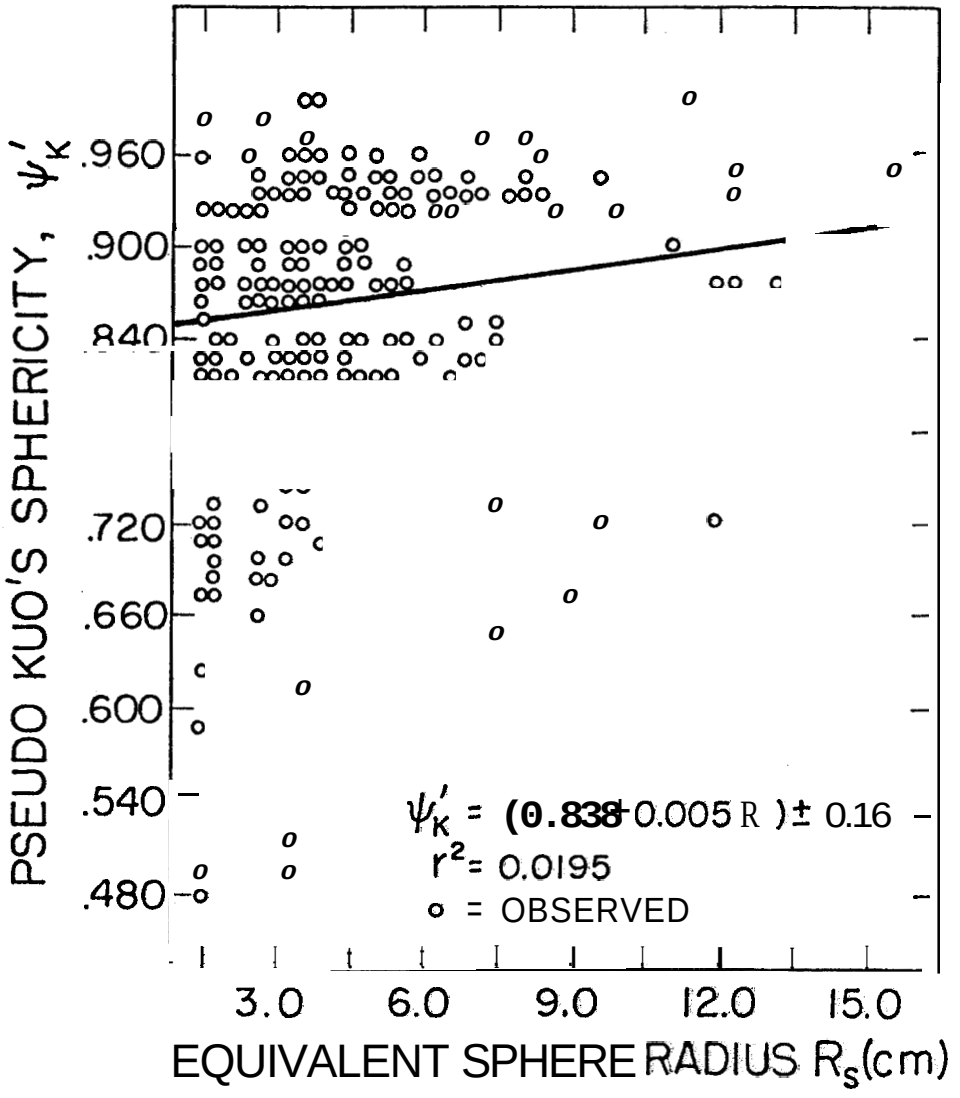

FIGURE 2-9. **Pseudo Kuo's sphericity as a function of equivalent sphere radius. Observed and predicted values from regression**

5.58 cm which is approximately three times the mean value of the equivalent sphere radius (2.05 cm). This is a particular property of a collection of rocks with the equivalent sphere radius exponentially distributed which is analyzed in Section 3.5.3.

The volumetric (or weight) fraction distribution is shown in Figure 2-10. It was calculated using Eq. B-17b from the frequency distribution of the rock volume shown in Appendix A. The mean values for each group are indicated to facilitate the calculations in Section 4. Note that the mean value of each group is different from the midpoint of the selected size interval for each group. Comparison of Figures 2-10 and 2-3 shows that the volume fraction distribution of the collection of rocks used in the laboratory model differ from those reported by Rabb (1970). The distribution in Figure 2-10 is only a small portion of the actual sizes covered in Figure 2-3. This was the effect of sampling with a shovel which preferentially "selects" the small sizes. On the other side of the distribution, the very small particles were deliberately extracted from the rock loading to protect the circulation system. The data in Figure 2-3 also show a higher volume fraction of larger rocks compared to the data in Figure 2-10, again probably due to the effect of the shovel "selecting" the smaller sized by dropping the larger ones.

2.2.4 Bulk Parameters

The major bulk parameters of the rock loading used in this study and the two loadings from prior studies are listed in Table 2-3. The definition of these parameters and the methodology for their measurement are as reported by Hunsbedt, Kruger, and London (1975b). The rock matrix volume refers to the total chimney volume occupied by rock. The void volume fraction was

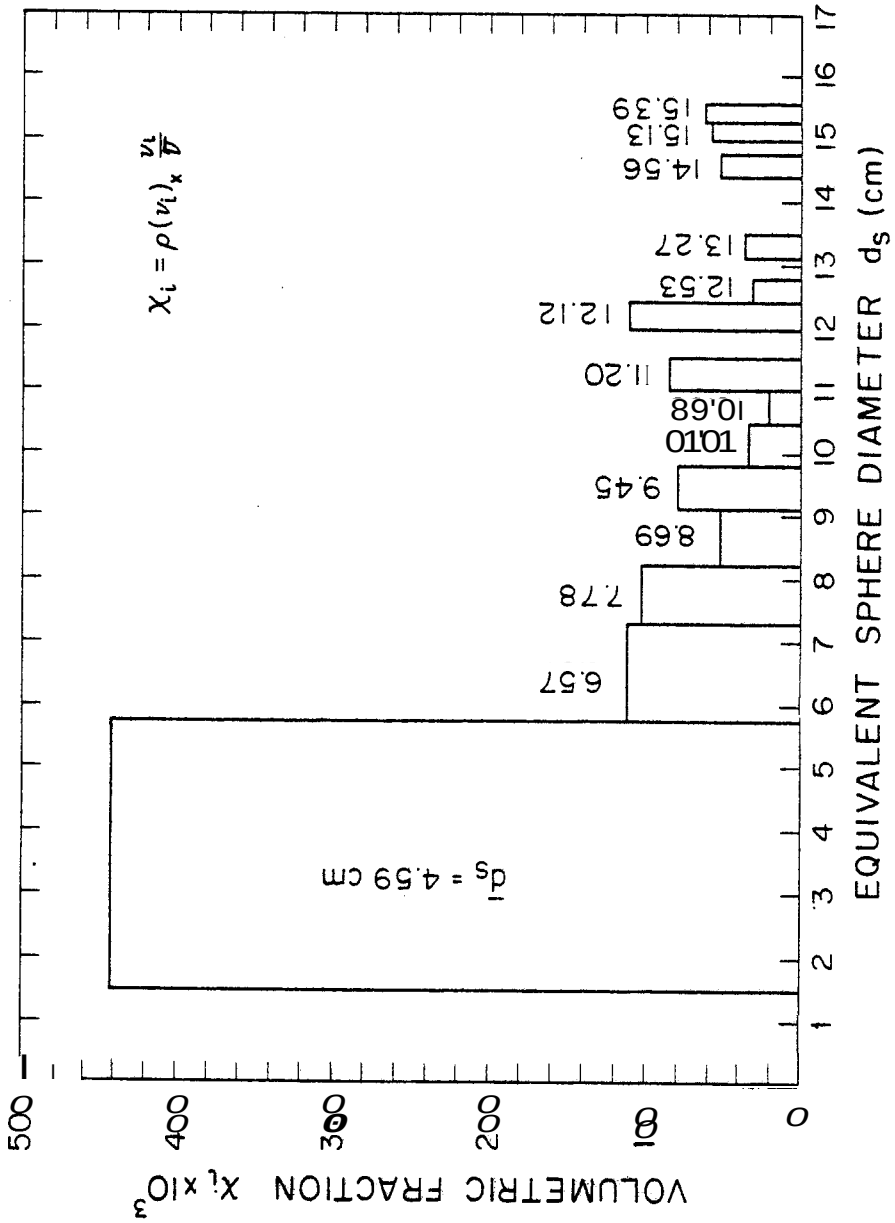

FIGURE 2-10 Volumetric fraction distribution

TABLE 2-3

Comparison of Major Bulk Parameters

Parameter	Gabbro	Granite	Piledriver Granite
Total Rock Mass (lbm)	1640	1818	1556
Mean Rock Density (g/cm^3)	2.79	2.61	2.64
Rock Matrix Volume (ft^3)	16.57	16.57	16.57
Rock Matrix Surface Area (est.) (ft^2)	748	546	690
Void Volume (ft^3)	7.25	5.72	7.2
Void Fraction (dimensionless)	0.437	0.345	0.43
Drainage Porosity (dimensionless)	0.44	0.35	0.42
Dead Volume between Valves (ft^3)	8.15	8.15	8.15
Rock Specific Heat (Btu/lbm-°F)	0.216	0.218	0.218
Rock Thermal Conductivfty (Btu/hr-ft-°F)	1.2	1.4	1.4
Rock Thermal Diffusivity (ft^2/hr)	0.032	0.039	0.039

found from the total rock mass and density measurements. The drainage porosity was measured by water displacement and differs from the pore fraction because of the irreducible water saturation. The thermal properties of the rock reported by Hunsbedt, and London (1975b) for granite were used for the Piledriver granite. They were assumed to be constant with temperature and pressure, and homogeneous throughout the collection of rocks.

An important characteristic of these three fractured rock loadings is very large porosity, on the order of 35 to 44 percent, and therefore an almost infinite permeability. A consequence of the high permeabilities is a negligible pressure drop through the rock matrix.

Another important characteristic is the rock size distribution which affects the total surface area. The effect is noted for the third loading which has a rock matrix surface area lower than the first loading

but higher than the second one, in spite of the similarity in size and its higher void fraction. The surface area fraction distribution shown in Figure 2-11 has most of the area fraction in the smaller sizes. A similar characteristic is also observed by comparing the void fraction of the Gabbro and Piledriver granite. The high volumetric fraction of the smaller sizes shown in Figure 2-10 makes the Piledriver rock very similar to the Gabbro in the volumetric characteristics in spite of the fact that the mean value of the Piledriver rock volume is almost eight times larger than that of the Gabbro.

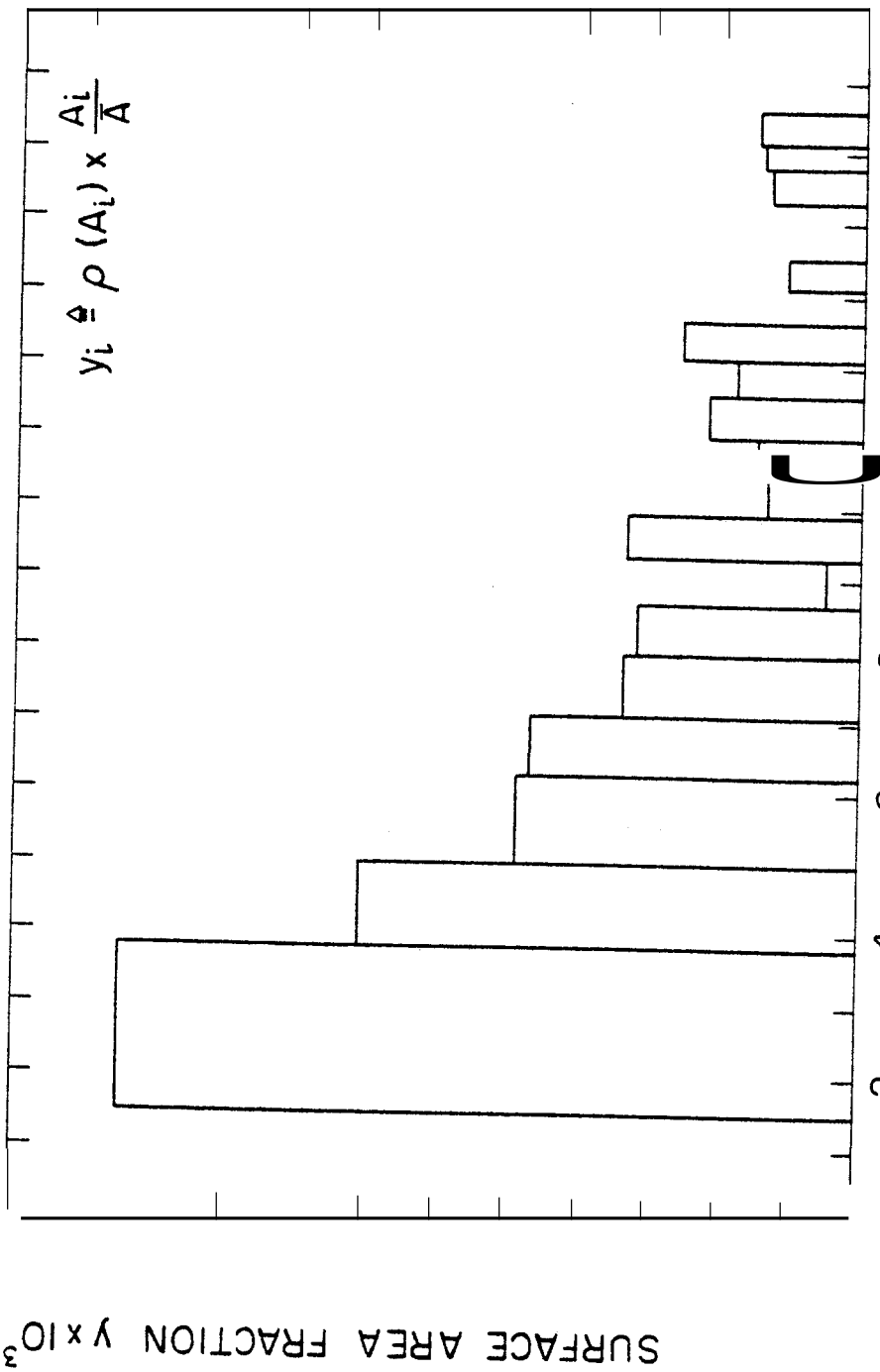

FIGURE 2-11 Distribution of the surface area fraction y

3. ANALYSIS

The analysis of the heat transfer limitations on the energy recovery from geothermal reservoirs requires a mathematical model that can predict the temperature of the reservoir rock relative to that of the geothermal fluid. The temperature transient behavior of individual rocks was first considered in developing such a model. To include the effect of the different rock sizes and shapes in the reservoir, the single rock model was applied to a collection of rocks with given size and shape distributions. Based on this model, the energy extraction process for the cold water sweep was analyzed, and a criteria was established to determine when the energy recovery may be heat transfer limited, and how this limitation can be measured.

3.1 Rock Temperature Transient Solutions

The prediction of the temperature transient behavior in the individual rocks must include conduction heat transfer inside the rock and convection to the geothermal fluid at the rock surface. Classical exact analytical solutions and simplified one-lump parameter solutions were formulated for spherical rock assuming constant fluid cooling rate conditions. The irregular shape of actual fractured rocks is accounted for by utilizing the shape factor correlation developed by Kuo, Kruger, and Brigham (1976). The validity of the one-lump solution was determined by comparing its accuracy to predict the energy extracted from a single rock to the exact analytical solutions, and eventually by comparing it to experimental rock temperature transients. The heat transfer model for individual

rocks was completed by formulating a solution for variable fluid cooling-rate conditions. Superposition of the solutions for constant fluid cooling rate was used for this purpose.

3.1.1 Exact Solution for Spherical Rock under Constant Fluid Cooling-Rate Conditions

A graphical representation of the temperature profile of a spherical rock and the surrounding fluid is shown in Figure 3-1. Both the rock and the surrounding fluid are initially at a uniform temperature T_1 (Fig. 3-la). The fluid temperature starts to decrease with time at a linear rate as (Fig. 3-lb)

$$T_f(t) = T_1 - \mu t \tag{3.1}$$

After a given time $t = t_P$ the fluid temperature has dropped to $T_f(t_p)$, and a temperature profile $T_r(r,t_P)$ has developed inside the rock as indicated in Figure 3-lc. In developing the mathematical model that governs the temperature inside the rock, the following idealizations were made: (a) The rock material is impermeable, homogeneous, and isotropic, with constant properties; (b) the fluid surrounding the rock is at a uniform temperature T_f; (c) there is a finite convection heat transfer coefficient constant with time and uniform throughout the rock surface.

The governing partial differential equation resulting from conservation of energy and heat transfer rate equations and its solution are given by Carslaw and Jaeger (1974) and by Hunsbedt, Kruger, and London (1975b). Heat transfer is initiated by the fluid temperature cooldown described as a non-homogeneous boundary condition at the rock surface. The solution for the partial differential equation is given in Appendix B.1.

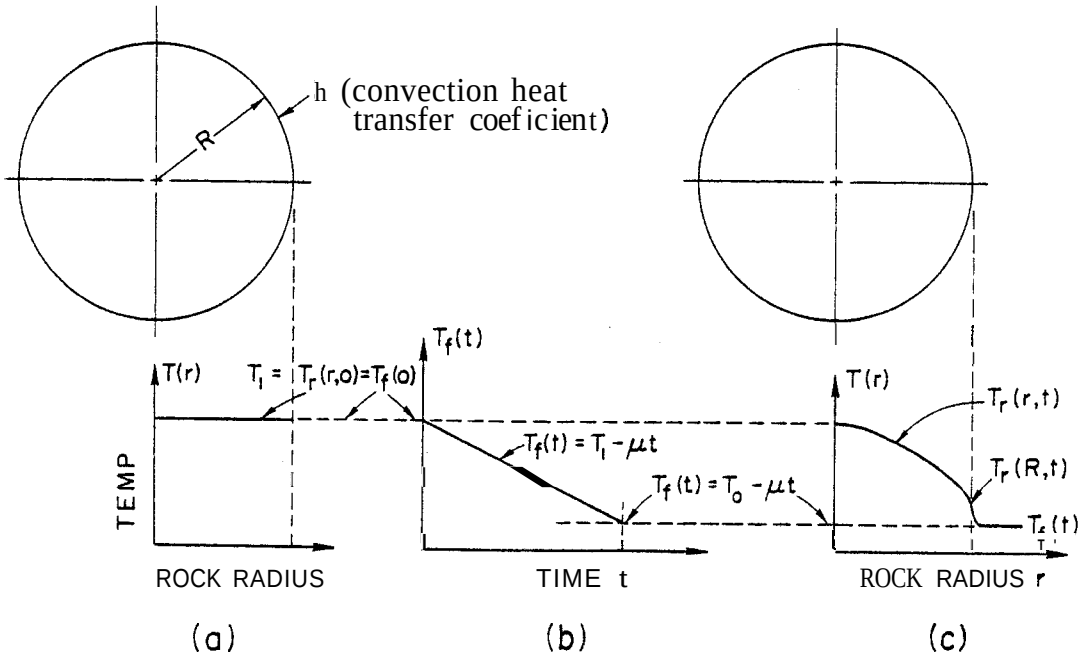

FIGURE 3-1. Development of the temperature profile in a spherical rock. (a) Initial condition. (b) Fluid temperature as a function of time. (c) Rock Temperature Profile after some time $t=t_P$

The solution for the rock center temperature for comparison to measured rock temperature transients is of particular interest. This solution is, in non-dimensional form,

$$\frac{T_r(0,t) - T_f(t)}{\mu R^2/\alpha} = \frac{(1/2 + 1/N_{Bi})}{3} - \sum_{n=1}^{\infty} \frac{2 N_{Bi}\, e^{-\beta_n^2 N_{Fo}}}{\beta_n [\beta_n^2 + N_{Bi}(N_{Bi} - 1)] \sin \beta_n} \quad (3.2)$$

It is important to analyze the physical meaning of the Biot number, $N_{Bi} = (hR/k)$. A large Biot number can result either from a big rock or, when the ratio of the convection heat transfer coefficient to the thermal conductivity of the rock (h/k) is large. Thus, for two rocks of the same size but of different material, the one which has the higher resistance to heat transfer inside the rock as compared to that at the rock surface (a larger h/k) will have the higher Biot number.

For purposes of evaluating the energy extracted from a rock, it is convenient to define a mean rock temperature as:

$$\bar{T}_r(t) \triangleq \frac{\int_V \rho c\, T_r(r^*,t)\, dV}{\rho c\, V} \quad (3.3)$$

Its physical meaning can be thought of as the temperature that would result if a rock initially at a non-uniform temperature, was left completely insulated for sufficient time to achieve a uniform temperature throughout the rock mass. Substituting Eq. B.1a (in Appendix B) into Eq. 3.3, the mean temperature results:

$$\frac{\bar{T}_r(t) - T_f(t)}{\mu R^2/\alpha} = \frac{(1/5 + 1/N_{Bi})}{3} - \sum_{n=1}^{\infty} \frac{6\, N_{Bi}^2\, e^{-\beta_n^2 N_{Fo}}}{\beta_n^4 [\beta_n^2 + N_{Bi}(N_{Bi} - 1)]} \quad (3.4)$$

Numerical results of Eqs. 3.2 and 3.4 are given in Figures 3-2 and 3-3, respectively. The following points are noted from these results:

(a) After a given time (expressed non-dimensionally as the Fourier number), the rock mean-to-fluid and rock-center-to-fluid temperature differences reach a steady value equal to

$$T_r(0,t) - T_f(t) = \frac{\mu R^2}{3\alpha} (1/2 + 1/N_{Bi}) \tag{3.5}$$

and

$$\bar{T}_r(t) - T_f(t) = \frac{\mu R^2}{3\alpha} (1/5 + 1/N_{Bi}) \tag{3.6}$$

It is readily seen from these equations that, for a given value of the Biot number, the rock-to-fluid temperature difference depends on the fluid cooling rate (characterized by μ), the square of the rock radius, and the rock thermal properties (characterized by the thermal diffusivity α).

(b) The rock-to-fluid temperature difference is very sensitive to changes in Biot number when it is less than 10. For values of Biot number larger than 10, the solution for rock-fluid temperature difference is approximately the same as if $N_{Bi} = \infty$. Physically, thismeans that for Biot numbers larger than 10, the thermal resistance at the rock surface is negligible as compared to the thermal resistance inside the rock mass.

(c) The difference between the magnitudes of the rock center to-fluid and mean rock to fluid temperature differences becomes greater for larger Biot numbers. The physical explanation of this is that a larger Biot number will produce larger non-uniformities in the temperature profiles inside the rock mass, and consequently a larger difference between the rock center and the mean temperatures will result.

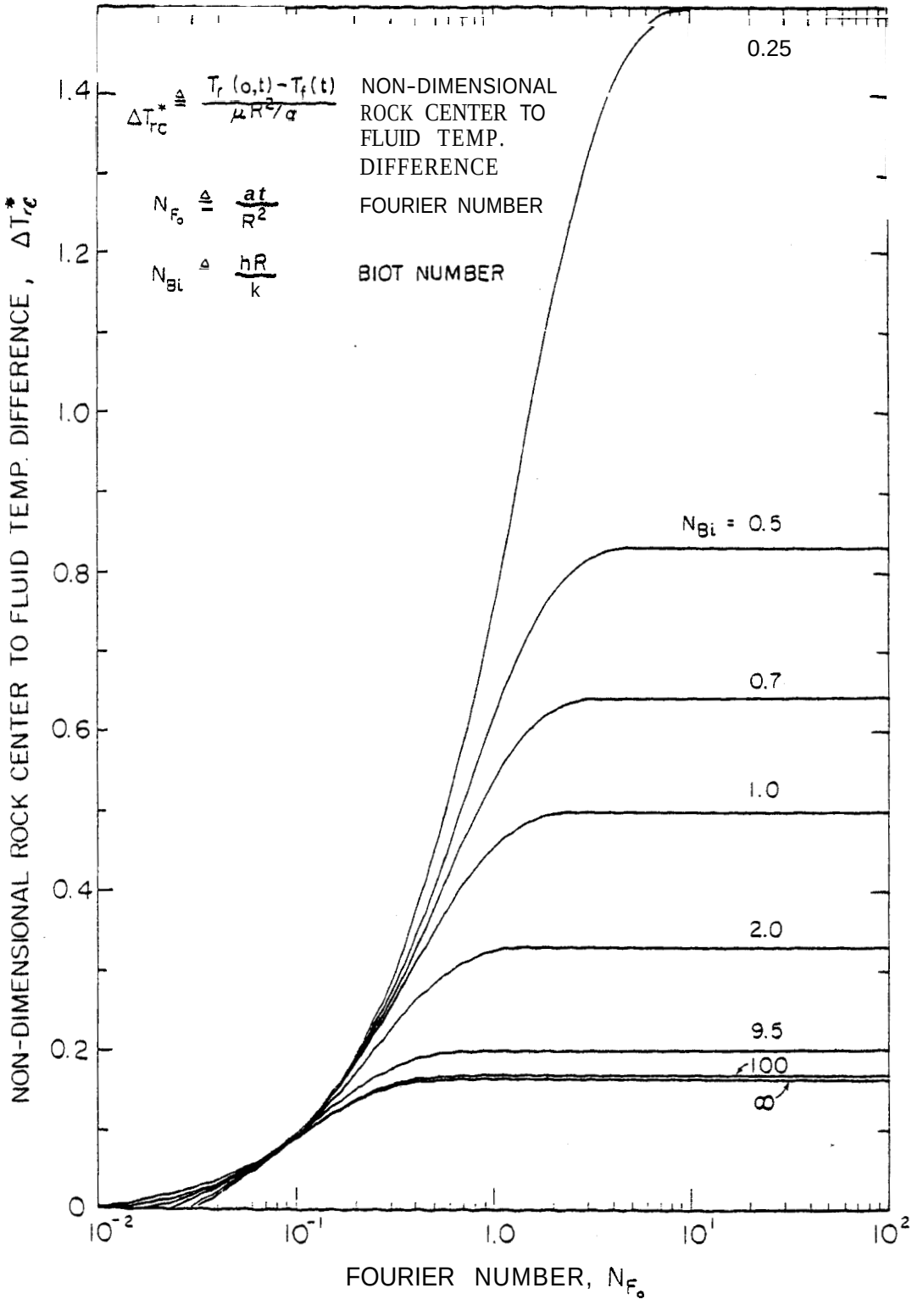

FIGURE 3-2. Rock center to fluid temperature difference as a function of Fourier number for different values of the Biot number

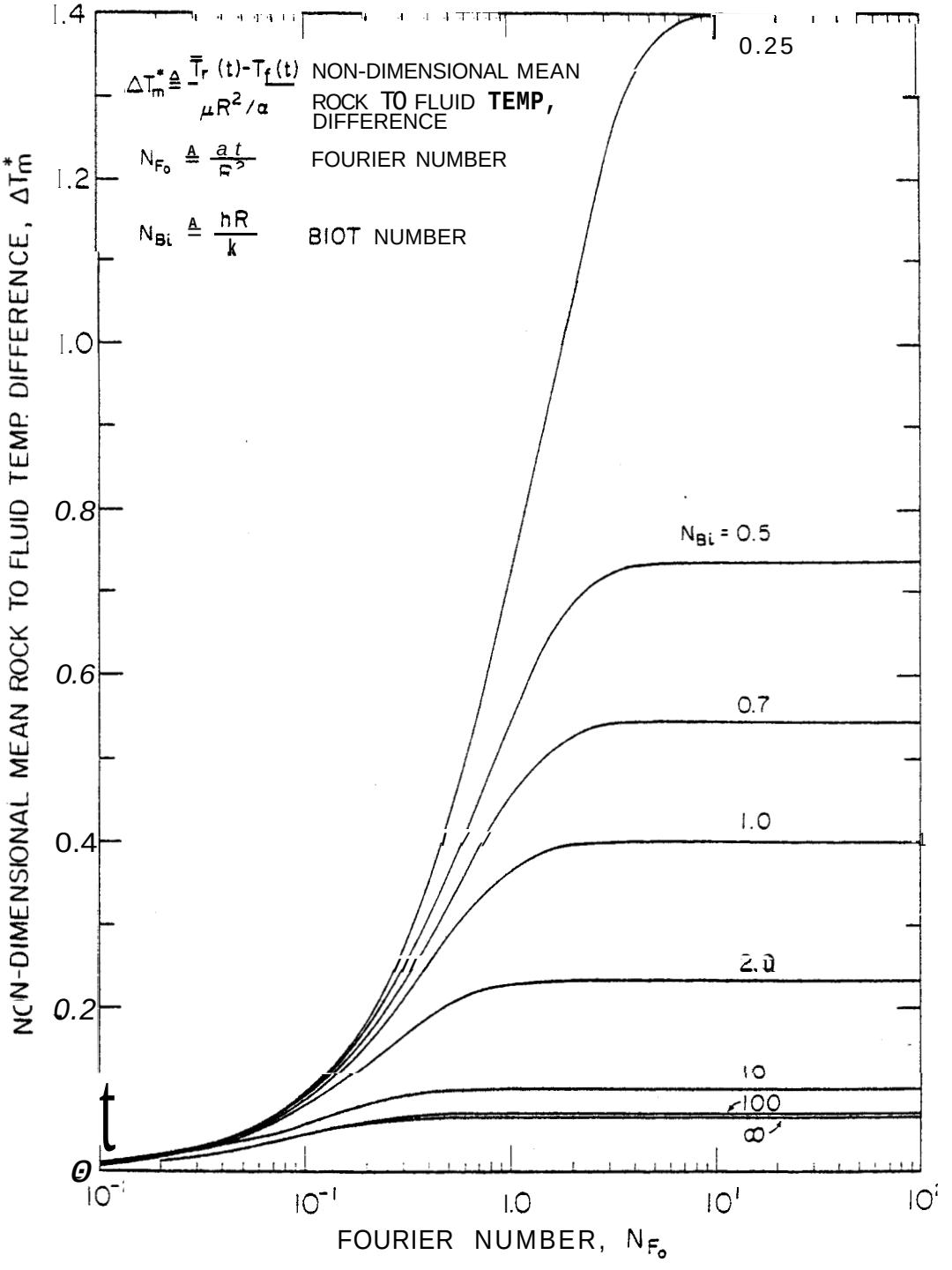

FIGURE 3-3. Mean rock to fluid temperature difference as a function of Fourier number for different values of the Biot number

(d) It was noted in the computational procedure that the rock center-to fluid temperature solution converges to a precision of 10^{-8} in the second term of the series expansion, whereas the mean rock to fluid temperature difference solution needed from 8 to 16 terms to converge to the same precision.

3.1.2 One-Lump Parameter Solution

The exact analytical solutions require a computer to evaluate the infinite series to an acceptable accuracy. This is impractical in the present study, because double summations result when the single-rock solutions are applied to a collection of rocks. Also, utilization of the superposition method to model variable fluid cooling rate conditions would be practically impossible without the use of a simple closed-form solution.

The one-lump parameter solution was reported by Hunsbedt, Kruger, and London (1975b) and is derived in Appendix B.2 by considering the total rock mass concentrated in a single point, which is located at some distance ℓ_{cond} (conduction path length) from the rock surface. It is given by

$$T_r - T_f = \mu R_o C(1 - e^{-t/R_o C}) \tag{3.7}$$

where the product $R_o C$ is called the time constant τ. It is a measure of the time needed to achieve 63.2 percent of the steady-state value of the rock to fluid temperature difference. As illustrated in Figure 3-4 the overall thermal resistance R_o is the reciprocal of the overall thermal conductivity times the rock surface area A, i.e.,

$$R_o \triangleq \frac{1}{U_o A} \tag{3.8a}$$

Physical Model

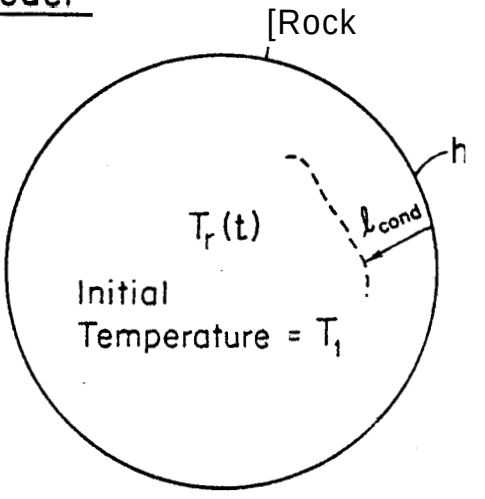

Surrounding Fluid

$T_f(t) = T_1 - \mu t$

Thermal Circuit

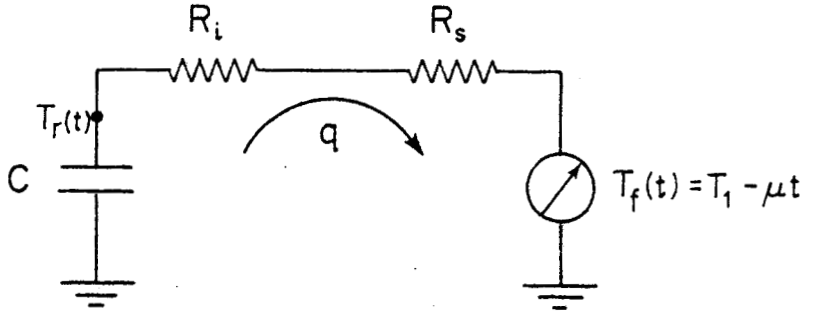

FIGURE *3-4.* **Notation and thermal circuit €or the one-lump parameter analysis**

where

$$U_o \triangleq \frac{1}{\left(\frac{\ell_{cond}}{k} + \frac{1}{h}\right)} \tag{3.8b}$$

The rock thermal capacitance C represents the energy that can be extracted from the rock mass for a temperature drop of one degree. It is given by

$$C \triangleq \rho_r c_r V \tag{3.9}$$

Then, the time constant of the rock is given by

$$\tau \triangleq \frac{C}{U_o A} = \frac{\rho_r c_r}{(A/V)} \left(\frac{\ell_{cond}}{k} + \frac{1}{h}\right) \tag{3.10a}$$

or, simplifying,

$$\tau = \frac{R^2}{3\alpha}\left(\frac{\ell_{cond}}{R} + \frac{1}{N_{Bi}}\right) \tag{3.10b}$$

It is observed from Eq. 3.10a that the surface area to volume ratio is the geometrical parameter that governs the temperature transient behavior in the rock. If the expression for the time constant is substituted into Eq. 3.7, the rock-to-fluid temperature difference becomes:

$$T_r - T_f = \frac{\mu R^2}{3\alpha}\left(\frac{\ell_{cond}}{R} + 1/N_{Bi}\right)\left(1 - e^{-N_{Fo}/\left(\frac{\ell_{cond}}{R} + 1/N_{Bi}\right)}\right) \tag{3.11a}$$

By comparing Eq. 3.11a to the exact solutions given by Eqs. 3.5 and 3.6, approximate values for the magnitudes of the conduction path lengths, ℓ_{cond}, can be determined. These magnitudes are taken such that Eq. 3.11a reproduces the quasi steady-state value of the exact solutions. Thus,

the magnitudes of the conduction path length that should be used in Eq. 3.11 become (Hunsbedt, Kruger, and London, 1975b).

$$\frac{\ell_{cond}}{R} = \frac{1}{2} \qquad (3.11b)$$

for the rock center temperature solution and

$$\frac{\ell_{cond}}{R} = \frac{1}{5} \qquad (3.11c)$$

for the mean rock temperature solution.

The one-lump parameter solution can be considered as an interpolation formula for the exact solution of the rock to fluid temperature difference from its zero initial value to its quasi steady-state solution. Its validity to predict intermediate values will be investigated in Section 3.2.

The conduction path length measures the internal thermal resistance of the rock. The larger it is, the larger the internal resistance for heat transfer is, and the larger the rock to fluid temperature difference will be. Clearly, large rocks represent long conduction path lengths and slow transfer of the stored thermal energy.

The one-lump parameter solutions represent simple and closed-form mathematical models for the rock temperature transient. They are also powerful "thinking tools" to understand the rock energy extraction process.

3.1.3 Shape Factor Correlation

The shape factor correlation developed by Kuo, Kruger, and Brigham (1976) is used to model the temperature transient for rocks of irregular shape. A summary of this correlation is presented here to provide some understanding of its physical meaning and to express it in an operationally convenient

form for its direct use in the temperature transient predictions as given by Eq. 3.11.

The shape factor correlation is based on the observation that the surface area to volume ratio is the geometrical parameter that governs the heat transfer from a solid of any shape to the surrounding fluid. The more surface area for convection to the surrounding fluid, the faster the stored energy in its volume will be extracted. This was clearly seen in Eq. 3.10a for the sphere. The larger the A/V ratio, the smaller the time constant will be. Thus, the rock will reach a lower magnitude of its steady-state rock to fluid temperature difference in a shorter period of time. Accordingly, it is expected that the temperature transient behavior of a solid with irregular shape will be similar to that of a sphere having the same surface area to volume ratio. Kuo (1976) defined the sphericity parameter for an irregularly shaped solid (referred to in Section 2.2.4), as the surface area of an equal volume sphere (Eq. 2.3) divided by the actual surface of the solid as

$$\psi_K \stackrel{A}{=} \frac{(A/V)_s}{(A/V)_{actual}} = \frac{A_s}{A_{actual}} = \frac{4\pi R_s^2}{A_{actual}} \qquad (2.3)$$

Since a spherical solid has the minimum surface area to volume ratio, the sphericity of a solid of any other shape will always be less than unity.

Kuo found that the temperature transient of an irregular shaped solid can be modeled as an equal volume sphere with radius R_s^*, and with the radii used in the Biot and Fourier numbers defined by

---

* Primes are used on K to differentiate it from the slightly different K used by Kuo in his original development.

$$\frac{R_{Bi}}{R_s} = K'_{Bi} \tag{3.12}$$

$$\frac{R_{Fo}}{R_s} = K'_{Fo} \tag{3.13}$$

where K'_{Bi} and K'_{Fo} are the correlation factors given in Figures *3-4* and *3-5* as a function of the sphericity and the length-to-width ratio of the rock a/b . Inspection of Figures 3-5 and 3-6 show that the correlation factors can be approximated with a fair degree of accuracy as

$$K'_{Bi} = K'_{Fo} \simeq \psi_K \tag{3.14}$$

An effective radius R_e is defined to replace R_{Bi} and R_{Fo} in the temperature transient solutions for spherical rocks. From Eqs. 3.12, 3.13, and 3.14 the effective radius is given by

$$\frac{R_e}{R_s} = \psi_K \tag{3.15}$$

This simplified correlation shows that the lower the sphericity is, the smaller the effective radius, and the better the heat transfer characteristics of rock are, from the energy extraction point of view.

3.1.4 Variable Fluid Cooling Rate Solutions

The analysis of the rock temperature transient has been done for constant fluid cooling rate. Only very special conditions will result in linear cooldown of an actual geothermal reservoir. The thermodynamics of the fluid cooling is governed by the production and recharge characteristics of the reservoir, and by the heat transfer from the hot rock. The heat transfer from the rock, in turn, depends on the cooling rate of the

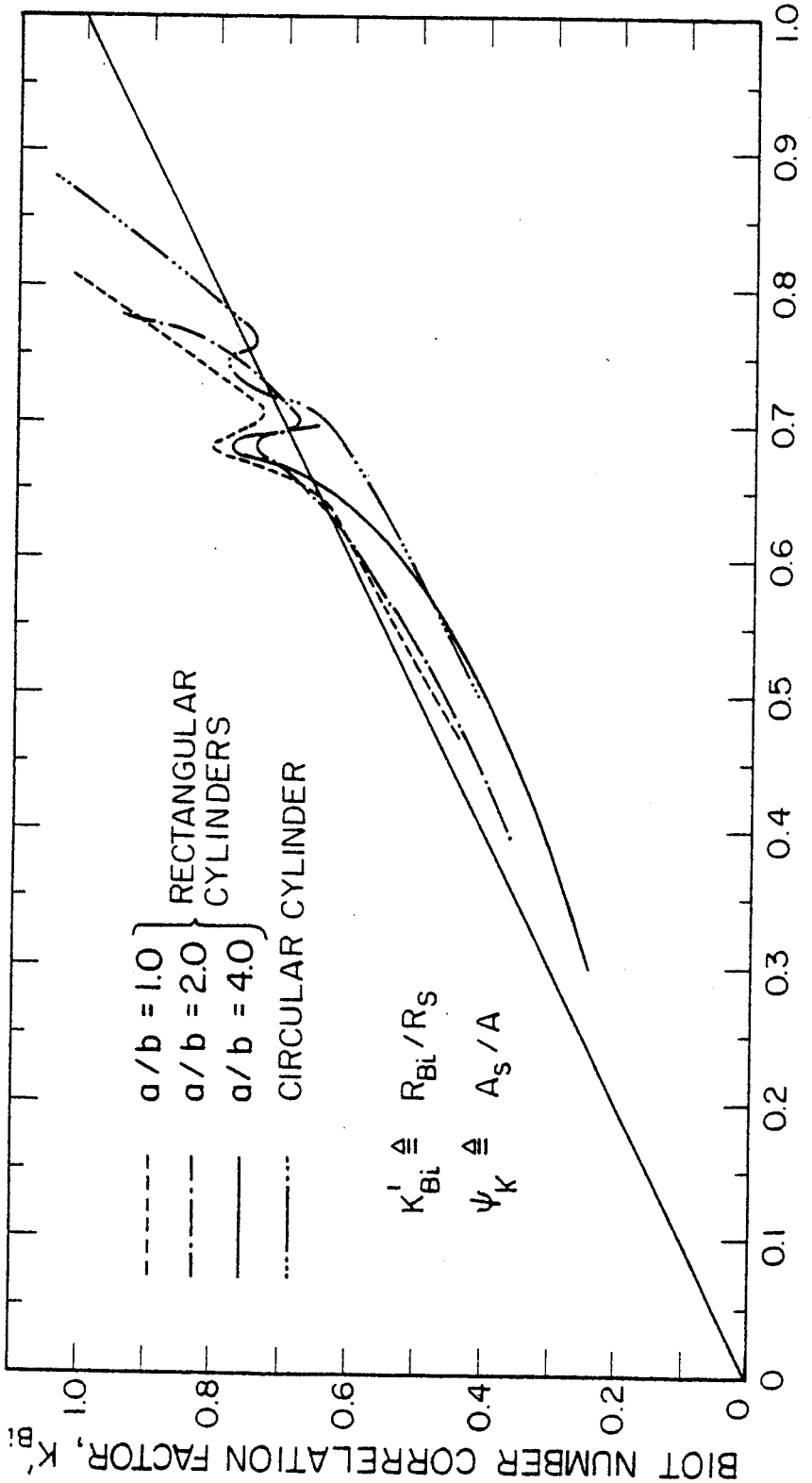

FIGURE 3-5. Biot number correlation factor as a function of sphericity and a/b ratio (from Kuo, Kruger, and Brigham, 1976).

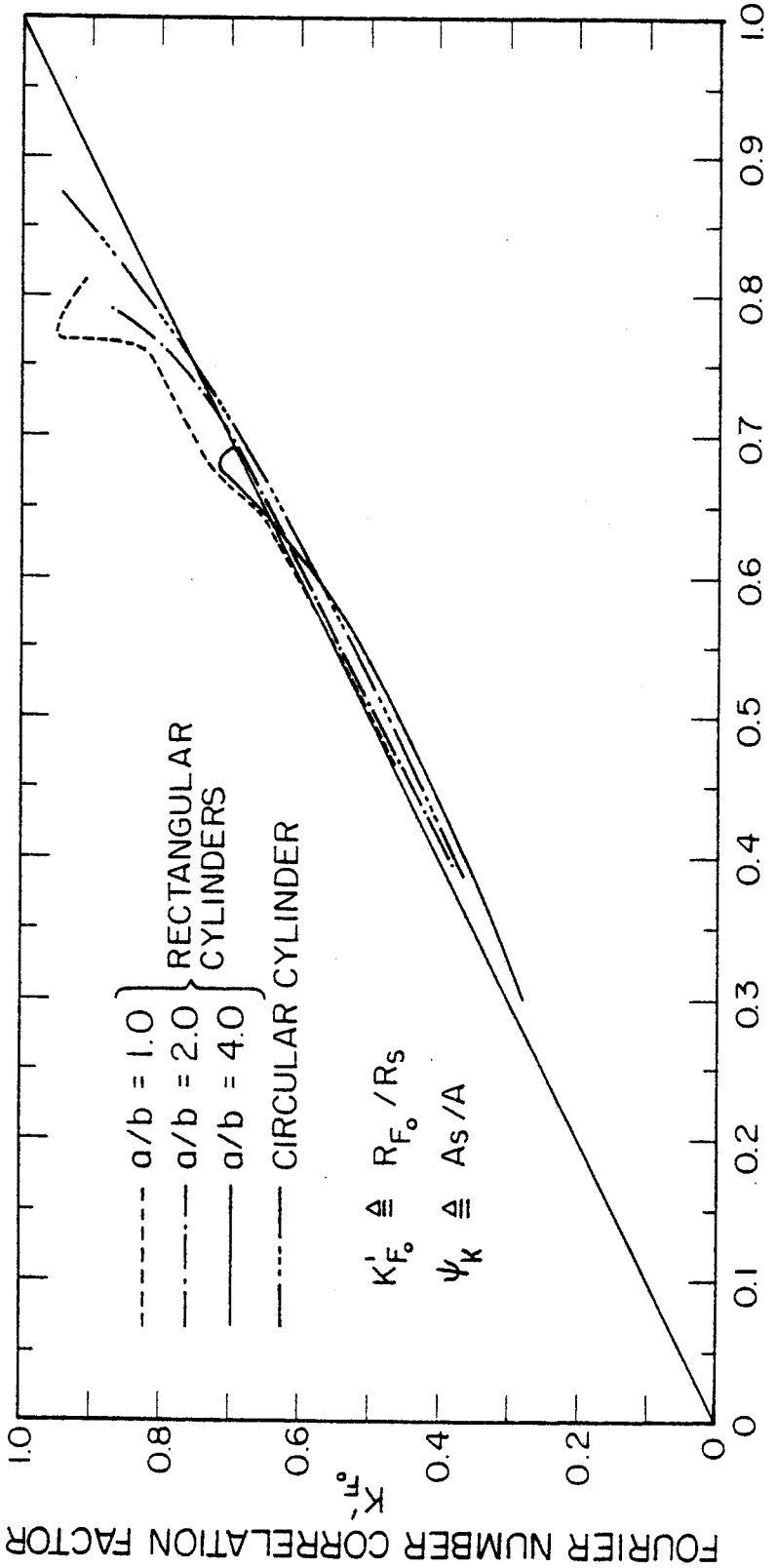

FIGURE 3-6. Fourier number correlation factor as a function of sphericity and a/b ratio (from Kuo, Kruger, and Brigham, 1976).

fluid. Therefore, the fluid cooling rate is actually a dependent variable. Thus, it can vary continuously in any manner as a function of the parameters controlled by the geothermal field developer, i.e., the independent variables.

The constant cooling rate solution is applied to variable cooling rate by superimposing a series of constant cooling rate solutions as indicated in Figures 3-7a and b. Then the cooling rate will behave as a series of steps. The rock temperature at any time t can then be determined by summing the contribution of each of the steps, either infinitesimal or finite. The time variable t is treated as a constant and a dummy variable ξ is used to designate the location of each step; ξ thus varies from 0 to t.

The derivation for the superposition technique is given in Appendix B.3. The resulting equation for the rock to fluid temperature difference is given by

$$T_r - T_f = \sum_{i=1}^{n} \tau \left(1 - e^{-(t-\xi)/\tau}\right) \Delta\mu_i \qquad (3.16a)$$

where

$$\Delta\mu_i = \mu_{i+1} - \mu_i \qquad (3.16b)$$

and

$$\tau = \frac{R_e^2}{3\alpha}\left(\frac{\ell_{cond}}{R_e} + \frac{1}{N_{Bi}}\right) \qquad (3.16c)$$

This equation can be evaluated in tabular form as indicated in Appendix C.1. A computer program given in Appendix B.4 was used when many steps were involved. The use of the one-lump parameter solution greatly simplifies the calculations as compared to the use of the exact analytical solutions.

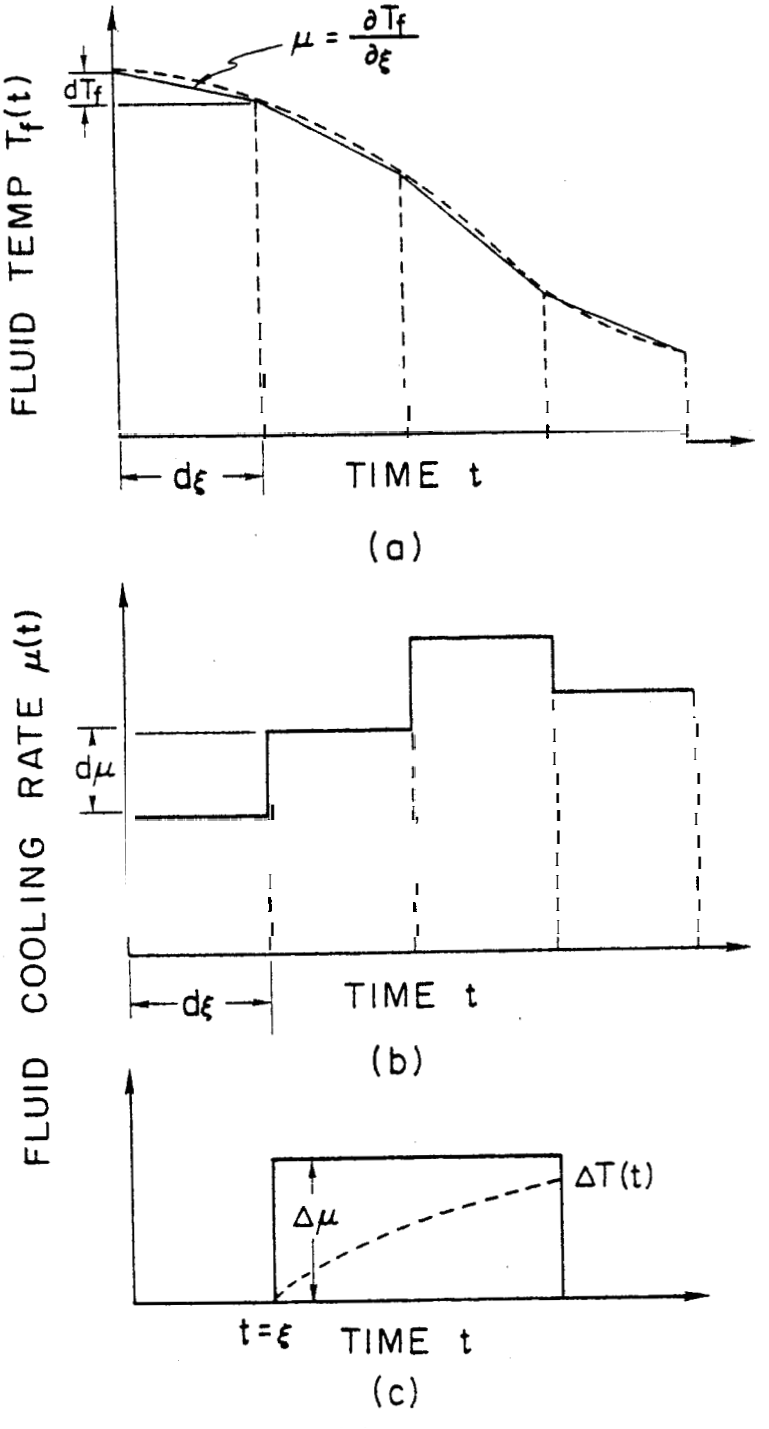

FIGURE 3–7. **Superposition of constant fluid cooling rate to model variable fluid cooling rate conditions**

3.2 Individual Rock Energy Extracted Fraction

The energy extracted fraction from a single rock is defined as the ratio of the thermal energy that is actually transferred from the rock to the surrounding fluid to the thermal energy that would be extracted if the rock were cooled uniformly to the fluid temperature at a given time t. It can be expressed in mathematical form as

$$F_E \triangleq \frac{Q}{Q_{max}} = \frac{\int_V \rho_r c_r [T_1 - T_r(r,t)]\, dV}{\rho_r c_r V[T_1 - T_f(X,t)]} \tag{3.17}$$

where X indicates the position at which T_f is being considered in a given reservoir, and it can be expressed in one, two, or three dimensions. For example in two dimensions, the fluid temperature would be expressed as $T_f(x,y,t)$. Performing the integration yields

$$F_E = \frac{T_1 - \left\{\frac{\int_V \rho_r c_r\, T_r(r,t)dV}{\rho_r c_r V}\right\}}{(T_1 - T_f(X,t))}$$

The second term in the numerator is the definition of mean rock temperature given in Eq. 3.3. Then,

$$F_E = \frac{T_1 - \bar{T}_r(t)}{T_1 - T_f(X,t)} \tag{3.18}$$

The individual rock energy extracted fraction F_E changes with time and position because $\bar{T}_r$ and T_f change with time and position. It can be seen that F_E approaches unity when the mean rock temperature approaches the fluid temperature. The individual rock energy extracted fraction measures directly the fraction of energy mined from the rock at a given time t and it can vary from zero to one. Clearly, $1-F_E$ represents the amount of energy left inside the rock because of temperature non-uniformities inside it.

This non-exploited energy is proportional to the mean rock to fluid temperature difference and is given by

$$(1 - F_E) = \frac{\overline{T}_r(t) - T_f(t)}{T_1 - T_f(X,t)} \tag{3.19}$$

An expression for the energy extracted fraction was derived assuming that the fluid is cooled at a constant rate. The non-dimensional temperature difference is expressed as

$$\Delta T^*_m \triangleq \frac{\overline{T}_r(t) - T_f(X,t)}{\mu R_e^2/\alpha} \tag{3.20}$$

where for constant cooling rate, μ is, by definition,

$$\mu = \frac{T_1 - T_f(X,t)}{t} \tag{3.21}$$

Substituting Eqs. 3.21 and 3.20 into 3.18 and rearranging results in a non-dimensional expression for the energy extracted fraction at a time t for constant cooling rate conditions:

$$F_E = 1 - \frac{\Delta T^*_m}{N_{Fo}} \tag{3.22}$$

The individual rock energy extracted fraction using the exact analytical solution for the temperature transient given by Eq. *3.4* for the rock to fluid temperature difference in Eq. 3.20 is given in Figure 3-8 (solid lines) for a range of Biot numbers. It is observed that the larger the Biot number, the higher the energy extracted fraction will be for a given value of the Fourier number. It is also observed that for all Biot numbers and for Fourier numbers greater than about 10 the energy extracted fraction is greater than 0.9. For Biot numbers greater than 10 most of the energy is extracted before the Fourier number reaches unity. In other words, the time necessary to extract most of the energy from a rock, when the Biot number is greater than 10, is given approximately by

$$t \approx \frac{R_e^2}{\alpha} \tag{3.23}$$

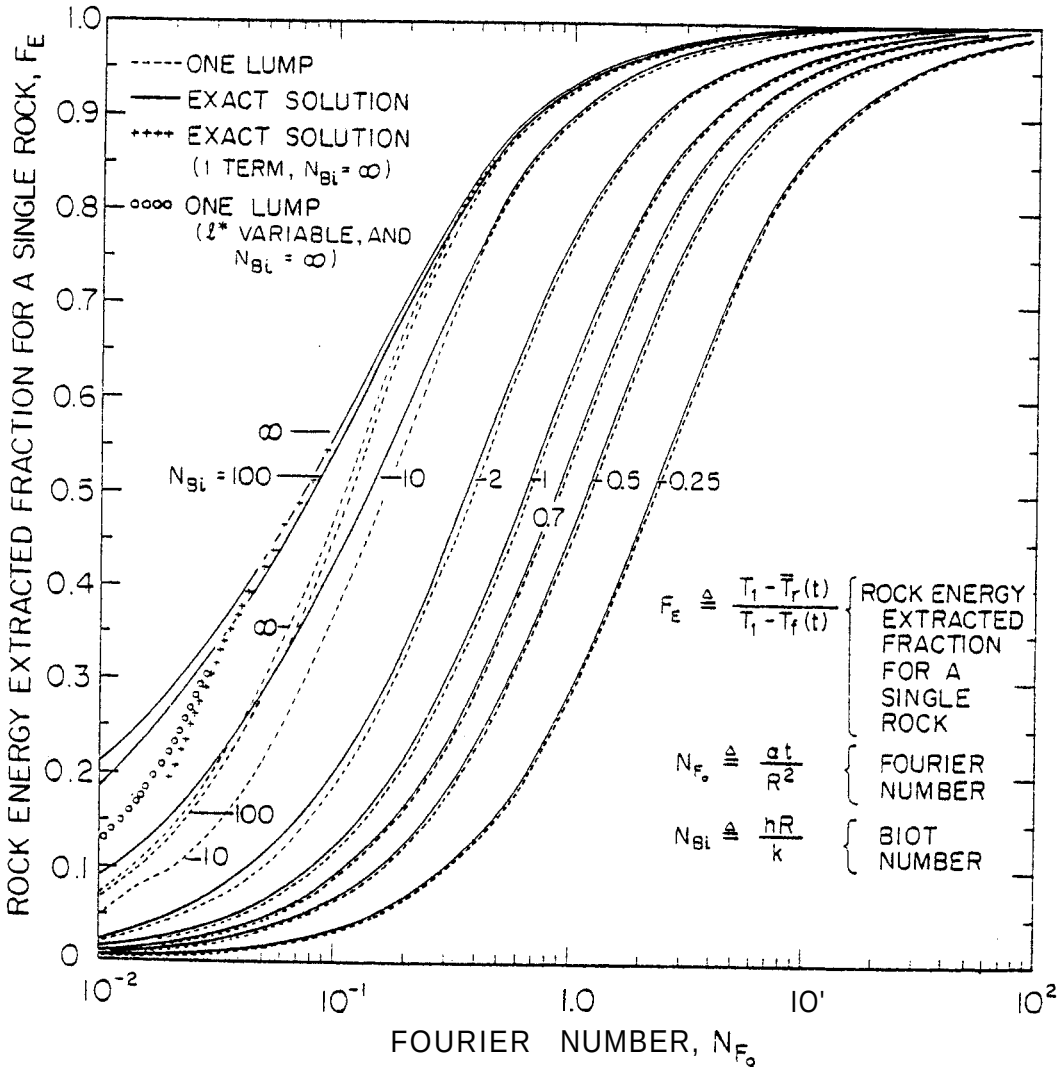

FIGURE 3-8. Rock energy extracted fraction for a single rock under constant fluid cooling rate conditions

3.3 Comparison of One-Lump Parameter and Exact Solution

The one-lump parameter solutions were derived for the rock center and rock mean temperature transients. The purpose of their derivations was to provide simple and closed-form mathematical approximate solutions. Simplicity makes the one-lump parameter solution a very powerful thinking tool.

The one-lump parameter solution is exact for the initial and steady-state values for the rock to fluid temperature differences because it was derived as an interpolation formula between the initial and the steady-state values of the exact analytical solution. Its validityforinter-mediate values was investigated by comparing the individual rock energy extracted fractions based on the one-lump parameter to the rock energy extracted fractions based on the exact solutions. Figure 3-8 shows this comparison for constant fluid cooling rate conditions.

It is observed that the one-lump parameter solution can be used to predict the energy extracted fraction provided that the following "rules of thumb" are kept in mind:

(a) It can be used for the complete range of Fourier numbers for Biot numbers less than 2 with an accuracy better than 10 percent. This is explained by the fact that a low Biot number means alowinternal thermal resistance, which is consistent with lumping the rock mass in a single point at uniform temperature.

(b) The one-lump parameter solution can be used for the complete range of Biot numbers if the Fourier number is greater than 0.3 with an accuracy better than 10 percent.

(c) An approximation for the time dependence of the conduction path length for Biot numbers greater than 10 and for Fourier numbers greater than *0.04* is

$$\ell^* = \frac{\ell_{cond}}{R_e} \simeq \frac{1}{3}\left[1 - e^{-8N_{Fo}}\right] \qquad (3.24)$$

The results of using this expression for the conduction path length in Eqs. 3.11 and 3.16 are given in Figure *3-8.*

(d) However, for infinite Biot numbers and for Fourier numbers greater than *0.04* it is simpler to use the exact solution which with only one term has the same accuracy as Eq. 3.24:

$$\Delta T_m^* = \frac{1}{15} - \frac{6}{\pi^4} e^{-\pi^2 N_{Fo}} \qquad (3.25)$$

The predicted energy extracted fraction obtained by using this expression are also given in Figure *3-8* for comparison.

3.4 Fluid Temperature Drop Fraction

To measure the degree to which the fluid temperature approaches a given temperature T_2, the fluid temperature drop fraction is defined as

$$F_C \triangleq \frac{T_1 - T_f(X,t)}{T_1 - T_2} \qquad (3.26)$$

The temperature T_2 can be *any* reference temperature, such as (1) Local fluid temperature at the end of the production period (then $F_c = 1$). *(2)* Temperature of the fluid being injected in the cold water sweep. (3) Temperature reference for resource base evaluation T_o. (4) Saturation temperature at the end of the production period..

3.5 Local Energy Extracted Fraction for a Collection of Rocks

3.5.1 Description of the Model

The analysis in Sections 3.1 through *3.4* concentrated on a **single** rock of irregular shape surrounded by a fluid that is being cooled at an

arbitrary rate. Let us now consider a fractured reservoir as indicated schematically in Figure 3-9. The rock formation consists of rock segments of different sizes and shapes. Also, let the sizes of this "collection" of rocks be distributed according to a given probability function $f(\bar{X},\sigma_{\bar{X}})$ in which the mean value $\bar{X}$ can be either the rock volume or the equivalent volume sphere radius, i.e.,

$$p(R_s) = f(\bar{R}_s,\sigma_{\bar{R}_s}) \tag{3.27a}$$

or

$$p(V) = f(\bar{v},\sigma_{\bar{v}}) \tag{3.27b}$$

where the standard deviation $\sigma_{\bar{R}_s}$ and $\sigma_{\bar{v}}$ measures directly the dispersions of R_s and v from their arithmetic mean values $\bar{R}s$ and $\bar{v}$.

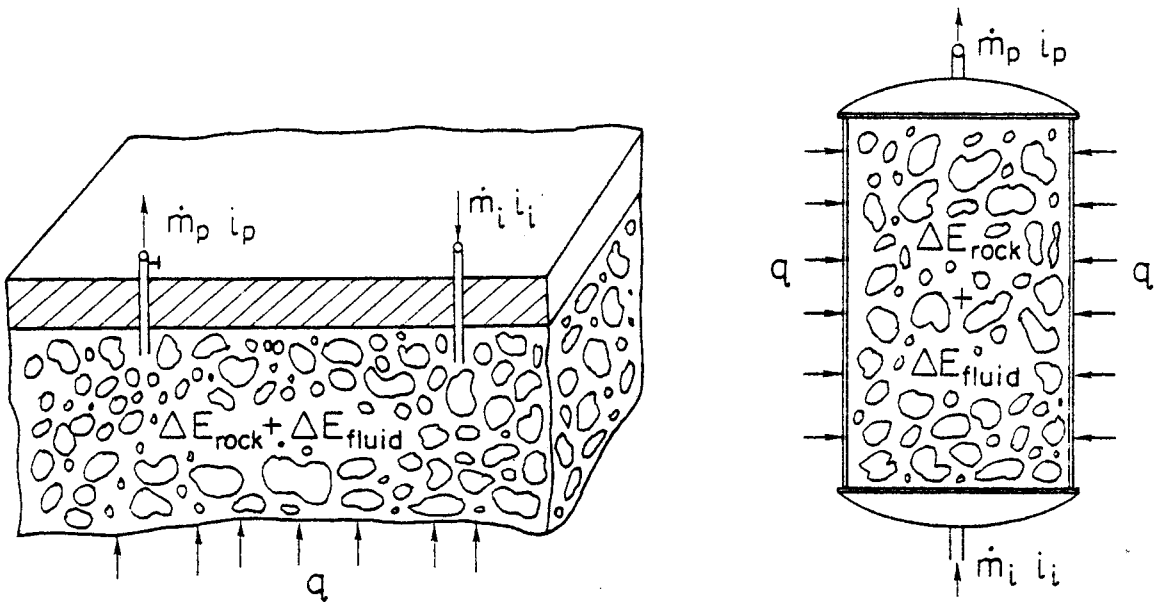

FIGURE 3-9. Physical and laboratory models of a fractured geothermal reservoir

The local energy extracted fraction for a collection of rocks measures the energy that has been extracted from a collection of rocks at a given location of the reservoir, as compared to the energy that would be extracted if all the rocks in the local sample were cooled uniformly to the local fluid temperature. From the definition of the individual rock energy extracted fraction and from conservation of energy, the local energy extracted fraction for a collection of rocks is defined as

$$F_{E,c} \triangleq \frac{Q_{actual}}{Q_{max}} = \frac{\sum_{i=1}^{N} F_{E,i}\, \rho_r c_r\, v_i (T_1 - T_f(X,t))}{(T_1 - T_f(X,t)) \sum_{i=1}^{N} \rho_r c_r\, v_i} \qquad (3.28)$$

where the terms of the summation in the numerator are the actual energy extracted from each individual rock as expressed by Eq. 3.18. The summation is performed from $i = 1$ to N where N is the total number of rocks in the sample.

The following idealizations were made in defining the local energy extracted fraction for a collection of rocks:

(a) The volume of the reservoir being considered is very large as compared to the space occupied by a representative collection of rocks.

(b) The heat transfer by conduction at contact points between adjacent rocks is neglected. The reason for this is that the temperature difference of rock surfaces will be negligible at contact points and consequently the heat transfer is negligible.

(c) At the end of the extraction period being considered, the fluid temperature $T_f(X,t)$ is uniform through the space occupied by the representative sample of the collection being analyzed.

(d) The idealizations made in modeling the temperature transient for individual rocks, as listed in Section 3.1.1, are also made here.

Simplifying Eq. 3.28 yields

$$F_{E,c} = \sum_{i=1}^{N} F_{E,i} \cdot \chi_i \tag{3.29a}$$

where the volumetric fraction χ_i of the rock i is defined as

$$\chi_i \triangleq \frac{v_i}{\sum_{i=1}^{N} v_i} \tag{3.29b}$$

The local energy extracted fraction for a collection of rocks is seen to be the summation of the energy extracted fractions of the individual rocks weighted by their volumetric fraction. An expression for the volumetric fraction as a function of the frequency distribution of volumes in a collection of rocks is derived in Appendix B.5. If N_L is the number of groups of different rock volumes, the local energy extracted fraction for a collection of rocks can be expressed as:

$$F_{E,c} = \sum_{j=1}^{N_L} p(v_j) \cdot \frac{v_j}{\bar{v}} \cdot F_{E,i} \tag{3.30}$$

where j indicates the volume group j. From this summation it can be seen that if the probability of having a rock size is very high, but its volume is small with respect to the mean volume, its effect on the total energy extracted fraction is small.

3.5.2 Bulk-Effective Radius and Time Constant for a Collection of Rocks

In Sections 3.1.2 and 3.1.3 it was observed that the surface-area-to-volume ratio is the main geometrical parameter that governs the heat transfer from a rock segment. Therefore, a collection of rocks of

irregular shape can be modeled thermally as a group of spherical rocks of equal size, provided that the total surface area to volume ratio of these spheres is equal to that of the actual rock collection.

The surface-area-to-volume ratio of a collection of rocks is given by:

$$(A/V)_c = \frac{\sum_{i=1}^{N} (4\pi R_{s,i}^2)}{\sum_{i=1}^{N} \frac{4}{3}\pi R_{s,i}^3} = 3 \times \frac{\sum_{i=1}^{N} \frac{R_{s,i}^2}{\psi_{K,i}}}{\sum_{i=1}^{N} R_{s,i}^3} \qquad (3.31)$$

This equation can be rearranged after introducing the probability function $p(R_{s,i})$ similar to what was done in Section 3.5.1 and Appendix B.3 as:

$$(A/V)_c = \frac{3 \times \sum_{j=1}^{N_L} p(R_{s,j}) \cdot \frac{R_{s,j}^2}{\psi_{K,j}}}{\sum_{j=1}^{N_L} p(R_{s,j}) \cdot R_{s,j}^3} \qquad (3.32)$$

For a sphere the surface-area-to-volume ratio is given by

$$(A/V) = \frac{4\pi R^2}{\frac{4}{3}\pi R^3} = \frac{3}{R} \qquad (3.33)$$

Therefore, the "bulk effective radius" for a collection of rocks can be defined as the radius of a sphere having the same surface-area-to-volume ratio as the collection,

$$R_{e,c} \triangleq \frac{3}{(A/V)_c} \qquad (3.34)$$

Equivalently, the bulk time constant for the collection is obtained

by replacing $R_{e,c}$ in Eq. 3.10b or 3.16c

$$\tau_e = \frac{R_{e,c}^2}{3\alpha}\left(\frac{1}{5} + 1/N_{Bi}\right) \tag{3.35}$$

The bulk time constant is the time necessary to achieve 63.2 percent of the quasi steady-state rock mean to fluid temperature difference. Thus, Eq. 3.35 can be replaced by Eq. 3.16c and substituted into Eq. 3.11 or 3.16a to calculated the overall mean rock to fluid temperature difference of the collection; the mean rock to fluid temperature difference can be substituted into Eq. 3.18 to obtain the local energy extracted fraction for a collection of rocks. The thermal transient computational procedure is largely simplified by using the bulk-effective radius because the overall mean temperature of the collection of rocks and the energy extracted fraction are those of a single rock of radius $R_{e,c}$

The validity of the procedure described above is investigated in Section 3.5.3 by comparing it to the rigorous procedure developed in Section 3.5.1 to calculate the local energy extracted fraction for a collection of rocks.

3.5.3 Validity of the Bulk-Effective Radius as a Single Parameter to Characterize a Collection of Rocks

The bulk-effective radius for a collection of irregularly shaped rocks was defined in Section 3.5.2 as the radius of a collection of spherical rocks that has an equivalent thermal behavior. It was derived by finding the radius of a spherical rock having the same surface-to-volume ratio as a collection of rocks with given size and shape distributions. This greatly simplifies the computations because Eq. 3.18 for a

single spherical rock can be used instead of Eq. 3.29 to predict the local energy extracted fraction for a collection of rocks.

The validity of the bulk-effective radius was evaluated by comparing the local energy extracted predicted from Eq. 3.30 to the one using Eq. 3.18. Equation 3.35 was used for the bulk-effective time constant needed to calculate the mean rock temperature transient in Eq. 3.18. In Section 2.2.5 it was shown that sphericity ϕ_K does not depend significantly on the rock size. It was also shown that the sphericity is distributed according to a normal distribution, and, as such, it can be appropriately defined by its mean value and standard deviation. In other words, the probability of finding a rock with a given sphericity is the same for any particular rock size (volume), and therefore, if a large number of rocks with the same size were taken from a given collection, a complete range of sphericity values would be found with a frequency given by a normal distribution. Thus, in this and the following sections, the rock collections will be considered as completely characterized by its size distribution (volume or equivalent sphere radius) and the mean value of the sphericity.

Several different size distributions are possible for a collection of rocks depending on which fracturing technique is used to produce it. Three hypothetical frequency distributions were assumed in this study, namely volume v normally distributed, and equivalent sphere radius R_s both normally and exponentially distributed. The normal distribution is given by

$$f(z) = \frac{1}{\sigma_{\bar{z}}\sqrt{2\pi}} e^{-\frac{1}{2}\left(\frac{z-\bar{z}}{\sigma_{\bar{z}}}\right)^2} \qquad (3.36)$$

where z can be either R_s or v. The normal distribution was selected because it is characterized by a mean value (arithmetic mean) and a standard deviation $\sigma_{\bar{z}}$. The standard deviation measures the dispersion of z from the mean value $\bar{z}$.

The exponential distribution is given by

$$f(z) = \frac{1}{\gamma} e^{-(1/\gamma)z} \qquad (3.37)$$

where $\bar{z} = \gamma$ and $\sigma_{\bar{z}} = y$. So it is characterized by a single value γ which is both the mean and the standard deviation, i.e., a larger dispersion of sizes will automatically mean a higher mean value and vice versa.

The validity of the bulk-effective radius was evaluated for two collections of rocks with different shapes. Both collections were normally distributed in R_s, but one consisted of spherical rocks (sphericity = 1.0) and the other of slabs with an average sphericity of 0.7. The mean equivalent sphere radius was 100 ft and the standard deviation was 30.7 for both collections.* From Eqs.3.32 and 3.34 the bulk-effective radius for the spheres is 116.4 ft and 81.48 for the slabs.

The energy extracted fraction was evaluated for both collections using the two computational methods and assuming constant fluid cooling rate (see Appendix C.2 for a sample calculation). Figure3-10 shows the results. The maximum difference between predicted results is less than 3 percent for the two rock collections. The difference tended to be

*A value of 30.7 for the standard deviation was selected to simulate maximum dispersion. (A dispersion of approximately $\pm 3 \times \sigma_{R_s}$ covers about 99.9 percent of the population.)

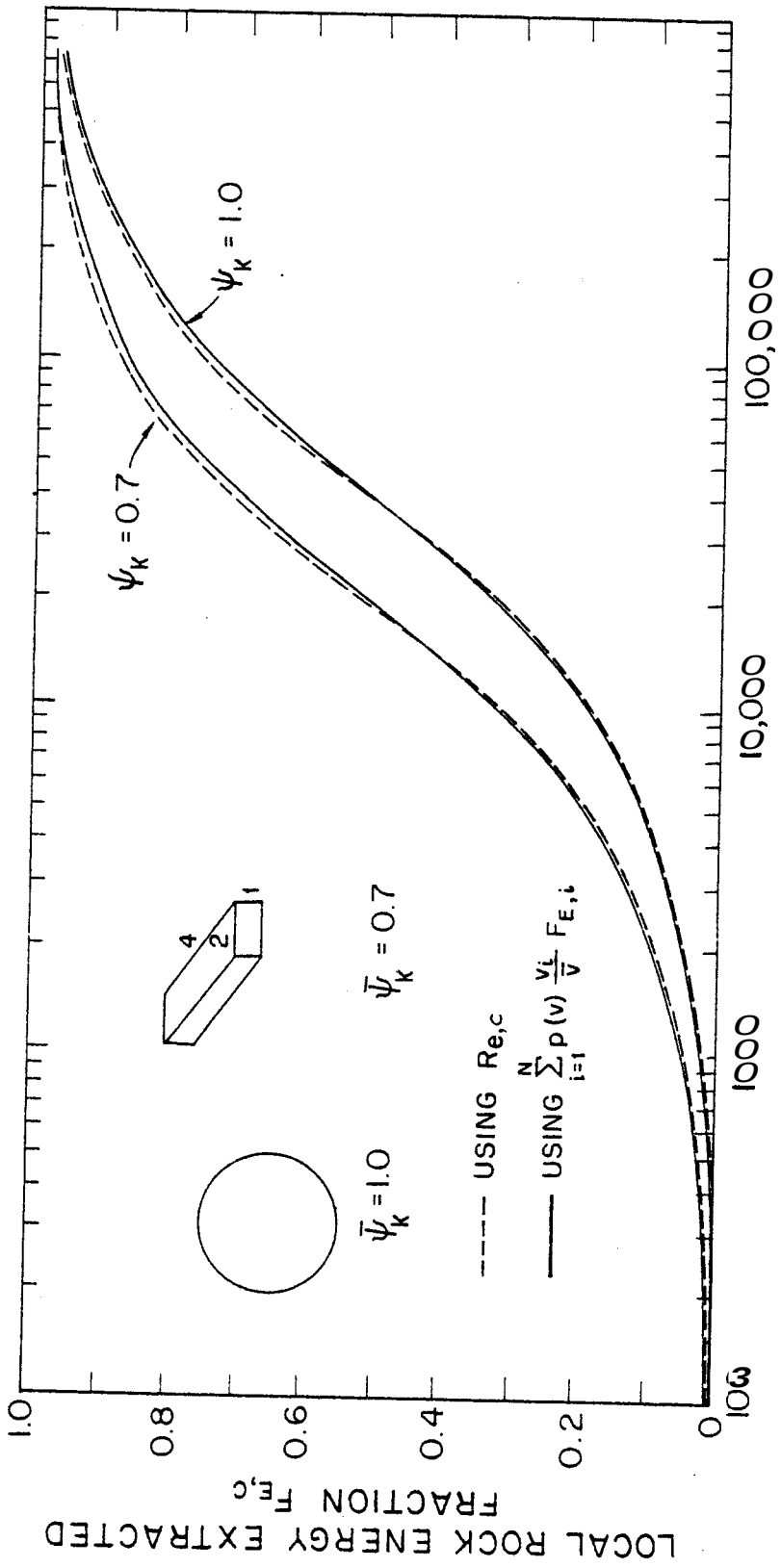

FIGURE 3-10 Validity of the b-lk-effective radius $R_{e,c}$

proportional to the number of groups of equal size rocks that the normal distribution was divided into in the numerical computation. In this particular example, 17 groups were used. Satisfactory results can be obtained with fewer groups. The effect of the number of groups was illustrated by evaluating the bulk-effective radius for two distributions both with $\bar{\psi}_K = 1.0$, Table 3-1 shows the results for the exponential and normal disrributions. If an infinite number of groups (infinitesimal size intervals) is taken, the bulk-effective radius of an exponential distribution is given by (see Appendix C.3 for derivation):

$$R_{e,c} = 3 \cdot \bar{R}_s \cdot \bar{\psi}_K \tag{3.38}$$

and for the normal distribution:

$$R_{e,c} = \bar{R}_s \cdot \bar{\psi}_K \frac{1 + \frac{3}{2}\sqrt{2\pi}\left(\frac{\sigma_{\bar{R}_s}}{\bar{R}_s}\right)^2}{1 + \frac{\sqrt{2\pi}}{2}\left(\frac{\sigma_{\bar{R}_s}}{\bar{R}_s}\right)^2} \tag{3.39}$$

Note from Table 3-1 that the exponential distribution is more sensitive to the marginal increase in number of groups when the number of groups is small, but it is not as sensitive as the normal distribution when the number of groups is large. Note also that the effect of the size dispersion is clearly seen in Eq. 3.39. A higher dispersion increases the numerator faster than the denominator, resulting in a larger bulk-effective radius and consequently lower energy extracted fractions. This subject will be considered in more detail in Section 4.

TABLE 3–1

Effect of the Number of Groups on the Calculated Bulk–Effective Radius

Normal, $\bar{R}_s$ = 100 and $\sigma_{\bar{R}_s}$ = 30.7		Exponential, $\bar{R}_s$ = 100	
Number of Groups	$R_{e,c}$ (ft)	Number of Groups	$R_{e,c}$ (ft)
5	112.35	6	247.4
17	116.4	12	283.6
∞	131.7	∞	300.0

3.5.4 Effect of Microfratures on the Energy Extracted Fraction

The main objectives of cracking large rocks are to convert them to smaller ones and to increase the formation permeability to enhance the energy extraction process. In addition, high–energy fracturing techniques might also produce microfractures in individual rocks which might be filled with geothermal fluid, and which might provide additional flow paths. The effect on the heat transfer process will depend on the thermal properties of the fluid as compared to those of the rock, and on the amount of fluid flow through the microcracks.

A simple one–dimensional model was developed to analyze the effect of the microfractures on the overall thermal behavior of a rock. The effect on the heat transfer will depend on the direction of the microfractures relative to the direction of the temperature gradient. If the cracks are perpendicular to the temperature gradient and there is no flow of fluid through them, the effective thermal conductivity is given by (see Appendix B.6 for details):

$$k_e = k_r \left\{ \frac{1}{1 + \eta t_c \left(\frac{k_r}{k_f} - 1 \right)} \right\} \tag{3.40}$$

where k_e is the effective thermal conductivity; η is the number of cracks per unit length; t_c is the crack width; and k_r and k_f are the thermal conductivities of the rock and fluid, respectively. If the cracks are parallel to the direction of the temperature gradient, the thermal conductivity is given by:

$$k_e = k_r\left\{1 - \eta t_c\left|1 - \frac{k_f}{k_r}\right|\right\} \qquad (3.41)$$

Similar expressions are derived in Appendix B.6 for the rock effective specific heat, effective density, and effective thermal diffusivity for the two cases.

Table 3-2 shows the correction factors $(Xe/Xr)^*$ for the rock properties when the rock is granite, the fluid is water, and there is no flow through the microcracks. As expected, the correction factors for the thermal conductivity and density are less than unity, since the corresponding water properties are less than for the granite. However, water has better volumetric heat capacity characteristics than the granite, resulting in a correction factor greater than unity for the specific heat. The combined effect of thermal conductivity, specific heat and density yields a correction factor less than unity for the thermal diffusivity. Consequently the conduction heat transfer from the rock will be reduced and so will the energy extracted fraction for a microfractured rock relative to a solid rock, provided that the fluid is stagnant in the microfractures.

---

* The symbol Xe stands for effective properties of the microcracked rocks, and Xr stands for properties of the solid rock.

TABLE 3-2

Correction Factors for Granite Thermal Properties When the Microfractures Are Filled with Stagnant Water

Property	Parallel (Xe/Xr)			Perpendicular (Xe/Xr)		
	Values of ηt_c			Values of ηt_c		
	0.005	0.01	0.05	0.005	0.01	0.05
Thermal Conductivity (Eqs. B.28 and B.21)	0.998	0.993	0.963	0.985	0.971	0.887
Specific Heat (Eq. B.23)	1.006	1.011	1.058	1.006	1.011	1.058
Density (Eq. B.22)	0.997	0.994	0.969	0.997	0.994	0.969
Thermal Diffusivity (Eqs. B.29 and B.24)	0.989	0.988	0.963	0.983	0.986	0.968
$k_r/k_f = 5$ $\frac{\rho_r c_f}{\rho_r c_r} = 1.5$ $\frac{\rho_f}{\rho_r} = 0.38$	q → 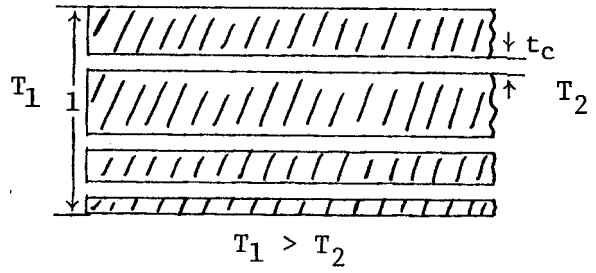 $T_1 > T_2$ η = # cracks/unit length (3 in this fig.)			q → 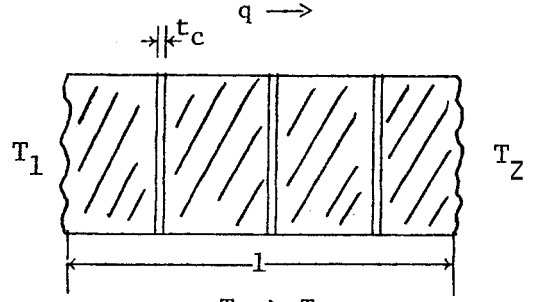 $T_1 > T_2$ η = # cracks/unit length (3 in this fig.)		

The parallel crack model was modified to include fluid flow through the cracks. For simplicity, the fluid was assumed to be in thermal equilibrium with the rock surface ($N_{Bi} = \infty$). The correction factor for the thermal conductivity when the fluid flows at a velocity u through the cracks and in the same direction as the heat transfer is given by (see Appendix B.6 for details):

$$\frac{k_e}{k_r} = 1 - \eta t_c \left(1 - \frac{k_f}{k_r} - \frac{\rho_f \, u \, c_f}{k_r} \right) \tag{3.42}$$

Figure 3-11 shows the effect of liquid water velocity through the microcracks in granite rock on the effective thermal conductivity as given by Eq. *3.42*. The correction factor (k_e/k_r) exceeds unity for velocities higher than approximately 0.002 ft/hr and exceeds unity significantly for larger velocities and high values of ηt_c. The parameter ηt_c can be thought of as a microfracture porosity and its values are expected to be no larger than about 0.01. A significant pressure gradient is required to drive the water through the microcracks and in the same direction as the heat transfer. Poiseulles' law was applied to estimate the required pressure gradient as indicated in Appendix B.6. From Figure 3-11 the velocity required for a 10-percent increase in thermal conductivity is approximately 0.3 ft/hr. Results show that a pressure gradient of approximately 17 psi/ft is required to achieve a velocity of 0.3 ft/hr assuming a crack width of 0.01 cm and one crack per cm ($\eta t_c = 0.01$). These magnitudes of pressure gradients might not be difficult to achieve in the vicinity of the wellbore. However, for highly fractured reservoirs like the one being considered, thesemagnitudes of pressure gradients will not

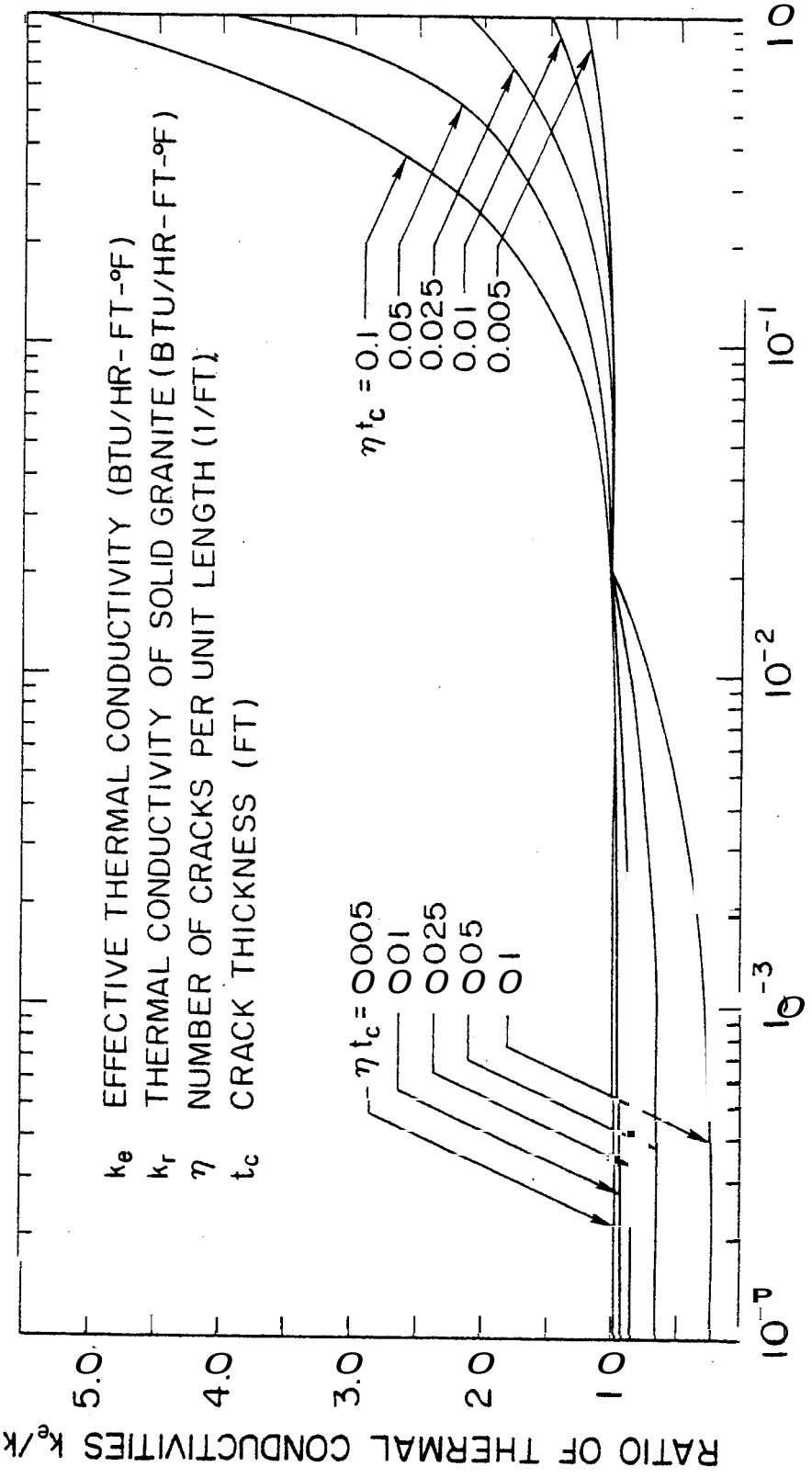

FIGURE 3-11 Effect of microfractures on thermal conductivity of granite for different water velocities

be found away from the wellbore. This means that the effect of the microfractures on the rock energy extracted fraction can be neglected compared to the rock cooling effect produced by flow in the much larger macrofractures.

3.6 Energy Balance of a Fractured Geothermal Reservoir

3.6.1 Reservoir Rock Energy Extracted Fraction

The reservoir rock energy extracted fraction is a reservoir parameter, and relates the thermal energy that has been extracted from the rocks in the reservoir to the thermal energy that would be extracted if the total rock mass was cooled uniformly to a mean fluid temperature. It is given by

$$\bar{F}_{E,c} \triangleq \frac{\text{thermal energy extracted from rock}}{V_{Re}(1-\phi)\rho_r c_r (T_1 - \bar{T}_f(t))} \qquad (3.43)$$

where,

$$\bar{T}_f(t) \triangleq \frac{1}{V_{Re}} \int_V T_f(X,t)\, dV_{Re} \qquad (3.44)$$

The reservoir rock energy extracted fraction measures the heat transfer limitations on the energy recovery from geothermal reservoirs. As $\bar{F}_{E,c}$ approaches unity, the heat transfer limitations decrease and the rock reaches thermal equilibrium with the surrounding fluid.

3.6.2 Reservoir Mean Fluid Temperature Drop Fraction

To measure the fluid flow and thermodynamic limitations on the energy recovery from geothermal reservoirs, the reservoir mean fluid temperature drop fraction was defined as:

$$\bar{F}_c \triangleq \frac{T_1 - \bar{T}_f(t)}{T_1 - T_2} \qquad (3.45)$$

It measures the degree to which the mean reservoir fluid temperature approaches a given temperature T_2. As described in Section *3.4*, the temperature T_2 can be any reference temperature. The degree to which the reservoir mean fluid temperature drop fraction approaches unity is limited by: (a) the formation permeability needed for adequate fluid circulation, (b) the creation of "hot spots" produced by fingering of the cold injected fluid to the production wells (in the cold water sweep process), (c) the formation of a superheated steam zone (in the in-place boiling process), (d) the minimum temperature level requirement on the production temperature for correct operation of the energy conversion system, such as an electric power plant or a space heating facility. Items (a) and (b) are essentially fluid flow limitations, whereas (c) and (d) are thermodynamic limitations.

3.6.3 Reservoir Energy Fraction Produced

The reservoir energy fraction produced relates the amount of energy that has been produced to the energy that would be produced if both fluid and rock were cooled uniformly to the reference temperature T_2. It is defined as

$$F_p \triangleq \frac{\text{energy produced at time } t}{V_{Re}\{\phi\ \rho_f c_f + c_r \rho_r (1 - \phi)\}\ (T_1 - T_2)} \qquad (3.46)$$

where the denominator is the thermal energy (rock and liquid) resource base referenced to a temperature datum equal to T_2.

3.6.4 Energy Balance

Let us consider the reservoir shown in Figure 3-9. Hot water or steam is produced at some rate $\dot{m}_p(t)$ with an enthalpy $i_p(t)$. Fluid is also injected at a rate $\dot{m}_i(t)$ with an enthalpy $i_i(t)$. If there is

no heat transfer from the bottom or the surrounding of the reservoir, conservation of energy yields the following expression in non-dimensional form (see Appendix *B.7* for details):

$$F_p = \frac{\overline{F}_{E,c} \cdot \overline{F}_c}{(1+\gamma)} + \frac{\overline{F}_c \cdot \gamma}{(1+\gamma)} + \frac{E_i \cdot \gamma}{(1+\gamma)(T_1 - T_2)V_{Re}} \qquad (3.47)$$

where γ is the "storage ratio" defined as the ratio of the energy stored in the fluid to the energy stored in the rock, i.e.,

$$\gamma \triangleq \frac{\rho_f c_f \phi}{\rho_r c_r (1-\phi)} = \frac{\phi}{c^*(1-\phi)} \qquad (3.48)$$

When the porosity ϕ is small, the storage ratio approaches zero. If besides, the energy injected is zero, Eq. *3.43* becomes

$$F_p \approx \overline{F}_{E,c} \cdot \overline{F}_c \qquad (3.49)$$

From Eq. *3.45,* it is seen that the fraction of energy produced can be small when the heat transfer limitations are high ($\overline{F}_{E,c}$ small), or when the reduction of the mean fluid temperature of the reservoir is limited ($\overline{F}_C$ small).

3.7 One-Dimensional Model of a Cold-Water Sweep Process

Analytical models for the rock temperature transient and rock energy extracted fraction were developed in Sections **3.3** to 3.5. It was assumed that the production and recharge characteristics of the reservoir were such that a given instant a variable fluid cooling rate resulted. In this section, the production and recharge characteristics of the reservoir are fixed, and a model is developed to calculate the fluid and rock matrix temperature distribution throughout the reservoir as a function of

time. This model is applicable to compressed liquid systems, where cold water is injected at one location of the reservoir, and hot water is produced at some distance from the injection point. This process is often referred to as the cold-water sweep process.

The reservoir model considered (shown in Figure B-2) is initially at a temperature T_1. Cold water is injected at a temperature T_{in} through a line of wells A, and produced at the same rate in a line of wells B. The distance between wells is L, and the cross section of the reservoir is S. In this arrangement the flow isone-dimensional. The size distribution of the rocks is assumed to be the same at different locations of the reservoir volume. Then, the collection of rocks can be completely characterized by the bulk-effective radius defined by Eq. *3.34*, and the rock mass will behave at each location of the reservoir as a collection of spherical rocks with a time constant given by Eq. 3.35. Heat transfer per unit length (Btu/hr-ft) q' from the bottom of the reservoir is assumed to be constant. Segregation of the cold fluid to the bottom of the reservoir is neglected.

It is important to point out that this analysis takes into account the temperature non-uniformities inside the rock segments produced by the long conduction path lengths and low rock thermal conductivity. Therefore, it is valid for any value of the Biot number. Previous analyses done by Schuman (1929) and Löf (1948) for air flowing through a rock matrix, have neglected the thermal resistance inside the rock itself, which makes them applicable only for low Biot numbers.

The governing equation for the fluid temperature as a function of time at different locations of the reservoir is derived in Appendix B.9.

Solution of this equation (B.59a) was done by the Laplace transform method. The inversion of the non-dimensional fluid temperature from the Laplace to the real space was performed numerically. It was found to be a function of

$$T_f^*(X^*,t^*) = f(N_{tu}, \gamma, q^*) \tag{3.50}$$

The non-dimensional parameters are defined and discussed separately to provide understanding of their physical meaning. These non-dimensional parameters are powerful analytical tools and useful parameters to extrapolate the results obtained from the laboratory model (see Section 4.3) to actual geothermal reservoir scales.

The non-dimensional'distance from the injection point;

$$X^* = \frac{X}{L} \tag{3.51}$$

expresses the distance as a fraction of the reservoir length L. Similarly, the non-dimensional time,

$$t^* = \frac{t}{t_{re}} \tag{3.52}$$

measures the time as a number of residence times (t_{re}). The meaning of the t_{re} is the time that an element of injected fluid takes to get to the production wells, and is given by

$$t_{re} = \frac{L}{w} = \frac{L\phi}{v_f} = \frac{V_{Re}\ \phi\ \rho_f}{\rho_f\ v_f S} = \frac{V_{Re}\ \phi\ \rho_f}{\dot{m}} \tag{3.53}$$

where w is the velocity at which the injected fluid front moves. It is equal to the Darcy velocity v_f divided by the porosity ϕ. Note that the Darcy velocity is defined so that $\dot{m} = \rho_f v_f S$. The non-dimensional

fluid temperature,

$$T_f^* = \frac{T_f(X,t) - T_{in}}{T_1 - T_{in}} \tag{3.54}$$

is equal to one, when the fluid is at the initial temperature T_1, and approaches zero when the fluid reaches the injection temperature.

The number of transfer units for the reservoir is

$$N_{tu} = \frac{t_{re}}{\tau_e} = \frac{t_{re}}{C_e/U_o A_e} = \frac{U_o A_e}{C_e} \cdot t_{re} \tag{3.55}$$

where C_e and A_e are the effective rock thermal capacitance (given by Eq.3.9) and surface area, respectively, and where τ_e is the effective rock time constant given by Eqs. 3.10a and 3.35. The number of transfer units is a parameter very similar to the N_{tu} used to size heat exchangers (Kays and London, 1969). The smaller the bulk effective radius, the larger the surface area for convection of the energy stored in the rock as measured by C_e, and the higher the number of transfer units. Also, the larger the residence time t_{re} with respect to the time constant τ_e, the higher the N_{tu}'s will be, and the more time the rock will have to adjust to fluid temperature changes. Therefore, large number of transfer units will result in high rock energy extracted fractions.

The storage ratio y defined in Eq. 3.48 represents the energy stored in the fluid, as compared to the energy stored in the rock volume.' The external heat transfer parameter,

$$q^* = \frac{q' L}{\dot{m} c_f (T_1 - T_{in})} \tag{3.56}$$

measures the heat transfer from the bottom or the surroundings of the

reservoir as a fraction of the energy produced (with T_{in} as datum), if the temperature of the produced water was T_1.

With the fluid temperature distribution as a function of time, the temperature transient of the "effective" rock (or any rock size in the collection) can be calculated using Eqs. *3.16* or *B.46* for any location of the reservoir. Also, if the reference temperature for energy fraction calculations is selected to be the injection temperature T_{in}, the reservoir mean fluid temperature drop fraction is given by (see Appendix B.9 for details):

$$\bar{F}_c(t^*) = 1 - \int_0^1 T_f(X^*, t^*)\, dX^* \qquad (3.57)$$

Similarly, the reservoir energy fraction produced is given by:

$$F_p = \frac{\int_0^{t^*} T_f^*(1,t^*)\, dt^*}{1 + 1/\gamma} \qquad (3.58)$$

From Eq. *3.43* the reservoir rock energy extracted fraction is

$$\bar{F}_{E,c} = \frac{F_p}{\bar{F}_c} + \gamma \left| \frac{F_p}{\bar{F}_c} - 1 \right| \qquad (3.59)$$

In Section *4.4* this model is verified experimentally, and an analysis of the effect of the non-dimensional parameters defined above on the energy extraction process is also performed.

4. RESULTS

4.1 Description of Experiments

Three verification experiments were performed in the reservoir model to verify the analytical models developed in this study. The corresponding measured fluid and rock temperatures were compared to the predicted results. Each experiment is described in the following paragraphs. The important parameters of the three experiments are given in Table *4-1*.

4.1.1 In-Place Boiling Experiment

The first experiment was of the in-place boiling type. Steam was produced from the top of the reservoir and there was no recharge. The purpose of this experiment was to verify the rock temperature transient model in both liquid saturated and superheat steam environments. Figure *4-1* shows the temperature distributions throughout the reservoir for different times. The dashes indicate the position of the liquid level. It can be seen that after some time the liquid level has dropped in the rock matrix and the initially saturated steam above the liquid/steam interface has become superheated. This is due to the heat transfer from the rocks. Details on the liquid level and pressure depletion behavior of this type of experiment were reported by Hunsbedt, Kruger, and London (1975b).

4.1.2 Cold-Water Sweep Experiment

A cold-water sweep experiment was performed to verify the rock temperature transient model under high and drastically varying fluid cooling rates. It is also used to verify the one-dimensional model derived in Section 3.7 for the fluid temperature distribution in the reservoir as a function of time which develops when cold water in injected. Water at

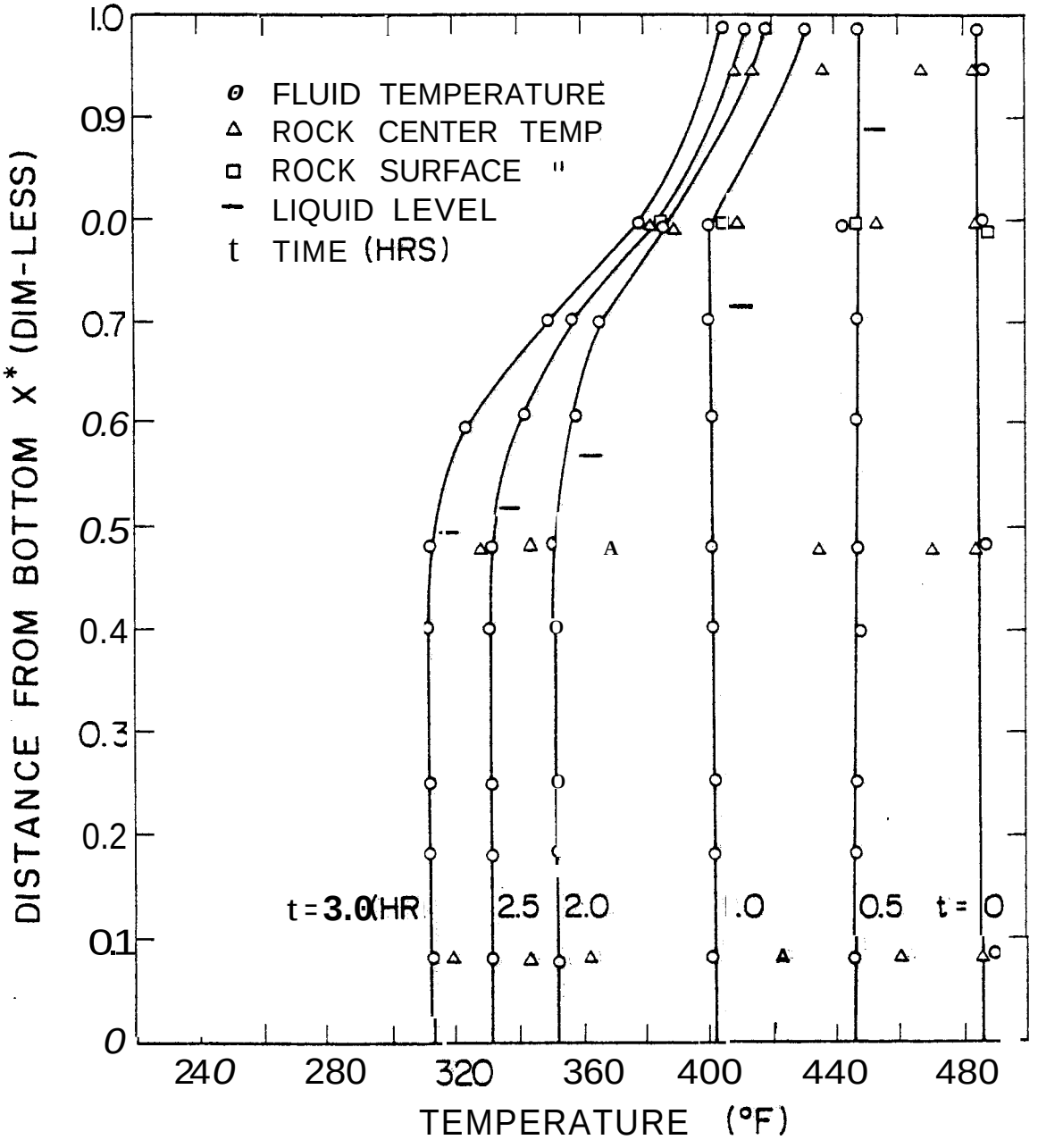

FIGURE 4-1. Measured temperature distribution for the in-place boiling experiment

TABLE 4–1

Main Parameters of Experiments

Parameter	In-Place Boiling (No Injection)	Cold-Water Sweep	In-Place Boiling (Hot-Water Injection)
Initial Temperature (°F)	485	461	443
Initial Pressure (psia)	625	531	487
Final Pressure (psia)	82	520	130
Final Mean Fluid Temperature (°F)	341	182	349
Duration of Experiment (hr)	3.0	7.0	2.75
Mean Fluid Cooling Rate (°F/hr)	48	40	34
Mass of Fluid Produced (lbm)	180	900.0	187
Mean Fluid Production Rate (lbm/hr)	60	133.3	68
Mass of Fluid Injected (lbm)	0.0	892	212
Mean Fluid Injection Rate (lbm/hr)	0.0	127.4	77
External Heat Transfer Parameter (Btu)	31,0 4	115,111	17,915
Drainage Porosity (dimensionless)	0.422	0.422	0.422
Mass of Rock in The Vessel (lbm)	1556	1556	1556
Temperature of Injected Fluid (°F)	-	70	$T_{sat}(P)$

approximately 70°F was injected from the bottom of the reservoir and fluid was produced from the top at approximately the same rate. The pressure in the reservoir was maintained higher than the saturation pressure. Figure 4–2 shows the water and rock temperature distributions throughout the reservoir as a function of time. It can be observed that the temperature gradients throughout the reservoir space as well as the rock/fluid temperature differences are much higher in the cold-water sweep process than in the in-place boiling process.

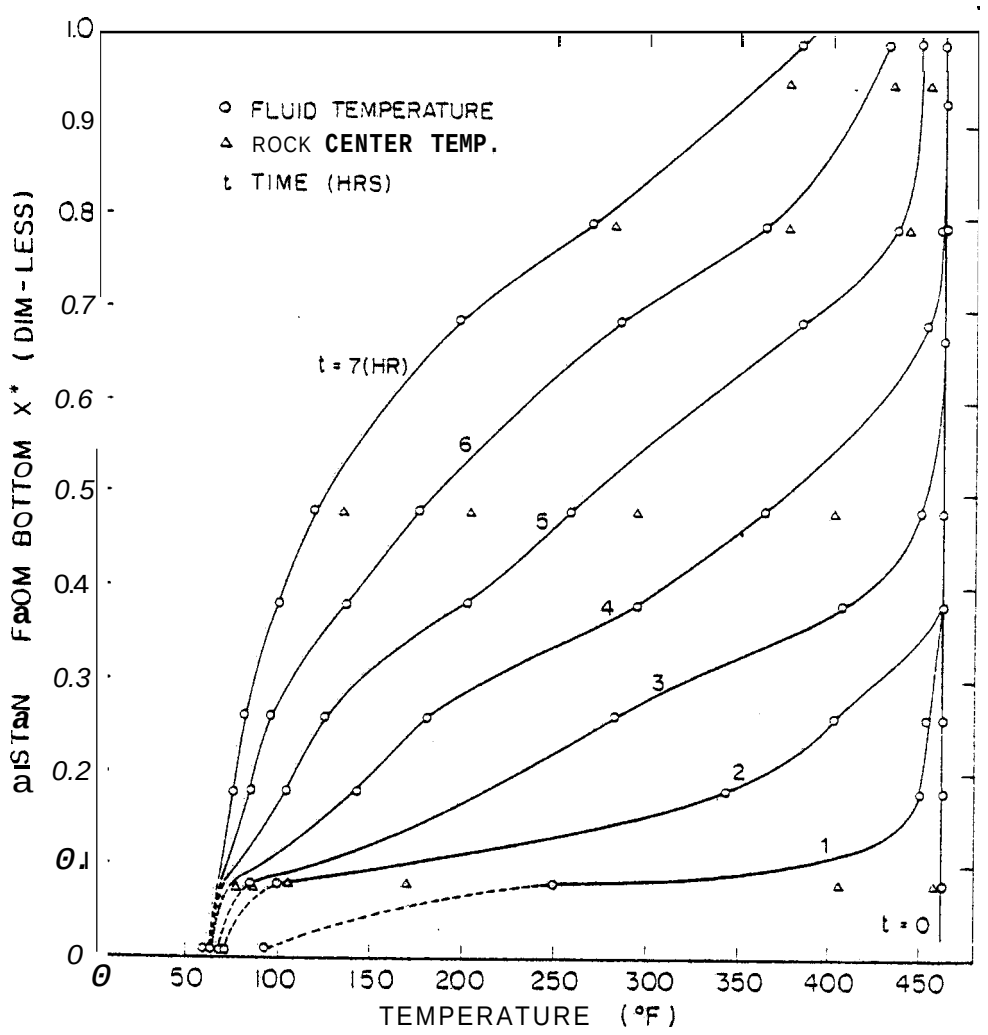

FIGURE *4-2.* **Measured temperature distribution for the cold-water sweep experiment**

4.1.3 In-Place Boiling Experiment with Hot-Water Injection

In the third experiment water at the initial saturation temperature was injected at the bottom of the model to maintain the liquid level near the top and a uniform fluid temperature distribution throughout the reservoir, as illustrated in Figure 4-3. The purpose of this experiment was to verify the model for the reservoir rock energy extracted fraction derived in Section 3.6. The reservoir rock energy extracted fraction can be readily evaluated, because the fluid temperature is uniform throughout the reservoir space which largely simplifies the computational procedure. In addition, it does not require the assumption of equal rock size distribution at different locations in the reservoir.

4.2 Experimental Rock Temperature Transient

The temperature transient data were compared to the transients predicted by the model developed in Section 3.1. An average convective heat transfer coefficient of 300 Btu/hr-ft^2-°F reported by Kuo, Kruger, and Brigham (1976) was used for the predictions in liquid environment. The one-lump parameter solution and superposition technique developed in Section 3.1.4 (Eq. 3.16) were used to model several rock temperature transients under different fluid cooling rates. The fluid temperature or fluid cooling rate was treated as the independent variable; therefore, the fluid temperature was first measured as a function of time, and these data were provided as input to predict the rock center temperature.

Figures 4-4 through 4-7 show the predicted and measured rock center and fluid temperatures for four different fluid cooldown histories. The data in Figures 4-4 and 4-5 are for Rock 81. In the former the relatively uniform and low fluid cooling rate of the in-place boiling test results in

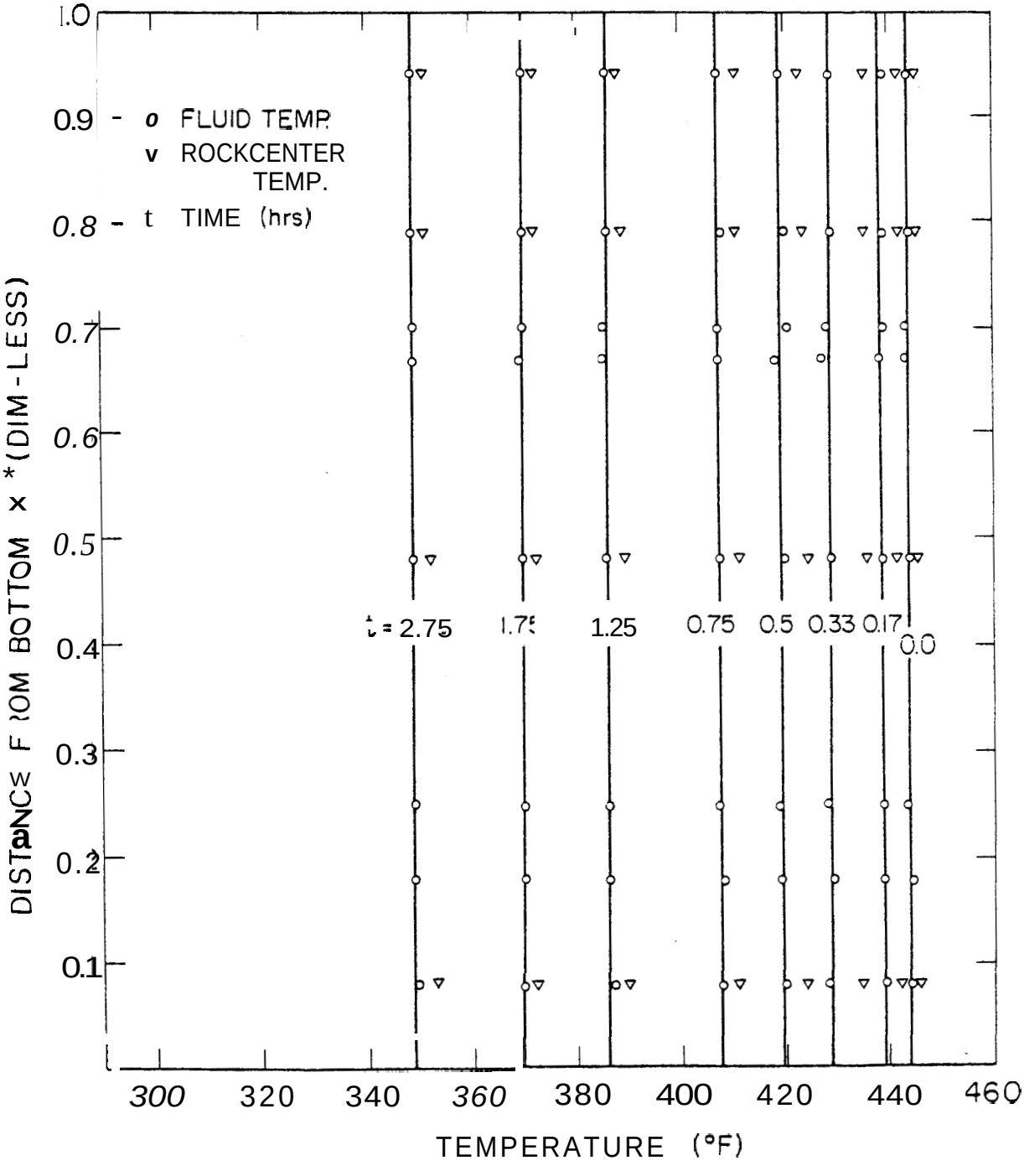

FIGURE 4-3. Measured temperature distribution for the in-place boiling experiment with hot-water injection

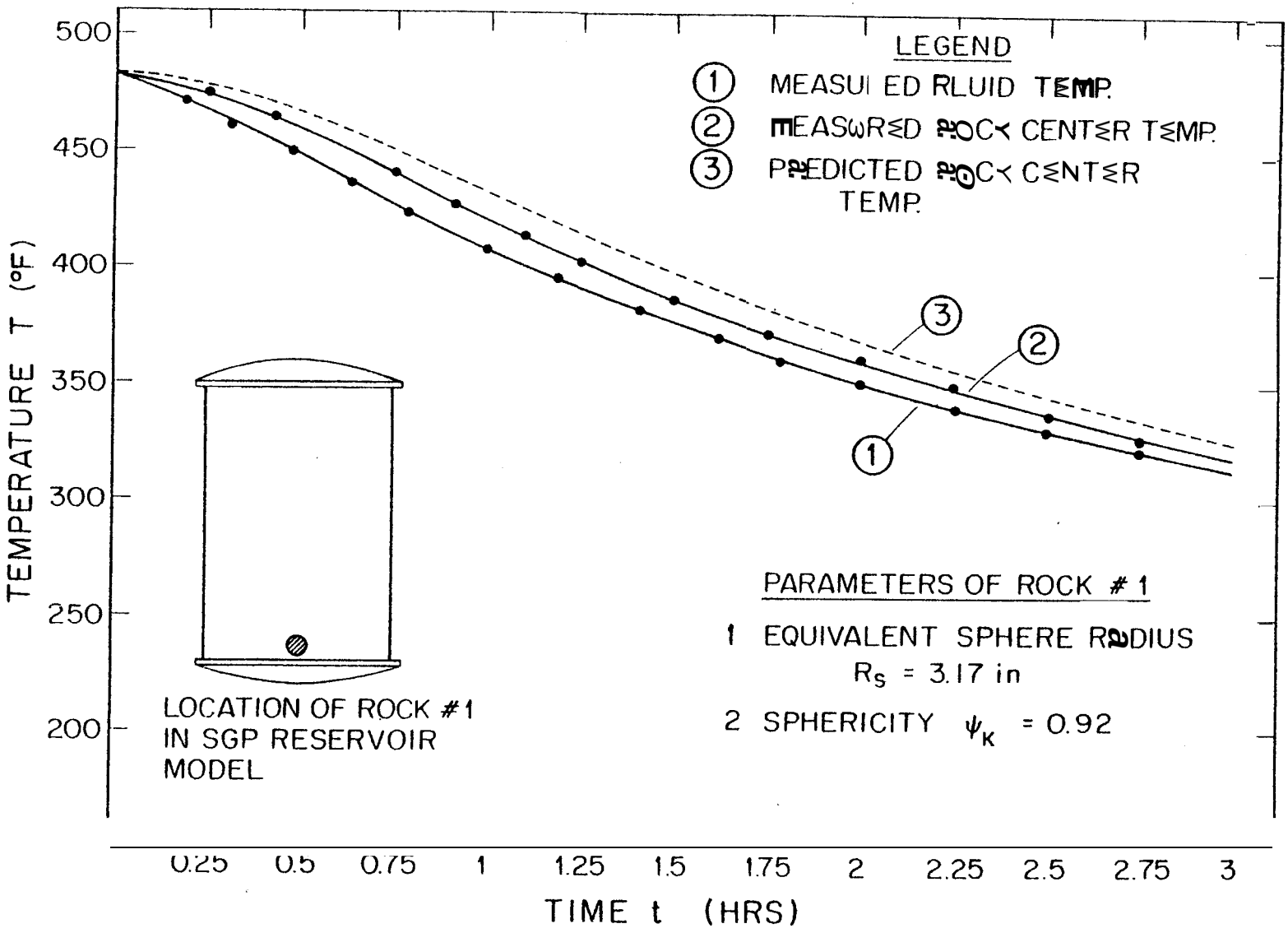

FIGURE 4-4 Measured and predicted rock center temperatures for rock number 1 in first test

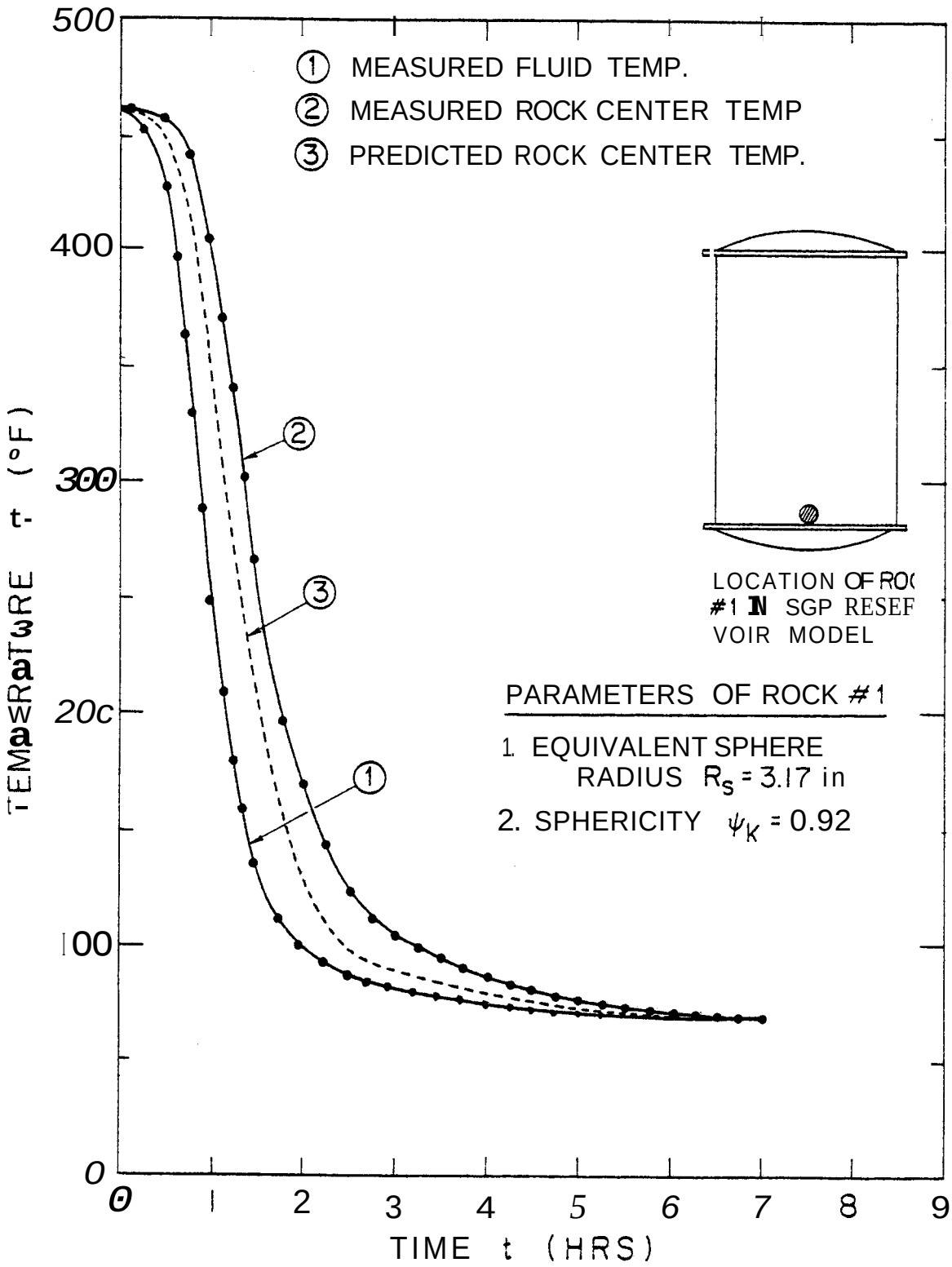

FIGURE *4-5.* Measured and predicted rock center temperatures for rock number 1 in second test

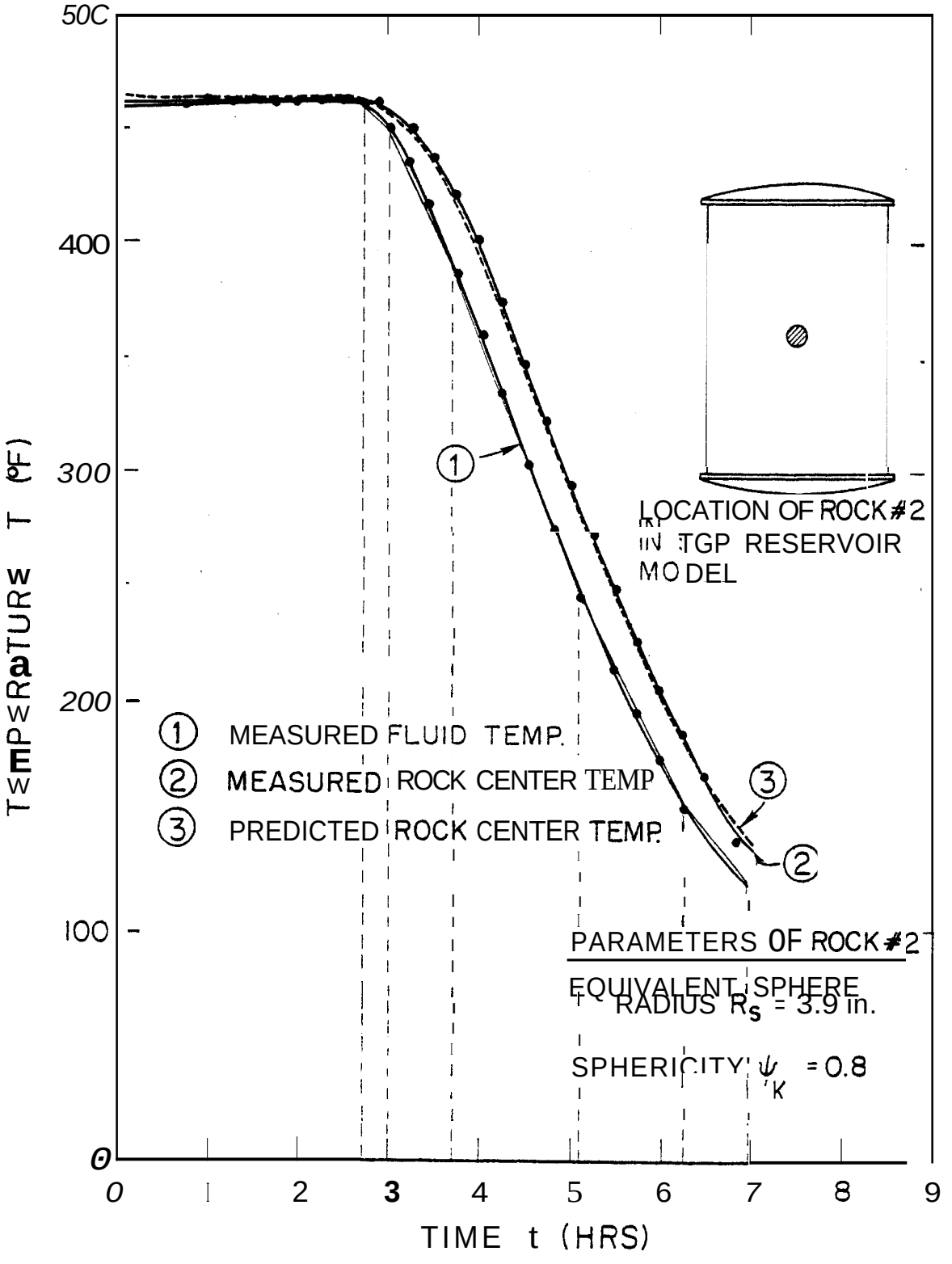

FIGURE 4-6. Measured and predicted rock center temperatures for rock number 2 in second test

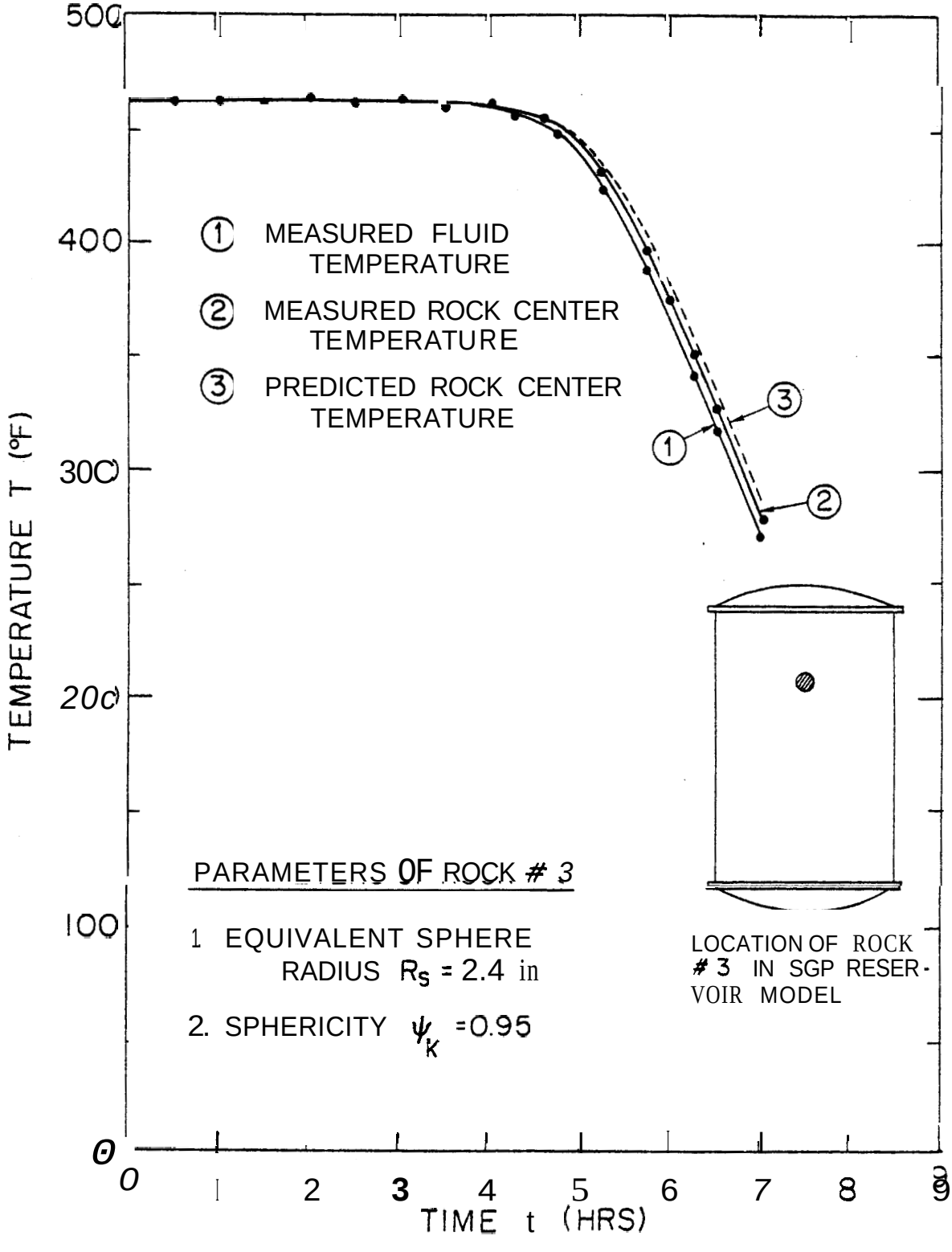

FIGURE *4-7.* Measured and predicted rock center temperatures for rock number **3** in second test

low rock center to fluid temperature differences. In the latter, the high fluid cooling rate of the cold-water sweep experiment, when the cold-water front passes through the rock, results in rather high rock center to fluid temperature differences. It can be seen in Figure 4-4 that the predicted rock center temperature is within 5 percent of the measured ones. However, the discrepancy between the measured and predicted rock center to fluid temperature differences is substantial (as high as 60 percent of measured). In Figure 4-5 the difference between the predicted and measured rock center temperature is about 20 percent in the worst cases. The inconsistencies in the results are believed to be caused by the mislocation of the thermocouple used to measure the fluid temperature. The effect of such a mislocation can be observed in Figure 4-2. The fluid temperature gradients at the location of Rock #1 ($X^* = 0.08$) are on the order of 25°F/in. The uncertainties in the location of the fluid thermocouple are as high as ±1 inches due to probable readjustments of the rock matrix as the reservoir was filled with rocks, or the probability that the thermocouple wire could have been pulled by the rocks during the loading process. Therefore, the measured rock center temperature predictions are within the uncertainties of the predicted ones (which can be as high as ±25°F).

Figures 4-6 and 4-7 show two cases where the predicted rock center temperatures were within 2 percent of the measured temperatures. These cases had considerably higher fluid cooling rates of 60°F/hr and 50°F/hr, respectively. A similar agreement between the experimental and predicted results was observed for Rocks #4, 5, and 6.

It is important to mention that the time dependence corrections for

the conduction path lengths given by Eq. *3.24* were not used since the small contribution of the final cooling rate steps (i.e., when $(t-\xi) \to 0$) made negligible the errors incurred by the one-lump solution at the early stages of the cooling process. This effect made the one-lump solution more accurate than expected when it was used with the superposition technique for variable fluid cooling rate conditions.

A sample calculation of the superposition technique using the one-lump solution is shown in Appendix C.1. The simplicity of the one-lump solution makes the computational procedure easy enough to do with a hand calculator. If a considerable amount of calculations is needed, a computer program is available in Appendix *B.4.*

4.3 Parametric Studies of the Local Rock Energy Extracted Fraction for a Collection of Rocks

The purpose of this section is to study the effect of important parameters on the local rock energy extracted fraction for a collection of rocks. In performing the parametric studies, three hypothetical frequency distributions were assumed, namely, rock volume v normally distributed, and equivalent sphere radius R_s, both normally and exponentially distributed. The normal and exponential distributions were described in Section *3.5.3* and given by Eqs. *3.36* and *3.37*, respectively.

A constant fluid cooling rate was assumed in evaluating the local rock energy extracted fraction for the hypothetical distributions selected. It was also assumed that the fluid temperature is uniform throughout the space occupied by a representative sample of the collection of rocks being considered. Equation *3.22* was used for the individual rocks, and Eq. *3.30* for the collection of rocks. A sample calculation is given in Appendix C.2.

4.3.1 Effect of Rock Mean Size

A collection of spherical rocks with volume normally distributed was selected to study the effect of the rock mean size on the energy extracted fraction. Figure *4-8* shows the results for three different mean sizes (arithmetic). As explained in Section 3.5.3, the values of the standard deviation was selected to simulate maximum dispersion. The following main points can be observed:

(a) The time required to achieve a certain energy extracted fraction is proportional to the square of the mean rock radius. Thus, to achieve a value of the energy extracted fraction equal to *0.78,* the collection of rocks with mean size equal to 10 ft requires 1,000 hours, whereas the one with a mean size of 100 ft requires 100,000 hours. This proportinality was clearly seen in Section 3.2 for individual rocks. From Figure 3-8 it is seen that for a given value of the Biot number, the energy extracted fraction depends on the Fourier number, which is inversely proportional to the square of the rock radius.

(b) If enough fracturing can be achieved to produce a mean value of the rock radius on the order of 10 ft, the energy stored in the rock collection can be totally exploited in one to two years under the idealized conditions assumed. However, if the fracturing produced a mean rock radius on the order of 100 ft, the time required to exploit efficiently the energy stored in the collection of rocks ranges from *30* to 100 years. Notice that witharock mean radius of about 0.1 ft, which is the range of sizes in the **SGP** reservoir model, the rock energy can be completely extracted in less than one day (see top left corner in Figure *4-8).* Notice also that if the geothermal fluid in a reservoir with a rock mean size on

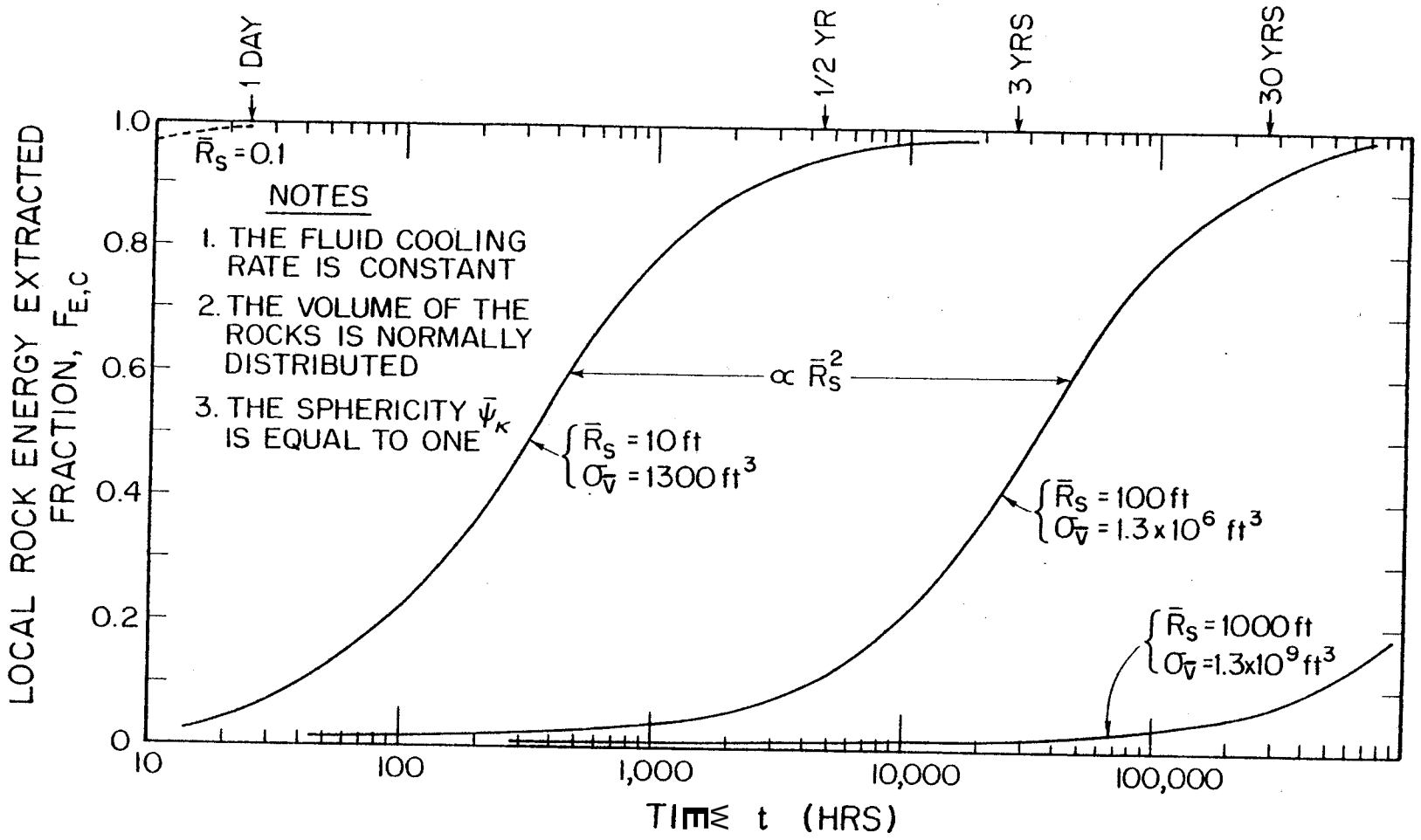

FIGURE 4-8. Effect of the mean size of a collection of rocks on the local rock energy extracted fraction

the order of 1000 ft is cooled in *30* years, less than 10 percent of the energy stored in the rock would be extracted.

4.3.2 Effect of Rock Size Distribution and Dispersion

The effect of the rock mean size on the local energy extracted fraction was observed in Section *4.3.1.* It was seen to depend significantly on the mean rock size. To study the effect of the dispersion of rock sizes from the mean value, three different size distributions were studied, all of them with a mean equivalent sphere radius of 100 ft and sphericity equal to one: rock volume normally distributed, and equivalent sphere radius both normally and exponentially distributed. The results are shown in Figure 4-9, and the distributions are schematically described in the top left corner. The following main points can be observed: for a given mean value of R_s, the size distribution strongly affects the energy extracted fraction. The difference between R_s normally distributed and v normally distributed is that, although the rock volumes can be highly dispersed from its mean value, the dispersion in terms of the rock radius is proportional to the cubic root of the dispersion in volume. Therefore, a collection of rocks with the normal distribution in rock radius has the greatest proportion of large rocks, as compared to the normal distribution in volume. Accordingly, the former distribution results in lower energy extracted fractions than the latter at a given time. The same situation is observed with the exponential distribution in which the probability of having more and bigger rocks is larger than in the normal distribution (the frequency of large rock radius decays only with the first power of the radius--see Eq. 3.37--whereas in the normal distribution it decays with the second power, Eq. *3.36).*

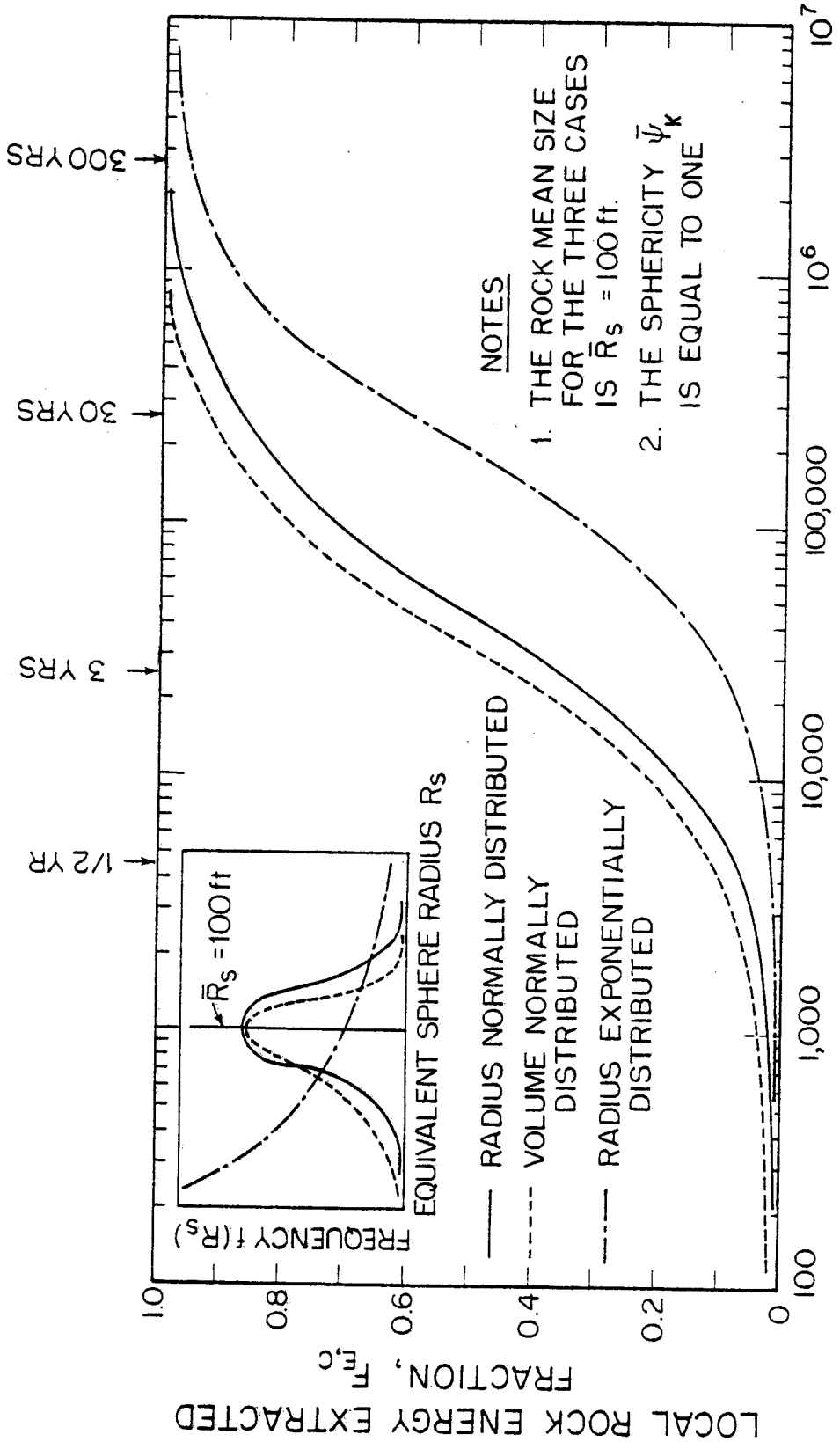

FIGURE 4-9. Effect of rock size distribution on the local rock energy extracted fraction

The effect of the rock size distribution on the energy extracted fraction can be clearly seen in terms of the size dispersion as measured by the standard deviation. In the case of the equivalent sphere radius the standard deviation is $\sigma_{\bar{R}_s} = 30.7$ ft whereas intheexponential distribution $\sigma_{\bar{R}_s} = \bar{R}_s = 100$ ft . As it was discussed in Section 3.5.2, the higher dispersion of the exponential distribution results in a larger bulk-effective radius for the collection of rocks, and therefore longer conduction path lengths, .i.e., lower rock energy extracted fractions.

4.3.3 Effect of Sphericity

A normal distribution (in R_s) with mean equivalent sphere radius equal to 100 ft and a standard deviation of 30.7 ft was selected in analyzing the effect of rock shape on the local energy extracted fraction for a collection of rocks. A mean value of the sphericity was assumed for the complete rock collection. The components of the collection with equivalent sphere radii $R_{s,i}$ will have an effective radius for heat transfer equal to (Eq. 3.18) :

$$R_{e,i} = R_{s,i} \times \bar{\psi}_K$$

Since the time required to achieve a given energy extracted fraction is proportional to the square of the mean radius, the curves of $F_{E,c}$ vs time will be displaced in time from the curve of $\bar{\psi}_K = 1.0$ in an amount that is inversely proportional to the square of the sphericity. To study this effect, three rock collections were considered. All of them are normally distributed in R_s equal to 100 ft and the same standard deviation $\sigma_{\bar{R}_s} = 30.7$ ft. One of them is a collection of spherical rocks, i.e., sphericity equal to unity, and the other two are slabs with sphericities

of 0.7 and *0.42* respectively. These values of the sphericity correspond to a proportion of the three dimensions as illustrated in the top left corner of Figure 4–10. As seen in Figure *4–10* the time required to achieve a given value of the energy extracted fraction is proportional to the square of the sphericity. Notice, for example, that the time required to achieve an energy extracted fraction of 0.6 for a sphericity of 0.7 is approximately one–half of that: for a sphericity of 1.0.

The physical significance of the sphericity was discussed in Section *3.5.2* when the concept of bulk–effective radius was introduced. A low value of the sphericity means shorter conduction path lengths (smaller bulk–effective radius), and therefore higher rock energy extracted fractions for a given time.

4.3.4 Effect of Variable Fluid Cooling Rate

The parametric studies evaluated the effects of the rock size, size distribution and dispersion, and rock shape for constant fluid cooling rate. A geothermal fluid cools according to the balance of the energy of the produced and recharge fluids and the heat transfer from the hot rock. The total heat transfer from the rock, in turn, depends on the fluid cooldown history. This effect was studied separately by fixing the size of the rocks and by letting the production and recharge rates be such that given fluid cooldown histories are obtained.

Three different fluid cooldown histories were selected for this study as shown in the right bottom corner of Figure 4–11. The initial temperature (rock and fluid) was assumed to be 500°F and the final fluid temperature 200°F. Constant cooling rate intervals were used to simplify the calculations. The local energy extracted fraction was evaluated for a

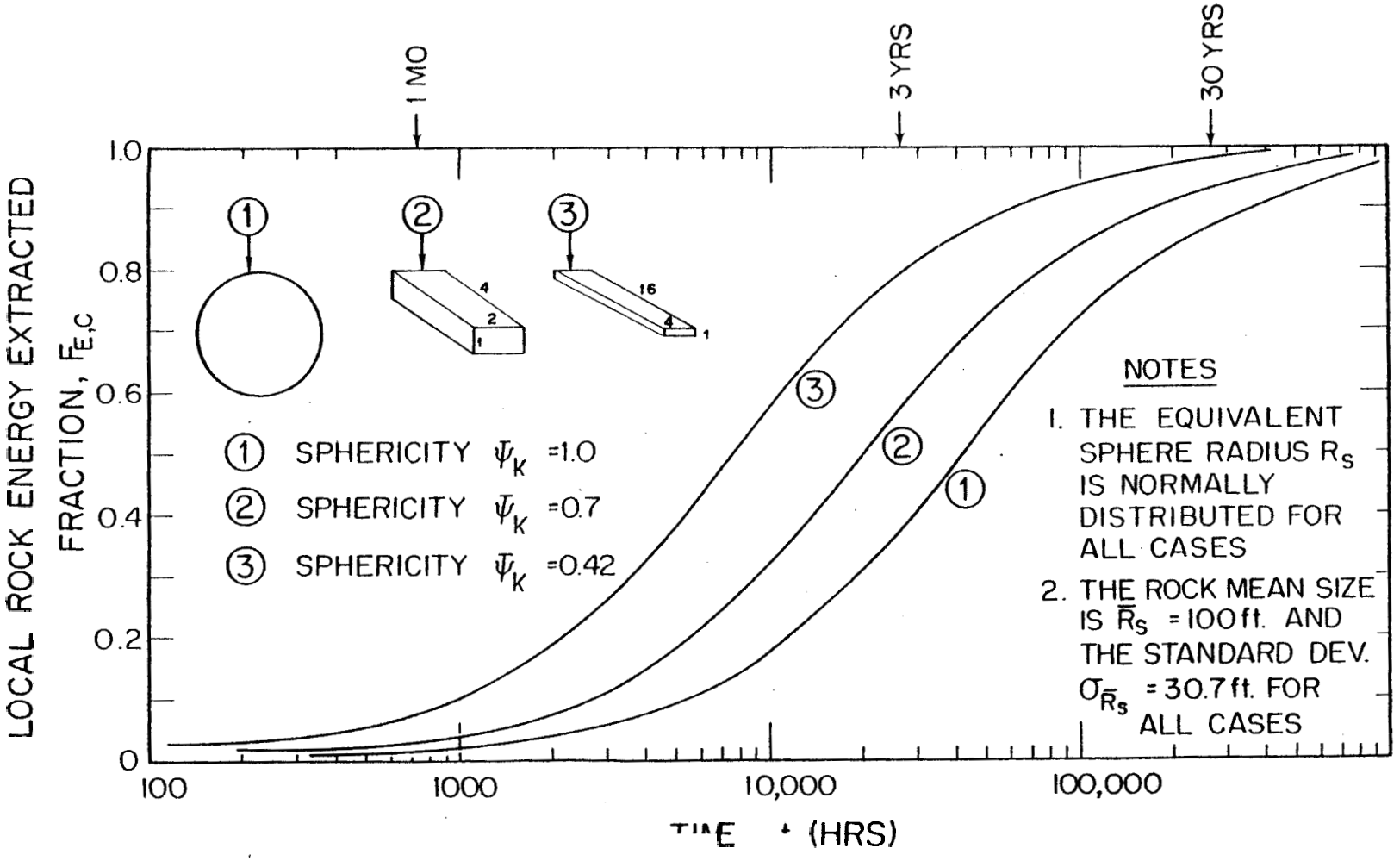

FIGURE 4-10. Effect of rock sphericiy on the local energy tracted fraction

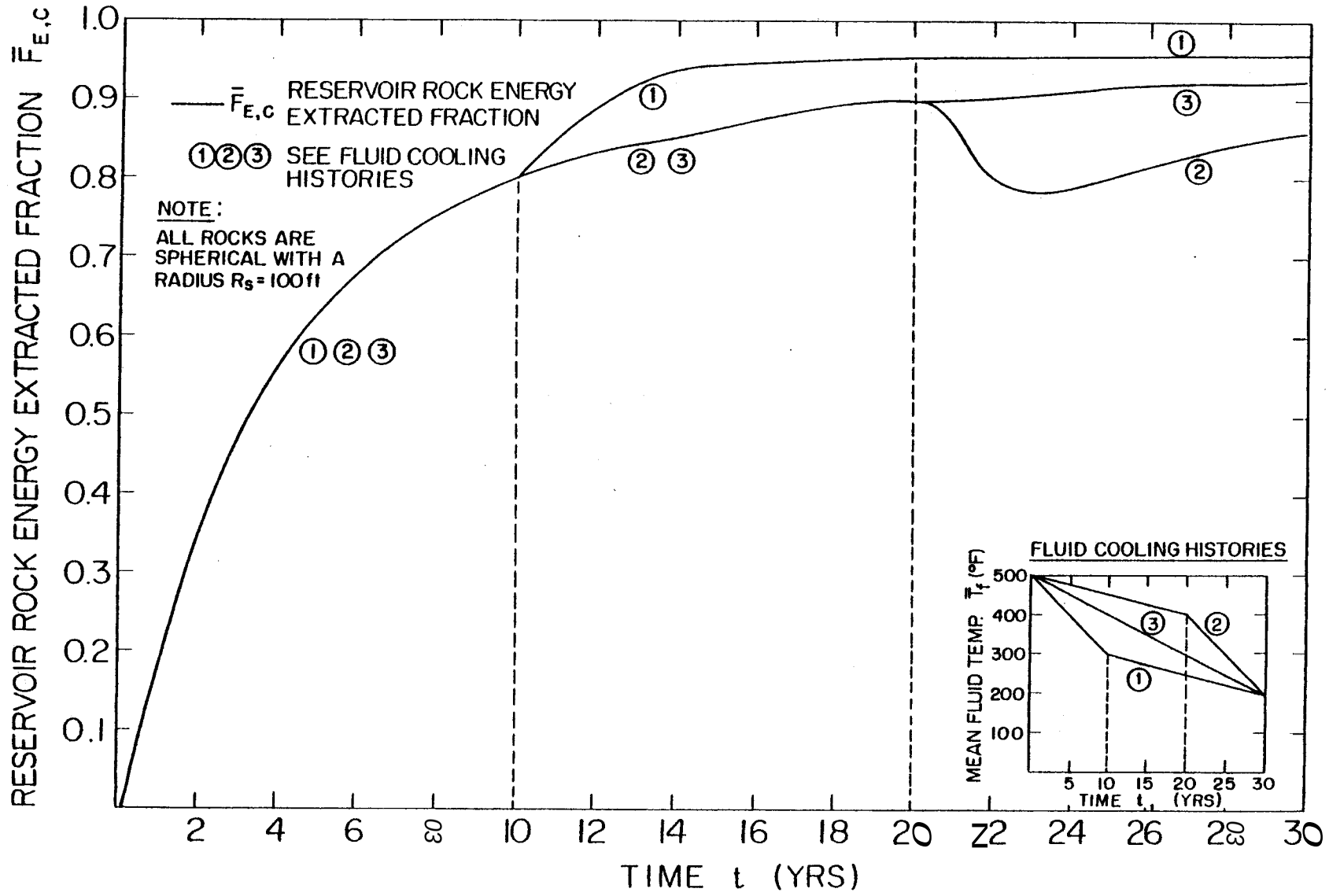

FIGURE 4-11. Effect of the variations of fluid cooling rate on the reservoir rock energy extracted fraction

collection of spherical rocks with a radius equal to 100 ft (time constant τ_e = 2 years). Figure 4-11 shows the results of the energy extracted fraction as a function of time for three fluid cooling paths. The following main points can be observed:

(a) The energy extracted fraction does not depend on the fluid cooling rate itself but rather on changes in the cooling rate. It can be seen that the energy extracted fraction is the same for the three fluid cooldown paths for times less than 10 years. After 10 years it is observed that when the fluid cooling rate decreases in curve number (1), the energy extracted fraction increases. The reason for this is that the rocks have more time to adjust to changes in the fluid temperature. The opposite occurs when the fluid cooling rate increases in curve number (2) after 20 years. In this case, the rock does not have as much time to adjust to fluid temperature changes. Notice that it takes about four years (two time constants) for the rocks to adjust to a quasi-steady state of the energy extracted fraction following a change in fluid cooling rate.

(b) To obtain a higher energy extracted fraction, a decreasing fluid cooling rate is preferred to an increasing one. The energy extracted fraction is about 0.87 for path number (2), whereas it is 0.97 for path number (1) at a time equal to 30 years. The temperature of the rock accumulative lags from the fluid temperature when the fluid cooling rate increases, and consequently low rock energy extracted fractions result.

4.4 Effect of the Variable Fluid Cooling Rate on the Reservoir Energy Fraction Produced

To study the effect of the variable fluid cooling rate on the reservoir energy fraction produced, the same procedure followed in Section

4.3.4 was used. However, instead of considering a representative sample of a collection of rocks to perform the analysis, the total reservoir volume was considered. To simplify calculations, it was assumed that the rocks are spherical with a radius equal to 100 ft, and that the fluid temperature is uniform throughout the reservoir volume. Thus, the local rock energy extracted fraction becomes the same as the reservoir rock energy extracted fraction, and the mean fluid temperature is equal to the fluid temperature at any location. Besides, it was assumed that the porosity is small, and that there is no recharge of fluid. Therefore, the storage ratio is small and Eq. 3.49 can be used to calculate the reservoir energy fraction produced. The reference temperature T_2 was selected as the final fluid temperature, i.e. 200°F.

Figure 4-12 shows the results for the three fluid cooldown histories considered in Section 4.3.4. The following points can be observed:

(a) The reservoir energy fraction produced depends on the magnitude of the fluid cooling rate mainly because the fluid temperature drop fraction is affected by the cooling rate itself. The fluid temperature drop fraction will increase with the cooling rate resulting in higher energy fraction produced, according to Eq. 3.49.

(b) The reservoir energy fraction produced also depends on the variations in the fluid cooling rate because the energy extracted fraction depends on the variations in fluid cooling rate. For example, at a time equal to 24 years path number (2) has reached a fluid temperature drop fraction of 0.6, whereas the increase in fluid cooling rate reduced the rock energy extracted fraction from about 0.92 to 0.8, i.e., 13 percent less than if the cooling rate had not changed.

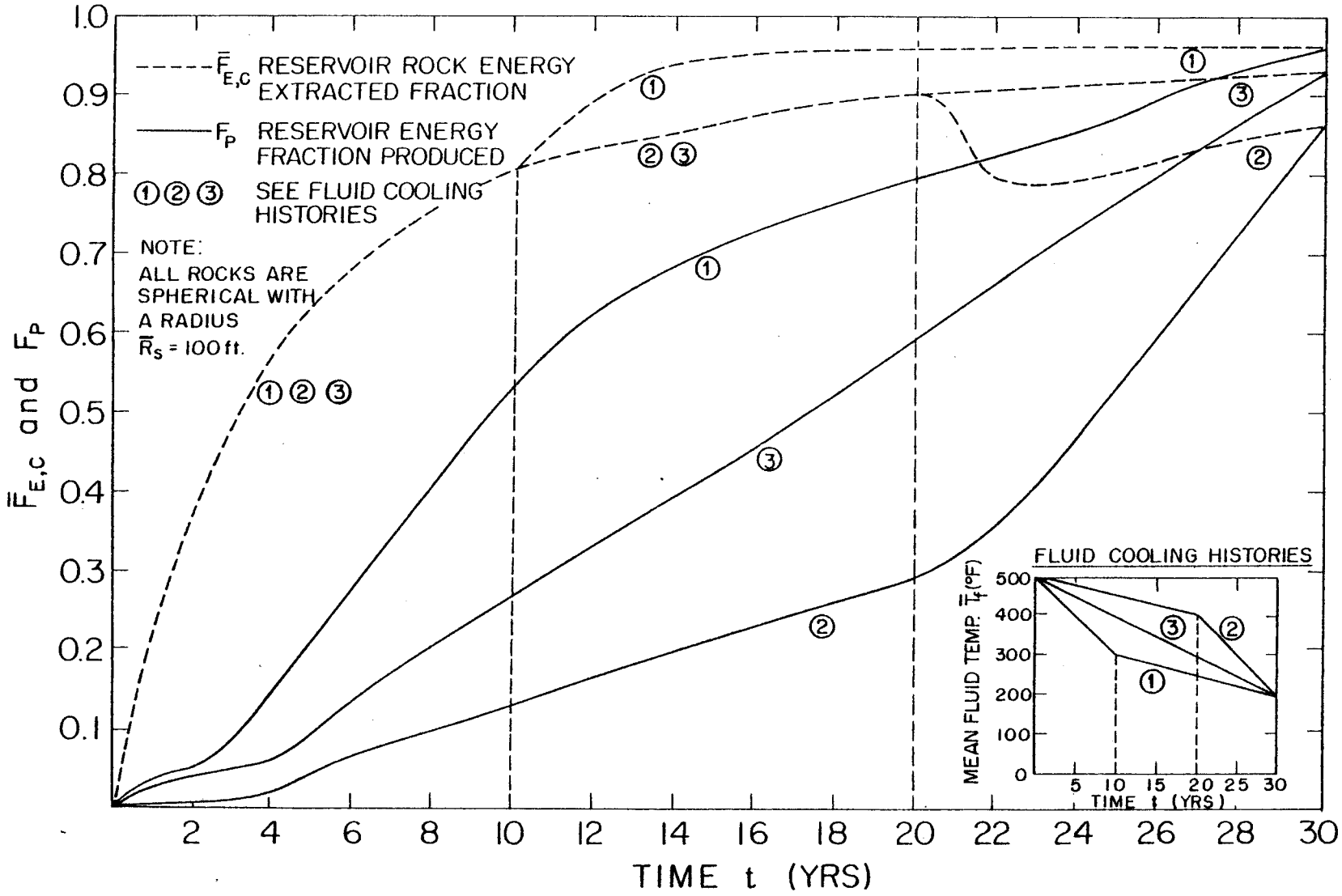

FIGURE 4-12. Effect of the variations of fluid cooling rate on the reservoir rock energy extracted fraction and energy fraction produced

(c) At the end of the production period, the reservoir energy fraction produced is equal to the reservoir rock energy extracted fraction, because the fluid has been cooled to the reference temperature T_2 equal to 200°F.

4.5 Experimental Reservoir Rock Energy Extracted Fraction

The reservoir rock energy extracted fraction evaluated from experimental data obtained during the third experiment was compared to the predicted results from the model developed in Chapter 3. The temperature of the fluid was maintained uniform throughout the reservoir (see Fig. *4-3)* during this experiment to enable the reservoir rock energy extracted fraction to be readily calculated for the collection of rocks with known characteristics contained in the SGP large reservoir model.

Table *4-2* shows the predicted and measured reservoir rock energy extracted fractions for the last three measurements of the experiment assuming an average production steam quality of 65 percent. It is observed that the estimated uncertainties for the experimental results are substantial, while the uncertainties in the predictions are relatively small. The procedure followed in evaluating the experimental results and corresponding uncertainties is described in Appendix C.4. The uncertainties in the predicted reservoir rock energy extracted fraction are evaluated in Appendix C.6.

Table *4-3* shows the experimental uncertainties for each one of the measured variables involved in evaluating the experimental reservoir rock energy extracted fraction. Notice that the major contributors to the large uncertainty are the production fluid enthalpy, the injection fluid enthalpy, and the specific heat of the rock.

TABLE 4-2

Measured and Predicted Reservoir Rock Energy Extracted Fraction

Time	$\overline{F}_{E,c}$ Measured	$\overline{F}_{E,c}$ Predicted
1.75	0.64 ± 1.3	0.98 ± 0.03
2.25	0.93 ± 1.4	0.99 ± 0.02
2.75	0.92 ± 1.5	0.98 ± 0.03

Parameter	± δX	$\left(\frac{\partial \overline{F}_{E,c}}{\partial X} \times \delta X\right)^2$
Production enthalpy (Btu/lbm)	50	1.0
Injection enthalpy (Btu/lbm)	10	0.14
Rock specific heat (Btu/°F-lbm)	0.02	0.74
Time (hr)	0.02	0.1
Rest of parameters	-	0.2

The relatively negligible uncertainty in the predicted energy extracted fraction is controlled by the uncertainty in the mean rock to fluid temperature difference, as illustrated in Appendix C.7. It is given by

$$\frac{\Delta \overline{F}_{E,c}}{\overline{F}_{E,c}} \approx \frac{6AT_m}{AT_m} \times \frac{(1 - \overline{F}_{E,c})}{\overline{F}_{E,c}}$$

Clearly, even if the prediction of AT_m is not very certain (the uncertainty in AT_m is about t30 percent, as evaluated in Appendix A.3), since $\overline{F}_{E,c}$ is some number close to unity, the uncertainty in $\overline{F}_{E,c}$ itself is very low.

The results of this evaluation show that complete verification of heat transfer model using this procedure will require improvements in the equipment such that production and injection fluid enthalpies can be measured with an accuracy of ± 5 percent. However, the earlier comparison of measured and calculated rock temperature transients showed good agreement and there is no reason why this present comparison should not be equally good if adequate data were available.

4.6 Cold-Water Sweep Process

4.6.1 Experimental Verification of the Model

The one-dimensional analytical model for the cold-water sweep process as derived in Section 3.7, was compared to experimental data obtained during the second experiment. The fluid flow in the reservoir model is approximately one-dimensional and the temperature can be considered uniform in the horizontal plane.

The reservoir was initially at a uniform temperature of *460* °F and water was injected at the bottom of the reservoir model at an approximately constant temperature of 70°F. Since the cold fluid being injected had to displace the hot water occupying the pipe line between the injection pump and the reservoir itself, the cold-water front actually reached the injection point about 30 minutes after the experiment was initiated. Then, for the purposes of the comparison with the analytical model predictions, the experiment actually started at a time equal to 30 minutes. The injection and production rates were maintained constant at approximately 133 lb/hr.

Table *4-4* presents a summary of the parameters of the experiment. The important non-dimensional parameters are noted with an asterisk. The calculation of the number of transfer units N_{tu} for the experiment is presented in some detail to illustrate the process.

TABLE 4-4

Summary of Numerical Input to the Cold-Water Sweep Heat Transfer Model

Initial Reservoir Temperature T_1 (°F)	460
Temperature of Injected Water: $\overline{T}_{in}$ (°F)	70
Production and Injection Flow Rates, $\dot{\overline{m}}$ (lb/hr)	133
* Reservoir Porosity, ϕ (dimensionless)	0.42
Reservoir Volume, V_{Re} (ft^3)	16.57
Reservoir Cross Section, S (ft^2)	3.27
Reservoir Length, L (ft)	5.08
External Heat Transfer, Q_e (Btu)	115,151
Electric Source Term in Q_e (Btu)	59,746
Heat Losses Term in Q_e (Btu)	56,455
Rock Bulk-Effective Radius, $R_{e,c}$ (ft)	0.152
Density of Fluid, $\overline{\rho}_f$ (lb/ft^3)	54.0
Density of Rock, $\overline{\rho}_r$ (lb/ft^3)	164.8
Specific Heat of Fluid, c_f (Btu/lb-°F)	1.0
Specific Heat of Rock, c_r (Btu/lb-°F)	0.218
Darcy Velocity, v_f (ft/hr)	0.7
Sweepage Velocity, w (ft/hr)	1.59
Residence Time, t_{re} (hr)	3.19
Bulk-Effective Time Constant, τ_e (hr)	0.058
* Heat Capacity Ratio, c^* (dimensionless)	0.62
* Storage Ratio, γ (dimensionless)	1.17
* Modified Storage Ratio, γ_{mo} (dimensionless)	0.52
* Number of Transfer Units, N_{tu} (dimensionless)	55
* External Heat Transfer Parameter, q^* (dimensionless)	0.33

* Stars indicate important non-dimensional parameters.

The bulk-effective radius was calculated using Eqs. 3.32 and 3.34. Using the mean value of Kuo's sphericity of 0.83 estimated earlier and the frequencies $p(R_{s,i})$ for each rock size $(R_{s,i})$ from Figure 2-7, the bulk-effective radius was calculated to be 0.152 ft.

The Biot number for a rock having the bulk-effective radius calculated above and with a convection heat transfer coefficient of 300 Btu/hr-ft^2-°F is 32.6. As discussed in Section 3.1.1, this indicates that the rocks behaved as if the Biot number was infinity, and that most of

the thermal resistance is located inside the rock mass. The overall heat transfer coefficient U_o given by Eq. 3.8b is 40 Btu/hr-ft^2-°F. The bulk-effective time constant was calculated from Eq. 3.35 to be 0.058 hr (3.5 min).

The residence time is calculated from Eq. 3.53 to be 3.14 hrs. The number of transfer units for the experiment is simply the ratio of the residence time and the bulk-effective time constant according to Eq. 3.55 and becomes 55.

It can be observed from Table 4-4 that the storage ratio is 1.17, which means that the energy stored in the fluid is 17 percent larger than the energy stored in the rock. This is the result of the relatively high porosity (42 percent) of the experimental rock system.

The magnitude of the non-dimensional external heat transfer parameter given in Table 4-4 shows that a significant amount of energy was transferred from the vessel steel wall to the fluid. The steel wall cools approximately as the rock contained inside the vessel. Therefore, the external heat transfer parameter cannot be considered uniform throughout the reservoir length; rather, it varies for different elevations of the reservoir. At a given elevation, the heat transfer from the steel will also vary with time similarly to the heat transfer from the rock. Also, the magnitudes of the terms in the heat transfer parameter in Table 4-4 show that the electric source term is approximately the same as the heat losses term. Thus, the energy released as a result of the decrease in steel wall temperature went to the fluid. The temperature of the steel wall can be assumed to respond to fluid temperature changes at the same rate as the rock (time constant for the steel wall ≈ 0.01 hr). These

observations were used to formulate a modified sweep process heat transfer model in which the steel wall is lumped in with the rock.

The mass of the steel vessel was assumed to be uniformly distributed throughout the reservoir volume. This equivalent rock mass is 206.8 lbm/ ft^3. In Appendix C.8, appropriate changes to the analysis performed in Appendix B.9 were made to account for the additional energy stored in the steel wall. The modified storage ratio (ratio of the energy stored in the fluid to that stored in the rock and steel) becomes 0.52 instead of the 1.17 found earlier. This means that the energy stored in the metal represents 56 percent of the total energy stored in the rocks and the steel. Also, the non-dimensional external heat transfer parameter can now be set to zero, because the heat losses and energy from the electric tape heaters cancel each other approximately.

Analytical prediction of the fluid temperature was performed using the procedure presented in Section 3.7 and Appendices B.9 and C.7. Figure 4-11 shows the experimental results and the analytical predictions (dotted lines). These are the same experimental data presented in Figure 4-2 except that time is plotted along the abscissa displaced 30 minutes (0.15 in non-dimensional units).

It is seen in Figure 4-13 that the time at which the non-dimensional fluid temperature starts to drop from its initial value of unity is longer for the predictions than for the experimental results. Moreover, this time delay increases at locations closer to the top of the reservoir ($X^* = 1.0$). The reason for this difference is explained by recalling that 56 percent of the total energy being received by the fluid comes from the steel wall. This means that the fluid in the center of the vessel will

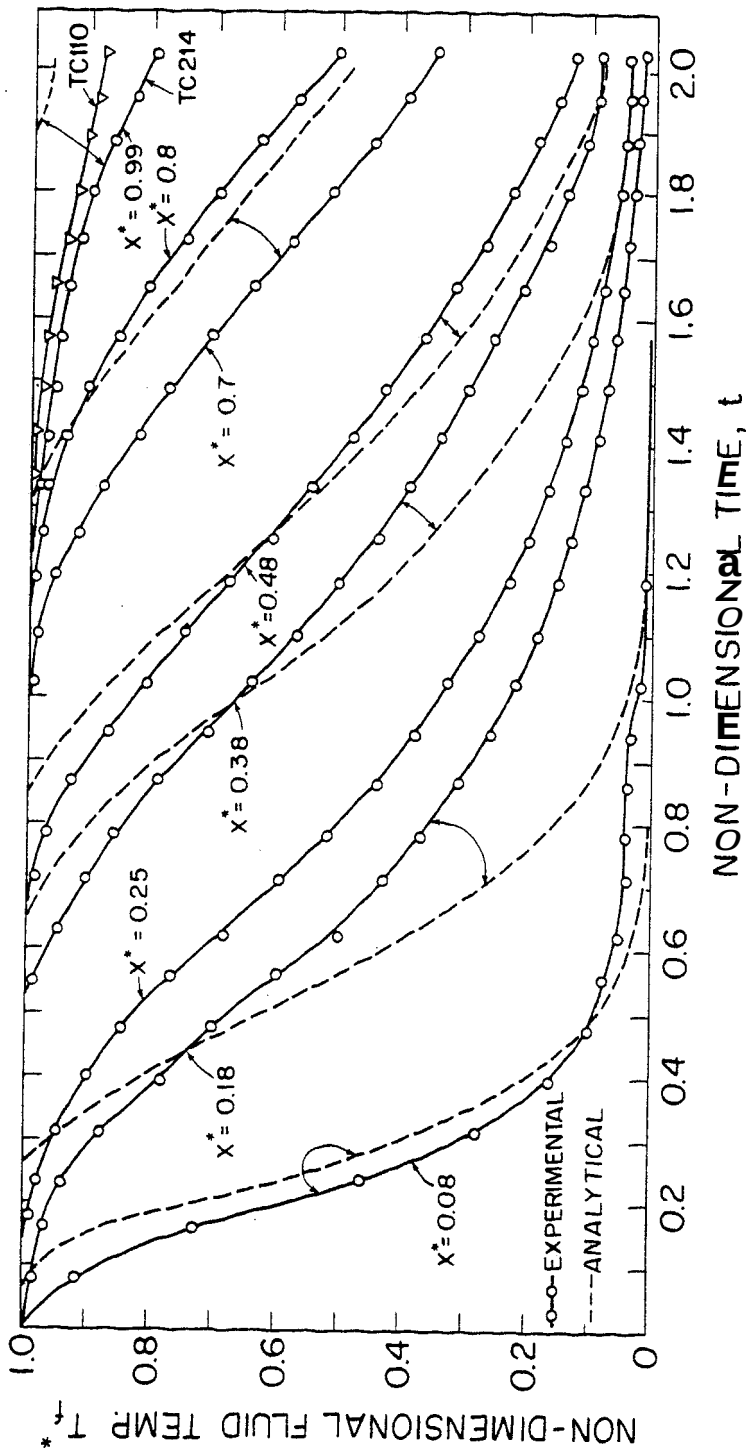

FIGURE 4-13. Non-dimensional fluid temperature vs non-dimensional time for different locations of the reservoir

be cooler than that close to the wall. Accordingly, the thermocouples located at the center (see Figure 2-15) tend to measure the cooler fluid. This effect was verified at the top of the reservoir where one thermocouple is located at the center of the rock matrix near the top (thermocouple 214 in Figure 2-15) and another one is located in the production line above the rock matrix (thermocouple 110). The fluid close to the wall mixes with the fluid flowing through the center before it reaches thermocouple 110. The temperature measured by thermocouple 110 is also given in Figure 4-11. Evidently, thermocouple 214 was measuring cooler fluid than thermocouple 110, indicating a two-dimensional temperature field instead of the one-dimensional assumed in the analytical model.

The measured fluid temperature drops more slowly than the predicted at locations in the lower half of the reservoir ($X^* \leq 0.5$). This is believedtobe caused by the significant amount of energy stored in the heavy flanges of the lower head (36 percent of the total mass of the vessel) as indicated in Figure 2-15. This results in a higher concentration of steel mass (approximately 372 lb/ft3) and more energy released per unit volume of steel and rock in this region as compared to the average. Numerical estimates show that the fluid will receive approximately 44 percent more energy from the steel and rock as compared to the uniformly distributed mass assumed in the analysis.

Several values of the number of transfer units were tried in the analysis to determine if a correct value for the bulk-effective radius was used. It was found that values smaller than the value of 55 computed earlier in this section fundamentally changed the shapes of the temperature vs time curves, whereas larger values had only a negligible effect

on these curves. It appears, therefore, chat the actual bulk-effective radius for the experimental rock system is very close to the one determined by the statistical sampling of the rocks described in Chapter 2. The effect of the number of transfer units on the energy extraction process is analyzed in detail in the following section.

4.6.2 Effect of the N_{tu} on the Energy Extraction Process

The reservoir number of transfer units measures the ability of the rocks to transfer the stored thermal energy to the surrounding fluid. The development in Section 3.7 showed that large number of transfer units would produce high energy extracted fractions. The effect of the number of transfer units on the energy extraction process is analyzed in this section. Before starting our analysis it is useful to recall which parameters are involved in its definition, and what conditions govern its magnitude. From the definition given by Eq. 3.55 it can be seen that the following parameters would increase the number of transfer units:

1. Reduce the rock-effective time constant which can be seen from the defining equation (Eq. 3.35) to be accomplished by: (a) reducing the bulk-effective radius of the rock collection, (b) increasing the convective heat transfer coefficient.
2. Increase the fluid residence time which can be seen from the defining equation (Eq. 3.53) to be accomplished by: (a) increasing fracture porosity, (b) reducing the injection or production rate, (c) increasing distance between wells.

A sensitivity analysis was performed to determine the effect of the number of transfer units on the reservoir rock energy extracted fraction

$\bar{F}_{E,c}$, the reservoir energy fraction produced F_p, and the produced fluid temperature $T_f^*(1,t^*)$. These parameters were defined in Sections 3.6.1 and 3.6.3 and were derived for the cold-water sweep process in Section 3.7. The computations were performed for assumed fracture porosity of 10 percent, granite rock cooled by saturated water ($c^* = 0.62$, $\gamma = 0.18$), and zero external heat transfer for all cases. The number of transfer units was varied from 5 to 200. The results are given in Figures 4-14 through 4-16.

The number of transfer units for the results in Figure 4-14 is 5.0. It is observed that the reservoir rock energy extracted fraction drops rapidly from 1.0 at time zero to about 0.14 at time 0.02. This drop occurs because there are not enough transfer units to rapidly cool the rock to the fluid temperature. In other words, either the rocks are so large that they do not have time to adjust to fluid temperature changes, or the rocks are reasonably small but the fluid flow rate is relatively high. After one residence time ($t^* = 1.0$), the reservoir rock energy extracted fraction reached 0.32. This means that the average rock temperature has dropped only 32 percent of the corresponding mean fluid temperature drop. As a result, the produced fluid did not receive enough energy from the rock, and its temperature $T_f^*(1,t^*)$ starts to drop soon. The life of the reservoir will be limited by the production temperature (if the flow rate remains constant), and when it drops beyond a certain limit the reservoir may have to be abandoned at a time when only a small fraction of the energy stored in the rock has been exploited. For example, if the reservoir is abandoned when the temperature of the produced fluid has dropped to $T_f^*(1,t^*) = 0.7$, the reservoir energy fraction produced,

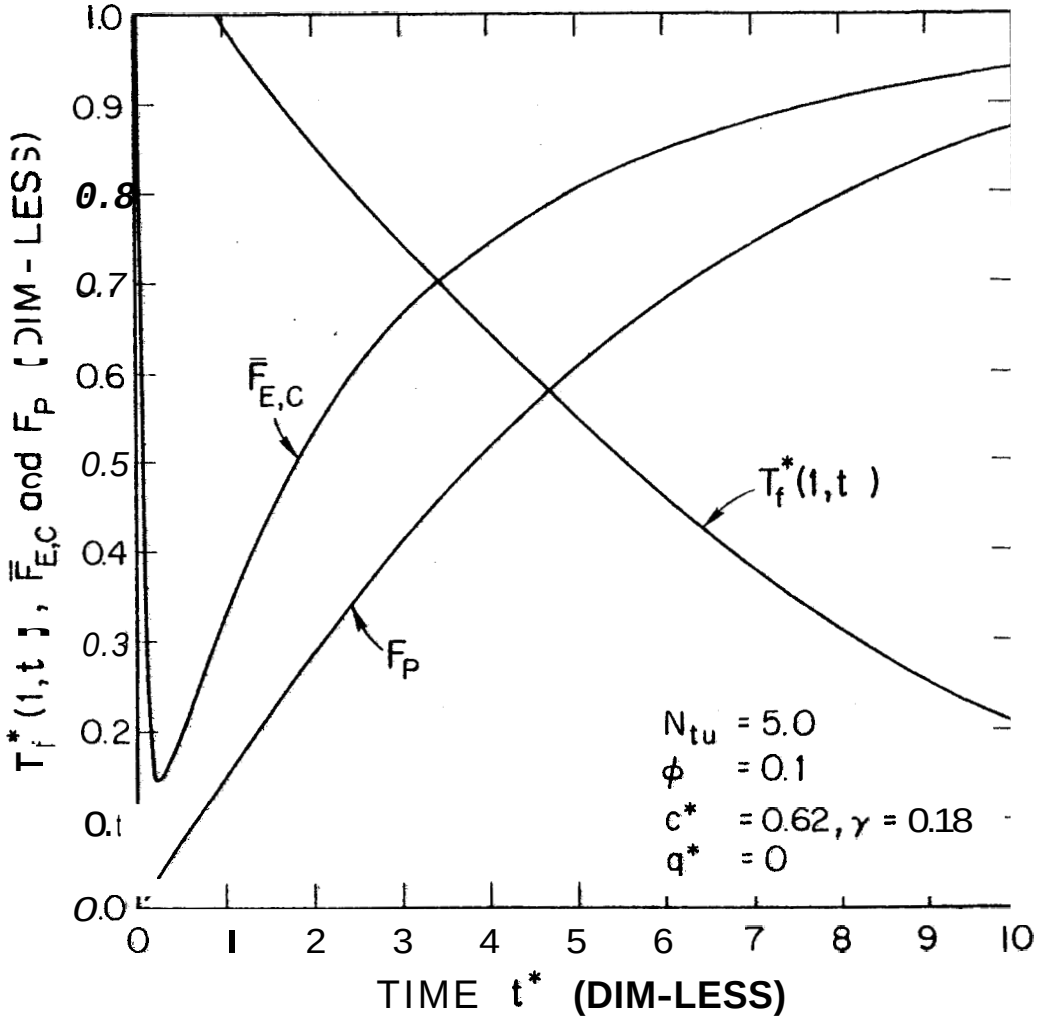

FIGURE *4-14.* **Effect of N_{tu} on the reservoir energy fraction produced F_p, reservoir rock energy extracted fraction $\bar{F}_{E,c}$, and produced fluid temperature $T_f^*(1,t^*)$**

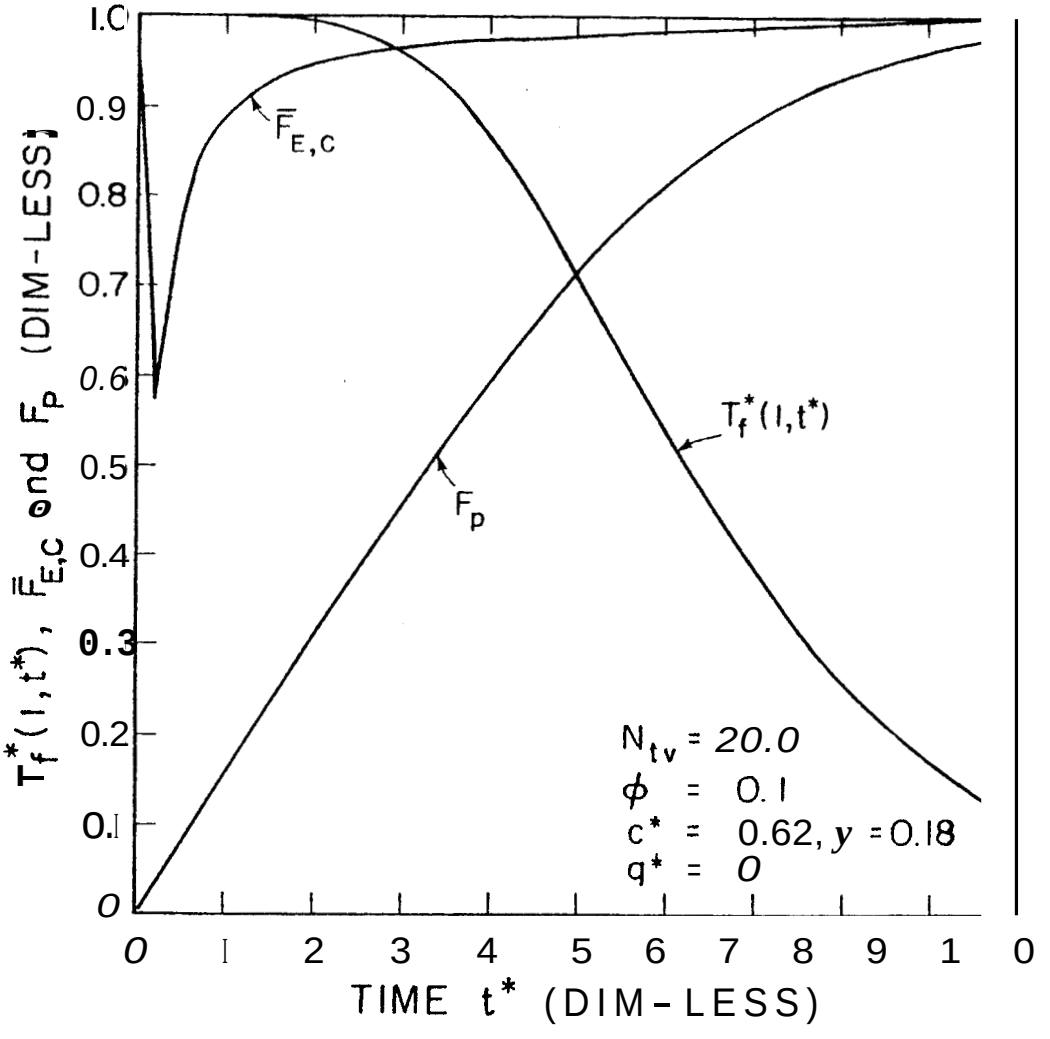

FIGURE 4-15. Effect of N_{tv} on the reservoir energy fraction produced F_p, reservoir rock energy extracted fraction $\bar{F}_{E,c}$, and produced fluid temperature $T_f^*(1,t^*)$

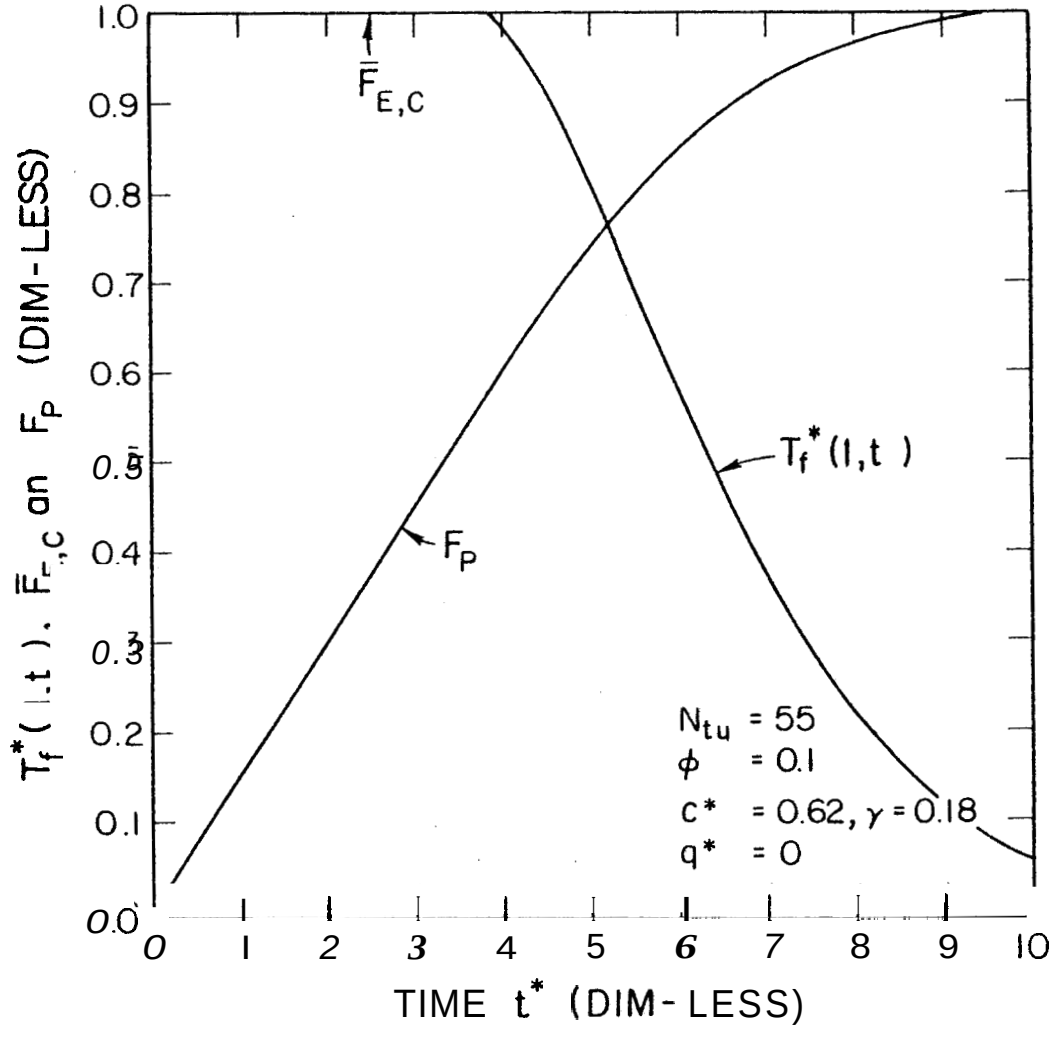

FIGURE 4-16. Effect of N_{tu} on the reservoir energy fraction produced F_p, reservoir rock energy extracted fraction $\bar{F}_{E,c}$, and produced fluid temperature $T_f^*(1,t^*)$

F_p, is 0.45 which means that only 45 percent of the recoverable energy would be exploited. The life of the reservoir would be 3.4 residence times.

The number of transfer units for the results in Figure 4-15 is 20. The reservoir rock energy extracted fraction is seen to drop initially, but after one residence time it has recovered and reached 0.9. Sufficient energy has been transferred from the rock to the fluid to keep the produced fluid at its initial temperature ($T_f^*(1,t^*) = 1.0$) for almost two residence times. If the reservoir was to be abandoned when the fluid temperature dropped to 0.7, about 72 percent of the recoverable energy would be exploited and the life of the reservoir would be 5 residence times.

The number of transfer units for the results in Figure 4-16 is 55, which is equal to that of the cold-water sweep experiment, except that there is no heat transfer from the surroundings of the reservoir and the rock porosity is 10 percent as compared to 42 percent in the experimental system. It is seen from Figure 4-16 that the reservoir rock energy extracted fraction is equal to one during the total production time. This means that the number of transfer units are sufficiently large to transfer the thermal energy from the rock to the fluid fast enough to maintain the rock in approximately local thermal equilibirum with the fluid. The produced fluid temperature remained at the initial reservoir temperature for 4 residence times. Also, if the reservoir was to be abandoned when the produced fluid temperature $T_f^*(1,t^*)$ reached 0.7, the reservoir energy fraction produced would be 0.8 and the reservoir life 5.4 residence times. The improvement in energy recovery was not significant when increasing the number of transfer units from 20 to 55.

A more detailed study showed that the energy extracted fraction approaches unity during the total production time for number of transfer units greater than approximately 30 for the particular conditions mentioned earlier (y = 0.18 , $ = 0.10). The physical meaning of this is that for N_{tu} greater than 30 the fluid flows slowly enough to allow essentially thermal equilibrium between the fluid and rock, irrespective of the rock size. Another interpretation is that the collection of rocks behaves approximately as infinitely small particules. This behavior is similar to fluid flowing through sedimentary porous rock media, which has been studied by Arihara (1974), Atkinson (1976), and Nathenson (1975).

The life of a reservoir will depend on its initial temperature and on the lowest temperature of the produced fluid acceptable for power generation (or any other energy utilization) and below which the reservoir will have to be abandoned. To characterize the reservoir life, a characteristic life time (denoted by t_C^*) is defined as the time when the produced fluid temperature $T_f^*(1,t^*)$ drops below unity.

Figure 4-17 shows the characteristic life time as a function of the number of transfer units. It also shows the reservoir rock energy extracted fraction and the reservoir energy fraction produced at time equal to t_C^*. The produced fluid cannot start to cool until one residence time for number of transfer units less than 10 for which $t_c^* = 1.0$. For N_{tu} between 10 and 50, t_c^* increases rapidly, and for larger values t_c^* starts to increase more slowly and approaches a value of approximately 4.5. It is observed that t_c^* started to increase slowly when the reservoir rock energy extracted fraction approached unity. Also, notice the similarity between the energy fraction produced and the

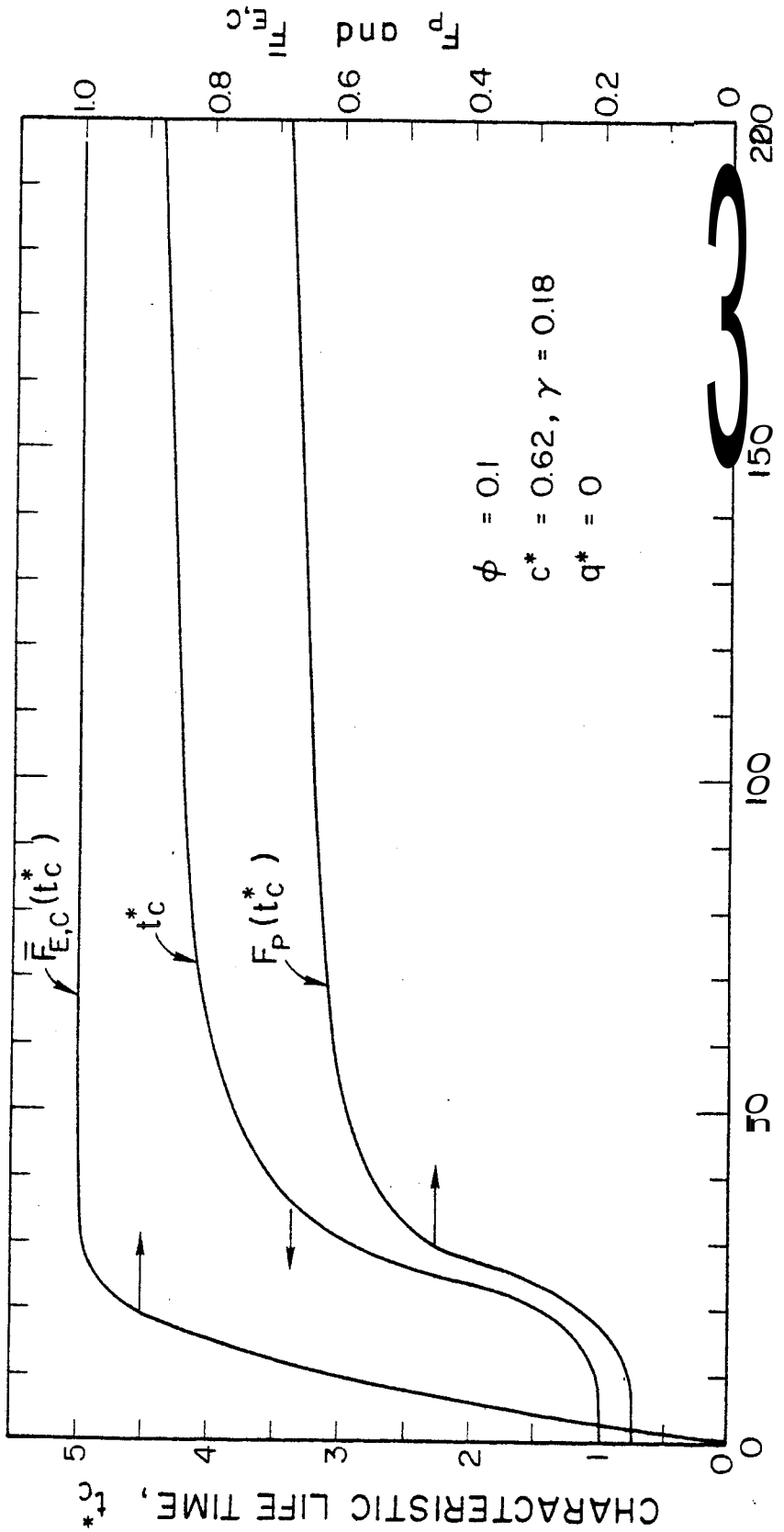

FIGURE 4-17. Effect of N_{tu} on the characteristic life time t_c^*, the reservoir rock energy extracted fraction $\bar{F}_{E,c}(t_c^*)$, and the reservoir energy fraction produced $F_p(t_c^*)$

characteristic life time curves. The reservoir energy fraction produced approaches 0.7 which means that to recover more than 70 percent of the energy stored in the reservoir, the reservoir must be exploited for a time longer than the characteristic life time t_c^* (i.e., the final produced fluid temperature $T_f^*(1,t^*)$ must be less than unity).

To achieve maximum energy recovery from a fractured geothermal reservoir the following should be kept in mind: (a) If the reservoir is to be produced at a given rate, sufficient fracturing should be performed to achieve a number of transfer units of approximately 50. Additional fracturing will not significantly improve the energy recovery. If the number of transfer units is less than *50*, the energy recovery from the reservoir is heat-transfer limited ($\bar{F}_{E,c}$ less than unity) and it decreases rapidly. (b) If there are limitations in fracturing the reservoir, it should be produced at rates such that the number of transfer units are approximately 50. If it is produced at lower rates, no significant additional energy recovery would be achieved, and if the rates are higher, a rapid decrease in the energy recovery would result.

4.6.3 Application of the Cold-Water Sweep Model

An example of an application of the methodology and model developed for the cold-water sweep process in the present study is presented. A hypothetical fractured geothermal reservoir with the parameters and conditions listed in Table *4-5* was selected for the study. Two energy extraction rates were assumed which correspond to power plant outputs of 10 and *50* MWe based on typical power plant specific flow rate of *85* lbm/kW-hr. The fluid residence times for the two extraction rates were evaluated from Eq. *3.53* to be *30* and 6 years for the 10 and 50 MWe power plant,

TABLE 4-5

Hypothetical Reservoir Parameters

Initial Temperature, (°F)	550
Injection Temperature, (°F)	70
Reservoir Volume, (km^3)	1
Specific Power Plant Flow Rate, (lb_m/kW-hr)	85
Distance between Injection and Production Wells, (km)	1
Reservoir Porosity, (dimensionless)	0.1[a]
"Power Generation" Rates, (MWe): Case 1	10[b]
Case 2	50
Bulk-Effective Rock Radius, (ft)	25-400

[a] Reservoir permeability assumed adequate to allow fluid circulation at the required rates 'in both cases.

[b] Power generation is based on the average specific flow rate given in the table.

respectively. Since the fluid residence time has been fixed, any change in the number of transfer units parameter is the result of changes in the mean effective rock radius which in the present analysis was varied from 25 ft to 400 ft. The produced fluid temperature, the reservoir rock energy extracted fraction, and the reservoir energy fraction produced are given as functions of time for the two cases considered in Figure 4-18. The following main points are noted from these results:

(a) The characteristic life time of the reservoir is increased by a factor of 4 when the rock size is reduced approximately by a factor of 2, as long as N_{tu} is less than about 50.

(b) For the 10 MWe case, a reservoir life of one residence time (30 years) can be achieved irrespective of the rock size. However, the

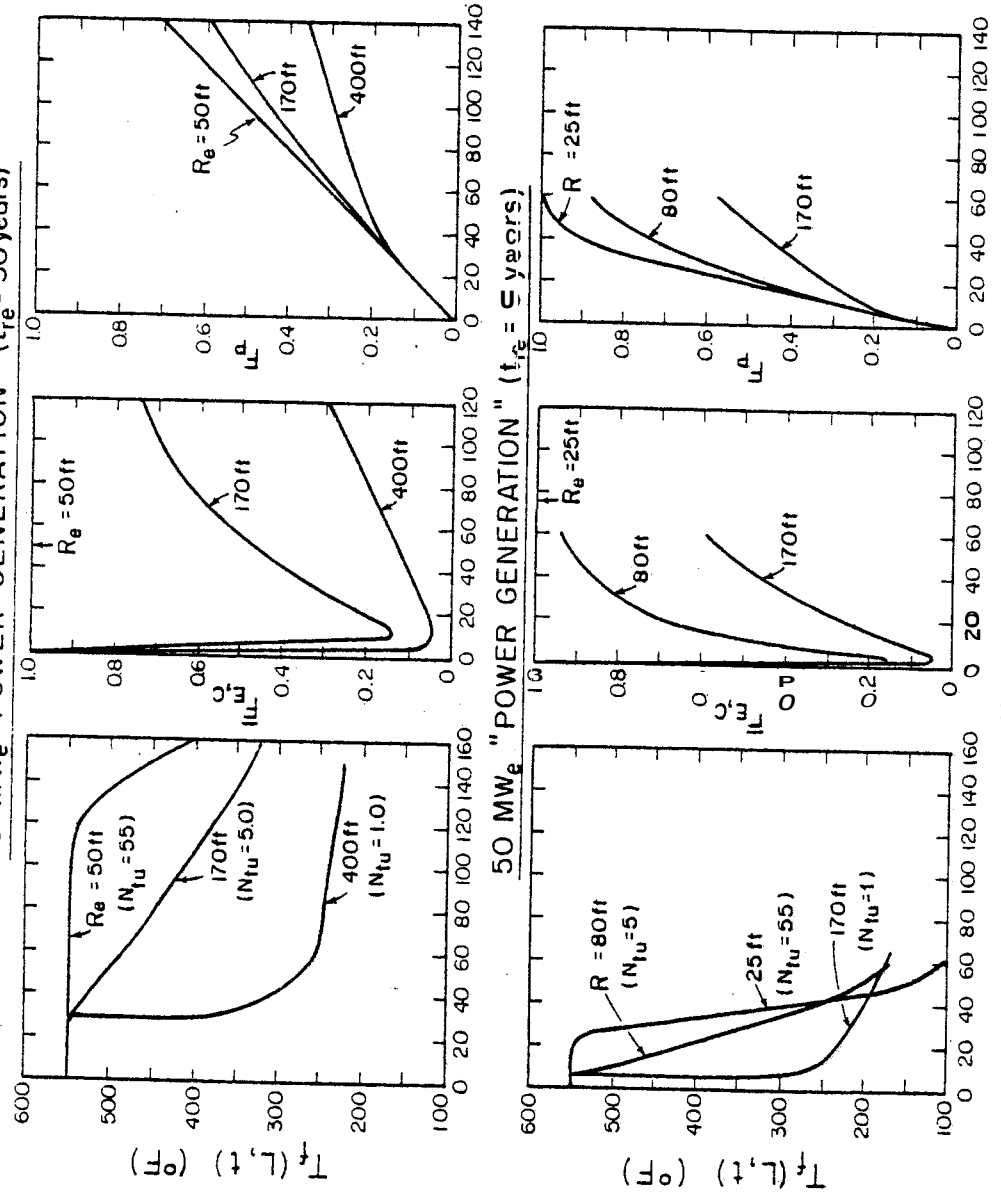

FIGURE 4-18. Example of the application of the cold-water sweep model to large-scale geothermal reservoirs

energy recovery will be only about 15 percent for all rock radii considered.

(c) For the 50 MWe case, the rock size required to achieve a reservoir life of one residence time is *25* ft. This is because the fluid flow rate is higher and its temperature is dropping at a faster rate.

(d) If the reservoir rock energy extracted fraction for the two cases is compared for an effective rock radius of 170 ft, it is noted that $F_{E,c}$ is almost identical for the two cases during most of the production time except for the first *6* years. This shows that the rock energy extracted fraction does not depend on the fluid cooling rate, but as shown in Section *4.3.4,* it depends on variations in fluid cooling rate. Variations in fluid cooling rate are occurring up to 5 times faster in the 50 MW_2 case during the first *6* years while being nearly equal for the two cases at later times.

(e) The mean fluid temperature drop fraction, and the reservoir rock energy extracted fraction are both larger for the 50 MWe case. This also results in a larger energy fraction produced because, as shown earlier, it is proportional to their product.

5. DISCUSSION

Energy extraction from the hot rock in a fracture-stimulated geothermal reservoir can be accomplished by two processes. In the first, net mass and energy removal from the reservoir produces a pressure reduction and eventually in-place boiling in the formation. The temperature of the geothermal fluid drops as the pressure of the saturated reservoir continues to decline. In the second case, the reservoir pressure is maintained at high values by reinjection of cold water. The cold water tends to cool the rocks and is heated as it flows towards the producing zone. Both processes produce a temperature difference between the hotter rocks and the surrounding geothermal fluid because of the resistance to heat transfer inside the rocks themselves (conduction), and at the rock surface (convection). This rock to fluid temperature difference is the "driving force" for heat transfer from the rock to the fluid and it varies for different rock sizes and shapes. However, as this temperature difference increases, the amount of energy that is left inside the rock mass as unrecoverable energy also increased.

The heat transfer limitations on the energy extraction process from fractured geothermal reservoirs were analyzed in the present study. The energy extraction from the rock was compared to the energy that would be extracted if the rock mass was cooled uniformly to the fluid temperature. Heat transfer from a single irregularly shaped rock was first studied for constant fluid cooling rate conditions. This analysis was extended to variable fluid cooling rate conditions, and the predicted rock temperature transients were compared to experimental results. The analysis was

subsequently applied to a collection of rocks with given size and shape distributions. Predicted results from the developed energy extraction model were compared to experimental data obtained for the in-place boiling and cold-water sweep processes. The energy recovered at the well head was related to the fluid cooling rate and the energy extraction from the rocks. Finally, the energy extraction model was applied to an hypothetical large-scale fracture-stimulated system using the cold-water sweep process.

5.1 Discussion of Analytical and Experimental Results

5.1.1 Single Rock Temperature Transient

Analysis of the temperature transient behavior of spherical rocks under constant fluid cooling rate conditions showed that for Biot numbers greater than 10, a rock behaves as if the Biot number were infinity. The minimum rock diameter for which the Biot number is greater than 10 is about 3.5 inches, assuming a non-boiling steam environment. The physical significance of large Biot numbers is that the resistance for heat transfer at the rock surface (convection) is negligible compared to the one inside the rock (conduction). The rock sizes in geothermal reservoirs can be hundreds of feet in diameter, and infinite Biot number thermal behavior can be generally assumed.

Analytical solutions for spherical rocks combined with the shape factor correlation developed by Kuo, Kruger, and Brigham (1976) were used to model the temperature transient behavior of irregularly shaped rocks. The Fourier and Biot numbers correlation factors were slightly modified to make them approximately equal to the sphericity factor (simple shape factor correlation in Kuo's development). This approximation is especially appropriate

for large Biot numbers (N_{Bi} greater than 10) because the Fourier number correlation factor is within 5 percent of the sphericity factor in the worst cases, whereas the Biot number correlation factor is within 25 percent. Since for Biot numbers greater than 10 the rock behaves as if N_{Bi} were infinity, a difference of 25 percent in the Biot number radius has a negligible effect in the rock to fluid temperature difference. This effect resulted in a satisfactory agreement between predicted and experimental results.

The one-lump parameter model was found to be within 3 percent of the exact analytical solution for spheres, when the Fourier number was greater than 0.3. Time-dependent corrections to the conduction path lengths were needed for smaller Fourier numbers. However, this correction was not needed when the solution for constant cooling rate was superimposed to model the variable fluid cooling rate conditions because of the relatively small contribution of the last constant fluid cooling rate intervals. The one-lump model was preferred over the exact solution because of the significant simplifications in evaluating the summations that resulted when the single rock solution was applied to a collection of rocks. Besides it represents a powerful "thinking tool" to analyze the energy extraction from fractured geothermal reservoirs.

The superposition of the one-lump parameter method to predict the temperature transients of irregularly shaped rocks was found to be in satisfactory agreement with experimental rock temperature data under variable fluid cooling rate conditions. Predictions were generally within 5 percent of the measurements. Predicted rock center temperatures were within the experimental uncertainties, in most of the cases. Higher

differences between the predicted and measured rock center temperatures were found when significant axial fluid temperature gradients were present. The thermocouples did not always measure the average fluid temperature surrounding the rock in those cases and a slight axial displacement would result in a large difference in the thermocouple reading.

5.1.2 Characterization of a Collection of Rocks

A statistical analysis of the granitic rock fragments used in the experiments revealed that the sphericity is essentially independent of the rock volume. It was also found that the sphericity is distributed according to a normal distribution and as such it can be fully described by its mean value and its standard deviation. Therefore, it was concluded that a collection of rocks can be completely characterized by the distribution of the equivalent sphere radius or the volume and by the mean value of the sphericity. The equivalent sphere radius R_s was distributed according to an exponential distribution and the mean value of the sphericity was determined to be 0.83. These observations were utilized in formulating a heat transfer model for a collection of rocks.

To characterize a collection of rocks with a single parameter, the concept of the "bulk-effective radius" was derived. It was defined as the radius of a sphere that has the same surface to volume ratio as a collection of rocks with a given size and shape distribution. In mathematical form,

$$R_{e,c} = \frac{3}{(A/V)_c}$$

where

$$(A/V)_c = 3 \times \frac{\sum_{j=1}^{N_L} p(R_{s,j})\, R_{s,j}^2}{\bar{\psi}_K \sum_{n=1}^{N_L} p(R_{s,j})\, R_{s,j}^3}$$

By analogy with the center of gravity, the "bulk-effective radius" can be thought of as the "thermal center" of a collection of rocks, i.e., the radius of a rock that behaves thermally as the collection of rocks. Evaluation of the bulk-effective radius for a collection of rocks with the equivalent sphere radius normally distributed showed that it is a function of the ratio of the standard deviation and the mean equivalent sphere radius. For the case of the equivalent sphere radius exponentially distributed, the bulk-effective radius is given by

$$R_{e,c} = 3 \cdot \bar{R}_s \cdot \bar{\psi}_K$$

Thus, the bulk-effective radius can be as large as three times the mean equivalent sphere radius depending on the value of the average sphericity.

The validity of the bulk-effective radius was verified by comparing the predictions of the energy extraction from a collection of rocks using the bulk-effective radius to the ones obtained by using the complete rock size distribution. It was found that the predictions using the bulk-effective radius were within 3 percent of the ones using the complete rock collection. The use of the bulk-effective radius significantly simplifies the calculations of the energy extraction from a collection of rocks. It is also the basis for the heat transfer model for the cold-water sweep model and the concept of the number of transfer units.

5.1.3 Energy Extraction from a Collection of Rocks

A methodology was developed to calculate the local energy extracted fraction for a collection of rocks with given size and shape distributions. It was found to be given by

$$F_{E,c} = \sum_{i=1}^{N} F_{E,i}\, \chi_i$$

where the energy extracted fraction from a single rock i is given by

$$F_E = \frac{T_1 - \bar{T}_r(X,t)}{T_1 - \bar{T}_f(X,t)}$$

and where the volumetric fraction of a single rock with volume v_i is given by

$$\chi_i = \frac{v_i}{\sum_{i=1}^{N} v_i}$$

The rock energy extracted fraction for a single rock measures how much energy has been extracted from a rock as compared to the energy that would be extracted if the rock mass was cooled uniformly to the surrounding fluid temperature.

In defining the local energy extracted fraction of a collection of rocks, it was assumed that the local temperature of the surrounding fluid is uniform through the space occupied by a representative collection of rocks. This assumption will generally require that the volume of the reservoir being considered be very large as compared to the size of a representative sample.

Based on this methodology, a sensitivity analysis was performed to determine the effect of the main physical parameters on the energy extraction from a collection of rocks. The parameters considered were: rock mean size, rock size distribution, and rock size dispersion characterized by the standard deviation about the mean. A summary of these results is given in Table 5-1. It shows the time required to extract 90 percent of the energy that would be

TABLE 5-1

Mean Equivalent Sphere Radii[a] (ft)	R_s Normal		R_s Exponential
	$\sigma_{R_s} = 0$	$\sigma_{R_s}/\bar{R}_s = 0.31$	
10	0.25	0.34	*0.4*	1.2
100	25 (1.0)[b]	*34* (1.36)	*40* (1.60)	115 *(4.6)*
1000	2500	*3400*	*4000*	11,500

extracted if the rocks were cooled uniformly to the fluid temperature under constant fluid cooling rate conditions. It can be seen that fracturing to produce rock mean radius of 100 ft or less is required to recover the energy in an average power plant lifetime of *30* years. However, it is not necessary to fracture too finely, as observed for mean equivalent sphere radius of 10 ft. For a given distribution, the time required to reach a specified value of the energy extracted fraction is proportional to the square of the mean equivalent sphere radius, if the ratio $\sigma_{R_s}/\bar{R}_s$ is kept constant. This is clearly seen in Table 5-1.

The rock size dispersion strongly affects the energy extracted fraction from a collection of rocks. If the volume normally distributed with a mean equivalent sphere radius of 100 ft is taken as a reference, a collection of rocks in which all the sizes are the same ($\bar{R}_s$ = 100 ft, $\sigma_{\bar{R}_s} = 0$), requires 36 percent more time to reach an energy extracted fraction of 0.90 (see ratios in parentheses in Table 5-1). If the radius is normally distributed and $\sigma_{\bar{R}_s}/\bar{R}_s = 0.31$, the collection requires 60 percent more time, and if

the radius is exponentially distributed the time required is 360 percent longer. The reason for this is that the volumetric fraction of the large rocks in the collection increases if the dispersion from the mean increases. This in effect displaces the "thermal center" of the collection towards larger values of the bulk-effective radius. Since the energy extracted fraction is inversely proportional to the rock radius squared, it decreased strongly as the dispersion from the mean radius increases.

The time required to reach a given value of the energy extracted fraction is also proportional to the square of the sphericity. Therefore, the smaller the sphericity, the shorter the time to reach a given energy extracted fraction, i.e., the further apart from a spherical shape, the better the heat transfer characteristics of the rocks are.

It was found that the energy extracted fraction does not depend on the fluid cooling rate itself but depends on the variations of the fluid cooling rate. It is better to have a decreasing fluid cooling rate than an increasing one to achieve high energy extracted fractions. The reason for this is that if the fluid cooling rate increases with time, the rock temperature accumulatively lags behind the fluid temperature. On the other hand, if the fluid cooling rate decreases, the rock has more time to adjust to changes in the temperature of the fluid.

The energy extraction model for a collection of rocks was applied to the laboratory model rock system and the predicted results were compared to the measured energy extracted fractions. The results showed that the uncertainties in the experimental measurements have to be significantly reduced to perform an adequate verification of the model. The main sources of experimental uncertainties resulted from the measurements of the production and injection fluid enthalpies.

5.1.4 Reservoir Energy Extraction

The "reservoir energy fraction produced" was defined as the energy that is actually produced at the well head as a fraction of the energy that would be produced if the final mean temperature of the fluid and rock was a given reference temperature. The overall rock energy extracted by the fluid in a reservoir is measured by the "reservoir rock energy extracted fraction," defined as the energy that is actually extracted from the rock in the reservoir as a fraction of the energy that would be extracted if the total rock mass was cooled uniformly to the mean fluid temperature. The "reservoir mean fluid temperature drop fraction" measures the degree to which the mean temperature of the fluid in the reservoir approaches a given reference temperature.

An energy balance of a geothermal reservoir was performed to relate the actual energy produced to the heat transfer limitations as characterized by the "reservoir rock energy extracted fraction," and to the fluid flow and thermodynamic limitations as characterized by the "reservoir mean fluid temperature drop fraction." The reservoir energy fraction produced is proportional to the "reservoir rock energy extracted fraction," and the "mean fluid temperature drop fraction." When the porosity is small enough so that the energy stored in the fluid is negligible, compared to the energy stored in the rock, the reservoir energy fraction produced is given by

$$F_p = \overline{F}_{E,c} \cdot \overline{F}_c$$

Thus, there are two main reasons why the energy fraction produced can be small: (1) Long conduction'path lengths which limit the heat

transfer from the rock to the fluid, i.e., low $\overline{F}_{E,c}$. (2) Limitations to cool the fluid such as fingering of the cold injected fluid to the production well, low permeability of the formation that does not allow enough circulation of the fluid, and the development of a superheated zone in the in-place boiling process, i.e., low $\overline{F}_c$.

5.1.5 Cold-Water Sweep Heat Transfer Model

A one-dimensional analytical model was developed to predict the temperature distribution in a cold-water sweep process with uniform external heat transfer from the boundaries. The non-dimensional fluid temperature was found to be a function of several non-dimensional parameters including the number of transfer units defined as the ratio of the fluid residence time to the bulk-effective rock time constant. The number of transfer units parameter was found to be an important measure to establish the conditions under which the energy recovery fromgeothermal reservoirs is heat-transfer limited. It is also a powerful tool to scale the energy extraction experiments performed in the laboratory model to full-scale geothermal reservoirs.

The heat transfer model was applied to the laboratory model and predicted results were compared to experimental data. To perform this comparison, the model was modified to account for variations in external heat transfer with location and time. It was assumed that the thermal capacitance of the vessel was uniform along the reservoir height. The comparison showed that predictions agreed qualitatively with the experiments. The differences are believed to be caused by the concentration of the vessel thermal capacitance in the heavy flanges in the lower portion of the steel vessel, which disagreed with the assumption of

uniform vessel thermal capacitance distribution. The high thermal capacitance of the vessel was found to cause a two-dimensional heat transfer effect resulting in slightly non-uniform cross-sectional temperature profiles in the reservoir model. A superposition of the solutions for different capacitance distributions is suggested for a more accurate modeling of the cold-water sweep experiments. The heat transfer model represents a significant addition to such analysis because it is valid for high Biot number systems. It is also simple to use.

It is important to point out that the present analysis takes into account the temperature noa-uniformities inside the rock segments produced by the long conduction path lengths and low rock thermal conductivity. Previous analyses, such as that by Schumann (1929) and by Löf (1948) for air flowing through a rock matrix, neglected the thermal resistance inside the rock itself. Therefore, these analyses are applicable to low Biot number systems only,

A sensitivity analysis was performed to study the effect of the number of transfer units parameter on the temperature of the produced fluid, the reservoir characteristic lifetime, the reservoir rock energy extracted fraction, and the reservoir energy fraction produced. It was found that the reservoir rock energy extracted fraction approaches unity when the number of transfer units are greater than 30 for the particular conditions analyzed. This means that the rocks approach thermal equilibrium with the surrounding fluid during the entire production period. For lower values of the number of transfer units, the reservoir rock energy extracted fraction decreases significantly and large amounts of recoverable energy are left inside the rock mass.

The reservoir lifetime is strongly affected by the number of transfer units when this is less than 30. For larger values the marginal improvement of lifetime for an increment in N_{tu} is very small. The same behavior was observed for the reservoir energy fraction produced. The reason for this is that the rock to fluid temperature difference is very small, when the reservoir rock energy extracted fraction approaches unity. Therefore, it is very difficult to extract the residual non-exploited energy in the rock mass, and large quantities of additional "transfer units" are needed to do it.

5.2 Applicability to Geothermal Reservoirs

The development of the energy extraction model for a collection of rocks and its application to model-scale geothermal reservoirs assumed that the rock size and shape distributions are known. This will generally not be the case in large-scale geothermal reservoirs. This information will have to be obtained by direct or indirect measurement, or it may be predicted if adequate fracturing models can be developed.

In a geothermal field, the developer obtains data on the formation, such as rock and fluid thermal properties, geochemistry, and fluid flow characteristics of the reservoir, from geologists, geochemists and reservoir engineers. These data can be currently obtained with fairly good accuracy, thanks to the state of the art of the oil and gas reservoir engineering. However, no data on the possible size and shape distributions on the rock in the formation is provided at the present time. The contribution of geologists and reservoir engineers to develop techniques to obtain this information is imperative for the development of the geothermal reservoir engineering in the area of naturally and artificially fractured reservoirs.

Analytic work is currently being performed to predict the rock size distribution produced by various fracturing techniques. Shockey et al. (1974) developed a model to simulate the conditions of dynamic impact experiments and compute the resulting fragment size distribution with Arkansas novaculite. The agreement between calculated and measured fragment size distribution illustrated that fragmentation behavior can be predicted from a few measurable rock properties. These and other techniques developed for underground nuclear explosions will have to be further evaluated. A very important technique is the utilization of thermal stress cracking in reducing the rock sizes.

Several methods have been developed for testing compact heat exchanger surfaces. Since the governing equations for transient heat transfer are very similar to the ones for flow in fluids through a collection of rocks, equivalent methods for testing geothermal reservoirs could be developed. Thesemethods utilize different techniques to determine the number of transfer units parameter, such as (a) maximum slope data reduction method; (b) zero intercept method; (c) direct curve matching method; and (d) first moment of area method.

For a broader range of number of transfer units, N_{tu}, Stang and Bush (1974) developed the "periodic method" to test compact heat exchanger surfaces. Description and references on these methods are reported in London and Sha (1976). However, it is questionable whether these techniques can be utilized in large-scale systems because of the large residence times involved.

6. CONCLUSIONS AND RECOMMENDATIONS

6.1 Conclusions

1. The resistance to heat transfer at the rock surface(convection)is negligible compared to the one inside the rock (conduction), for the rock sizes expected to be found in geothermal reservoirs. Therefore, significant amounts of energy may be left inside the rock mass as unrecoverable energy.

2. The sphericity factor appears to be independent of the rock size. Therefore, a collection of rocks may be fully characterized by the mean value of the sphericity and the distribution of the rock equivalent sphere radius. These can be combined into a single parameter defined as the bulk-effective radius.

3. The temperature transient in irregularly shaped rocks under variable fluid cooling rate conditions can be predicted with acceptable accuracy using superposition of the one-lump parameter solutions for spherical rocks, and applying the sphericity factor to account for the irregular shape. This solution is applicable for any value of the Biot number.

4. The energy recovery from a geothermal reservoir is limited by two main factors: (1) the degree to which the mean temperature of the fluid can be reduced, and (2) the amount of thermal energy that can be transferred from the rock to the fluid. The former is essentially a thermodynamic and fluid flow limitation and it is measured by the reservoir mean fluid temperature drop fraction. The latter is a heat transfer limitation, and it is measured by the reservoir rock

energy extracted fraction. The reservoir energy fraction produced is proportional to the product of the two factors.

5. The reservoir rock energy extracted fraction depends strongly on the rock size and shape distributions, and thermal properties of the rock. The time to reach a given value of the reservoir rock energy extracted fraction is inversely proportional to the square of the bulk-effective radius.

6. The reservoir rock energy extracted fraction depends on the variation in the fluid cooling rate and not on the fluid cooling rate itself. A decreasing fluid cooling rate produces a higher reservoir rock energy extracted fraction as compared to constant or increasing rates.

7. The number of transfer units parameter measures in a single parameter the dependence of the reservoir rock energy extracted fraction on the bulk-effective radius and the variations of fluid cooling rate for the cold-water sweep process. The reservoir rock energy extracted fraction approaches unity when the number of transfer units parameter is greater than a certain value determined by other reservoir parameters (storage ratio and external heat transfer parameters), which means that the rocks approach thermal equilibrium with the surrounding fluid during the entire production period. For lower values of the number of transfer units, the reservoir rock energy extracted fraction decreases rapidly and large amounts of recoverable energy are left inside the rock mass.

8. In the cold-water sweep process, the characteristic life time of the reservoir, t_c^*, depends on the number of transfer units and the

fluid residence time. The life of the reservoir approaches its maximum value, equal to several times the residence time, when the number of transfer units exceeds a certain value which depends on the values of the storage ratio and the external heat transfer parameter. The actual life of the reservoir may be longer, depending on the limitations imposed on the allowable drop in the produced fluid temperature.

9. The reservoir mean temperature drop fraction depends on the fluid residence time, the formation permeability for adequate fluid circulation, the creation of "hot spots" produced by fingering of the cold injected fluid to the production wells (in the cold-water sweep process), and the formation of a superheated steam zone (in the in-place boiling process). It also depends on the allowable drop in the production fluid temperature determined by the energy conversion cycle utilized.

10. The effect of microfractures resulting from high-energy fracturing techniques on the energy recovery from the rock is significant only when substantial flow of the geothermal fluid exists through the cracks. Signficant microfracture flow rates can only be achieved where the pressure gradient is high such as might be the case in the vicinity of a production well.

6.2 Recommendations

1. Improvement in the one-dimensional model to predict the fluid temperature distribution of the Laboratory model for the cold-water sweep process is recommended. A superposition technique is suggested to account for the variations of wall thickness throughout the vessel.

2. The development of a two-dimensional model for the cold-water sweep

process is recommended to assess the limitations on the energy recovery from geothermal reservoirs created by the production of "hot spots" and "fingering" of the cold injected fluid to the production wells.

3. It is recommended that improved instrumentation be installed in the production and reinjection lines of the laboratory model. Uncertainties in the measured production and injection fluid enthalpies should be reduced to about 5 percent, to reduce the uncertainties involved in the energy balance to an acceptable value.

4. Testing methods for indirect measurements of the number of transfer units (bulk-effective radius for a collection of rocks and fluid residence time) should be developed for the laboratory model based on the techniques developed for testing compact heat exchangers. The applicability of these techniques to large-scale systems should also be evaluated.

5. The simulation code developed by Shockey et al. (1974) should be applied to predict the rock size distribution for granite rock. These predictions should be compared to field data available from fractured rock chimneys created by nuclear explosives.

APPENDIX A

ROCK COLLECTION CHARACTERIZATION

To study the energy extraction process from a collection of rocks, certain parameters have to be properly characterized. The relevant parameter in the energy extraction from a single rock and a collection of rocks are described in Section 2.2.1. The characteristics of the rock loading were obtained in three forms:

1. Instrumented rock geometrical parameters. They are required to study and verify analytical models for the rock temperature transients.
2. Mean geometrical parameters and their distributions. These parameters describe the size and shape of the rocks which govern their temperature transient behavior.
3. Bulk parameters, which determine the total amount of energy that can be stored (or recovered) in the rock and the fluid.

Details on the size and shape measurements of individual rocks, the methodology to determine the required number of rocks that must be measured to obtain a representative sample of the rock collection, the sampling procedure, and some of the results not presented in Section 2, are described in the following.

A.1 Size and Shape Parameters

As described in Section 2.2.1, the relevant geometrical parameters intheenergy extraction process from an irregularly shaped rock are the

equivalent sphere radius R_s and the Kuo's sphericity ψ_K. The equivalent sphere radius is defined in Eq. 2.2 as the radius of a sphere with a volume equal to that of the irregularly shaped rock. Thus, the equivalent sphere radius can be readily determined from the weight and the density of the rock.

The Kuo's sphericity ψ_K is defined in Eq. 2.3 as the ratio of the surface area of a sphere of equal volume to the actual surface area of the rock. The determination of the actual surface area of the rock can be performed utilizing the paraffin coating technique developed by Kuo, Kruger, and Brigham (1976). This technique was used to determine the actual surface area of the instrumented rocks and a brief description of the process is presented in Section 2.2.2.

The measurement of the surface area of each individual rock in a collection of rocks (or a representative sample) using the paraffin technique is not practical. Therefore, an approximate method to determine either the rock surface area or the value of the Kuo's sphericity had to be determined. Hunsbedt, Kruger, and London (1975b) reported an approximate formula to evaluate the surface area of a rock as the area of a triaxial ellipsoid, whose three axes are estimated from the three orthogonal dimensions of a rock as illustrated in Figure A-1. The surface area of a triaxial ellipsoid was reported to be given by

$$A = \pi\left(\frac{b+c}{4b}\right)\left[b^2 + \frac{ab}{\sqrt{1-\left(\frac{b}{a}\right)^2}}\sin^{-1}\sqrt{1-\left(\frac{b}{a}\right)^2}\right] \qquad (A.1)$$

However, as it will be demonstrated in Appendix A.3.1, the difference between the surface area calculated from Eq. A.1 and the actual surface

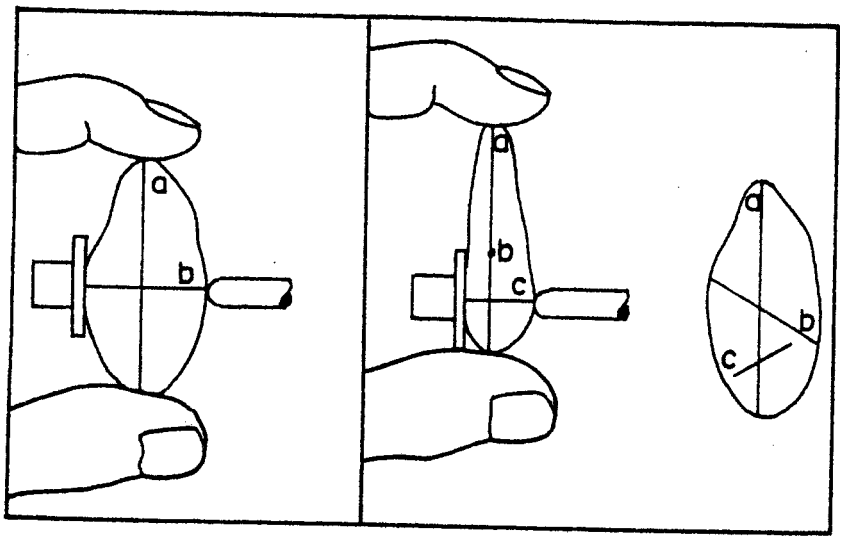

a = length
b = breadth
c = thickness

FIGURE A-1. Orthogonal dimensions of .the rock **(Hunsbedt,** Kruger, and London 1975b)

area of the rock can be as high as 55 percent depending on how close the shape of the rock is to that of a triaxial ellipsoid. Then, it was decided that instead of trying to approximate the actual surface area of the rock, the value of the Kuo's sphericity could be estimated directly as the Kuo's sphericity of a triaxial ellipsoid whose three axes are the rock orthogonal dimensions a , b , and c . Thus, the errors incurred in estimating the volume of the ellipsoid to calculate the surface area of an equal volume sphere, and the errors incurred in the calculation of the surface area (Eq. A.1) would tend to cancel each other, when their ratio was performed. The volume of a triaxial ellipsoid is given by

$$v = \frac{\pi\, abc}{6} \tag{A.2}$$

Therefore, the surface area of an equal volume sphere is given by

$$A_s = (36\pi)^{1/3}\, v^{2/3} = \pi(abc)^{2/3} \tag{A.3}$$

Recalling the definition of the Kuo's sphericity given by Eq. 2.3, the Kuo's sphericity of the triaxial ellipsoid referred to as the "pseudo Kuo's sphericity," ψ_K' , in this study is given by

$$\psi_K' \triangleq \frac{A}{A_s} = \frac{\pi(abc)^{2/3}}{\pi\left(\frac{a+b}{4b}\right)\left[b^2 + \frac{ab}{\sqrt{1-\left(\frac{b}{a}\right)^2}}\sin^{-1}\sqrt{1-\left(\frac{b}{a}\right)^2}\right]}$$

where A and A_s were substituted from Eqs. A.1 and A.3, respectively. Simplifying and rearranging:

$$\psi_K' = \frac{4}{\left(\frac{bc}{a^2}\right)^{1/3}\left(\frac{b}{c}+1\right)\left[1+\frac{(a/b)}{\sqrt{1-\left(\frac{b}{a}\right)^2}}\sin^{-1}\sqrt{1-\left(\frac{b}{a}\right)^2}\right]} \qquad (2.6)$$

The first factor in the denominator is the Krumbein sphericity used by Hunsbedt, Kruger, and London **(1975b),** which is defined as the cubic root of the ratio of the rock volume approximated by that of a triaxial ellipsoid to the volume of a circumscribing sphere:

$$\psi_H \triangleq \left(\frac{\pi\ abc/6}{\pi\ a^3/6}\right)^{1/3} = \left(\frac{bc}{a^3}\right)^{1/3} \qquad (2.7)$$

The accuracy of the pseudo Kuo's sphericity in estimating the actual value of the Kuo's sphericity was evaluated by comparing the estimated (ψ_K') and the actual values (ψ_K) for the six instrumented rocks. This comparison is presented in Section **2.2.2.**

A.2 Determination of the Size of a Representative Sample

A.2.1 Statistical Analysis

A basic principle in statistical inference is the so-called "Central Limit Theorem" which says that the arithmetic mean tends to be normally distributed as the number of samples increase in size, almost independently of shape of the original population. This is graphically explained in Figure A-2 which shows how the sample mean converges to the actual or "true mean" as the sample size increases. If the frequency distribution of the estimated sample means were plotted as the sample size increases, the shape of the distribution would tend to be that of a normal distribution as illustrated in Figure A-3. As the sample size

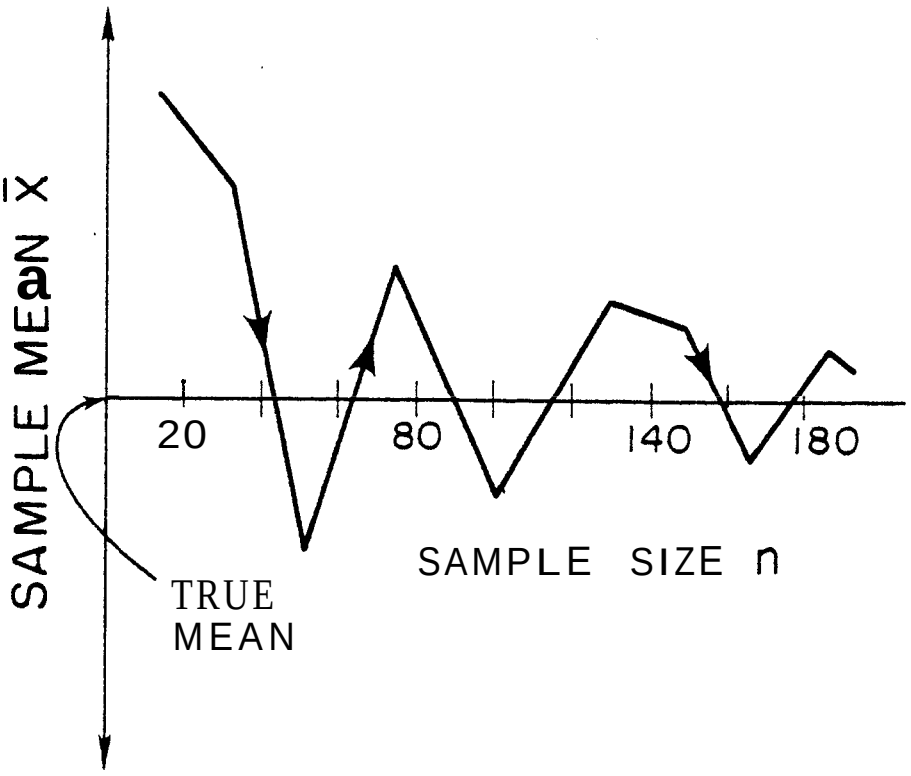

FIGURE A–2. Convergence of the sample mean to the true mean as the sample size increases

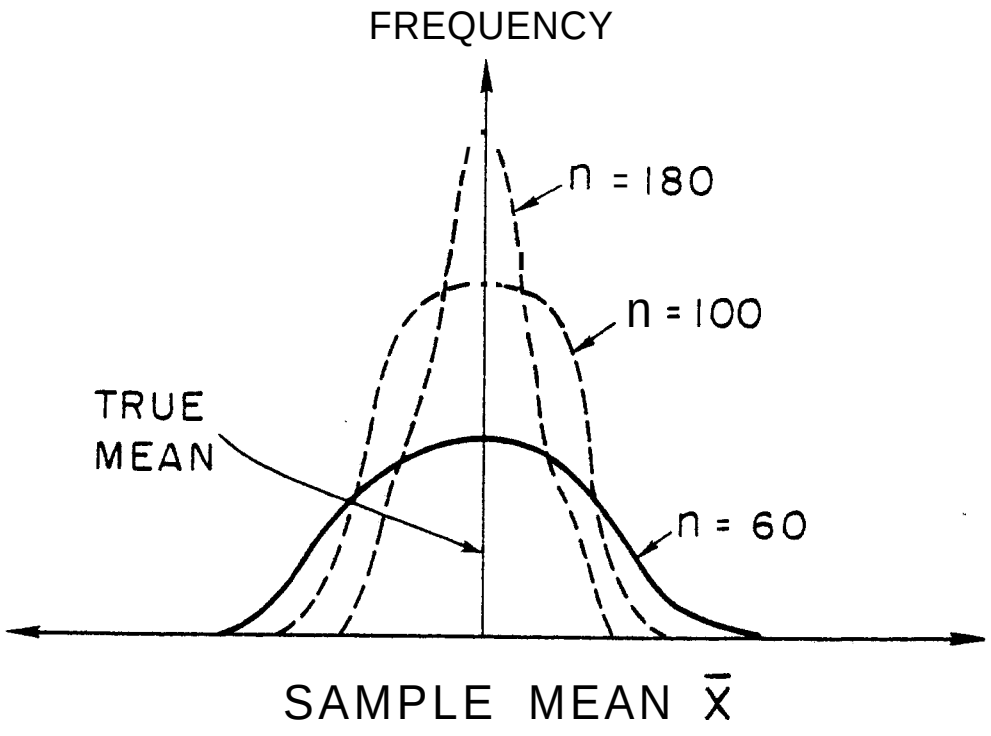

FIGURE A–3. Decrease of the dispersion of the sample mean from the true mean as the sample size increases

increases, the frequency of estimated means close to the actual mean increases.

Then, provided that the sample size is large, the distribution of sample means is normal or nearly so; and therefore it can be completely described by its mean and its standard deviation. Furthermore, these values may be estimated from a single large sample.

The standard deviation of the distribution of sample means is called the "standard deviation of a mean," and it measures (inversely) the precision of the sample estimate; that is, how closely the sample mean value is likely to approach the true mean value. When the population is large enough with respect to the sample size, the standard deviation of the mean or just standard error is given by:

$$\% \triangleq \frac{\sigma}{AT\cdot} \tag{A.4}$$

where σ is the standard deviation of the population which can be estimated from an initial sample as

$$\sigma_{\bar{X}} = S_{\bar{X}} = \frac{S}{\sqrt{n}} \tag{A.5}$$

where n is the sample size, and S is the estimated standard deviation of the population given by

$$S = \sqrt{\frac{\sum (X - \bar{X})^2}{n - 1}} = \sqrt{\frac{\sum X^2 - \left(\sum X\right)^2 / n}{n - 1}} \tag{A.6}$$

Therefore, as $\bar{X}$ and S can be estimated from an initial random sample, the standard error can also be fixed by the precision required, and the sample size can be computed from

$$S_{\bar{X}} = \frac{S}{\sqrt{n}} \quad \therefore \quad n = \left(\frac{S}{S_{\bar{X}}}\right)^2 \tag{A.7}$$

where $S_{\bar{X}}$ is given by the required level of confidence which has to be set in advance. The level of confidence is defined as the probability that the estimated mean will be within a certain affordable error. For example, for 95 percent level of confidence, $\bar{X}$ will be given by

$$\bar{X} \pm 1.96\ \sigma_{\bar{X}}$$

where the value $1.96\ \sigma_{\bar{X}}$ has to be equal or less than the affordable error. Thus, if $\bar{X}$ is desired to be within a certain value,

$$\bar{X} = \bar{X} \pm \delta_{\bar{X}}$$

for a desired 95 percent confidence level that it will happen, the probability that $\bar{X}$ will be less than $\bar{X} + \delta_{\bar{X}}$ and larger than $\bar{X} - \delta_{\bar{X}}$ should be 0.95 (or 95 percent, or 20:1 odds). Since the means are normally distributed,

$$p(\bar{X} - \delta_{\bar{X}} \leq X \leq \bar{X} + \delta_{\bar{X}}) = 0.95 = \int_{\bar{X}-\delta_{\bar{X}}}^{\bar{X}+\delta_{\bar{X}}} \frac{1}{\sqrt{2\pi}\,\sigma} e^{-\frac{1}{2}[(X-\bar{X})/\sigma]^2}$$

performing the integration and solving for $\delta_{\bar{X}}$ will yield

$$\delta_{\bar{X}} = 1.96\ \sigma_{\bar{X}}$$

The main problem in defining the minimum sample size is the predetermination of the permissible error $\delta_{\bar{X}}$. Once $\delta_{\bar{X}}$ is determined, the standard error of the mean is fixed for a given confidence level.

A.2.2 Uncertainty Analysis and Specification of the Standard Error of the Mean

The driving force for heat transfer from a rock to the surrounding fluid is the rock to fluid temperature difference. To minimize the uncertainty in the prediction of the energy extraction from a collection of rocks, the uncertainties on the required parameters to predict the rock to fluid temperature difference have to be minimized. The mean rock to fluid temperature difference is calculated for the quasi-steady state using Eq. 3.6:

$$\Delta T = \bar{T}_r - T_f = \frac{\mu R_s^2}{3\alpha} (0.2 + 1/N_{Bi}) \qquad (3.5)$$

It can be seen that this temperature difference is proportional to the square of the equivalent sphere radius. To find the allowable uncertainty on the mean value of the rock equivalent sphere radius, a sensitivity analysis of the uncertainty on the rock to fluid temperature difference was performed. For a first-order replication uncertainty and 95 percent confidence level, the uncertainty of the rock to fluid temperature difference is given by

$$6AT = \left\{ \left(\frac{\partial \Delta T}{\partial \alpha} \delta\alpha \right) 2 + \left(\frac{\partial \Delta T}{\partial \mu} \delta\mu \right) 2 + \left(\frac{\partial \Delta T}{\partial k} \delta k \right)^2 + \left(\frac{\partial \Delta T}{\partial h} \delta h \right) 2 + \left(\frac{\partial \Delta T}{\partial R_s} \delta R_s \right)^2 \right\}^{1/2} \qquad (A.8)$$

For the values given in Table A-1, the percentage uncertainty of the rock to fluid temperature difference is shown in Figure A-4 as a function of the rock equivalent sphere radius, R_s, and several values of the uncertainty on R_s. The convective heat transfer coefficient for vapor

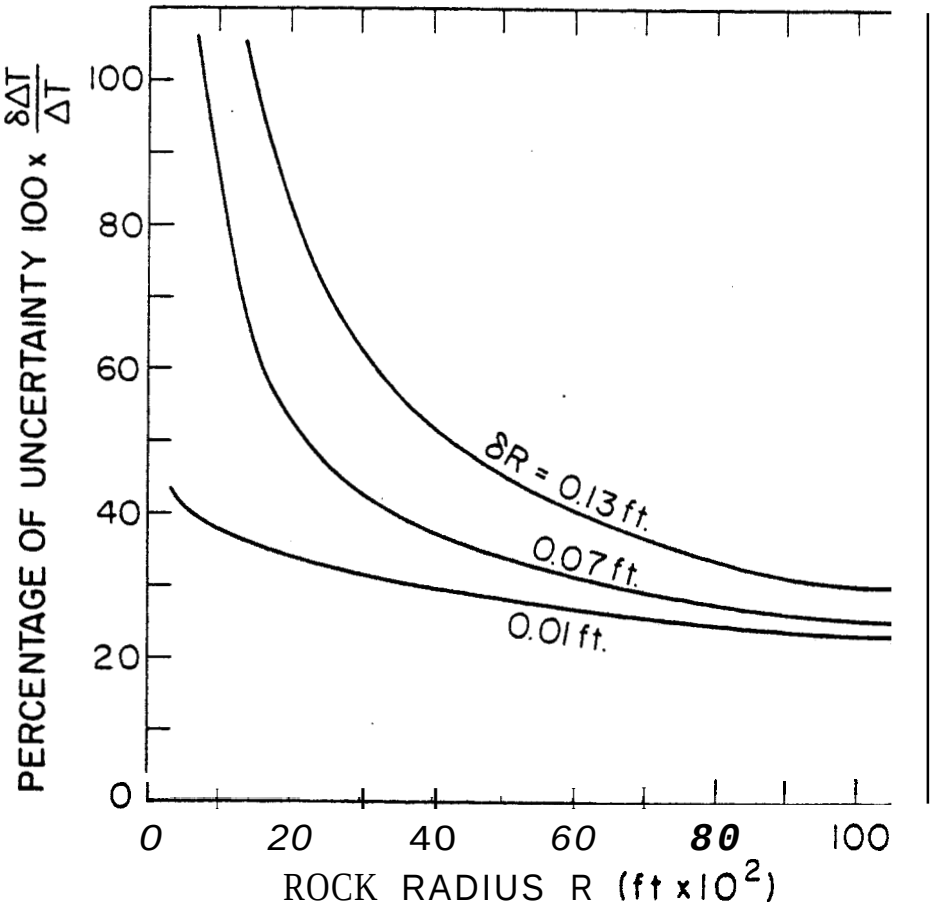

FIGURE *A-4.* Percentage of uncertainty as a function of rock radius and uncertainty of the rock radius

TABLE A-1

Parameter	Value
Thermal Diffusivity, α (ft^2/hr)	0.039 ± 0.005
Fluid Cooling Rate, μ (°F/hr)	12 ± 1.0
Thermal Conductivity, k (Btu/hr-ft-°F)	1.4 ± 0.2
Convective Heat Transfer Coefficient, h (Btu/hr-ft-°F)	3 ± 1[a]

environment was selected to consider the worst condition. It can be observed that the percent uncertainty increases strongly as the equivalent sphere radius decreases. It appears that independently of the value of R_s itself, the uncertainty δR_s must be 0.01 feet or less to have an acceptable value of the percent uncertainty on the rock to fluid temperature difference.

From this analysis, it was concluded that for an irregularly shaped rock, the maximum affordable uncertainty in any rock dimension should be equal or less than 0.01 feet (3 mm), i.e.,

$$\delta_a \leq 0.01 \text{ ft}$$
$$\delta_b \leq 0.01 \text{ ft}$$
$$\delta_c \leq 0.01 \text{ ft}$$

and for 95 percent confidence level, the standard deviation should be

$$S_a \leq 0.01/1.96 \text{ ft}$$
$$S_b \leq 0.01/1.96 \text{ ft} \qquad \text{(A.9)}$$
$$S_c \leq 0.01/1.96 \text{ ft}$$

Since individual rock weight measurements were used to find the volumes of the rocks, and the rock volumes, in turn, were used to calculate the equivalent sphere radius, the uncertainty in the equivalent sphere radius is given by

$$\delta R_s = \left(\frac{3}{4\pi}\right)^{1/3} \times \frac{1}{3} v^{-2/3} \delta v$$

It can be seen that the uncertainty on the rock volume is not very sensitive to the uncertainty in the equivalent sphere radius. Therefore, the number of rocks required to have a representative sample of the collection of rocks was based on the allowable standard deviation of the mean for the three rock dimensions, a , b , and c , as indicated in Eq. A.9.

A.2.3 Rock Sampling Procedure

A programmable calculator (HP-65) was used to compute the mean values, the standard deviation, the standard error of the mean, and consequently the required number of rocks to be measured. The following sampling procedure was performed:

1. A random sample of a convenient size was taken and the rock dimensions, a , b , c , and rock weight were measured. The sample standard deviation s was computed as an estimate of σ , the standard deviation of the collection of rocks.
2. The desired value of the standard error of the mean $\sigma_{\bar{X}}$ and the estimated standard deviation of the rock collection σ were used to calculate the required sample size n from Eq. A.7).

3. If the computed value of n was larger than the original random sample size, additional rocks were measured and a new standard deviation was computed to find a new n . This process was continued until the required and measured number of rocks were reasonably close.

A.3 Results

A.3.1 Instrumented Rocks

Six instrumented rocks were installed at different locations of the reservoir, as shown in Figure 2-5, to study the temperature transient behavior of individual rocks. Thermocouples were installed in the center of all of them and at the surface of rock number 3 to measure convection heat transfer coefficients. Prior to installing the instrumented rocks, their geometrical parameters were determined. The paraffin coating technique developed by Kuo, Kruger, and Brigham (1976) was used to measure the surface area. The volume was determined by water displacement in a calibrated tank, and the average density of the granite was calculated for the six rocks from their weight and volume measurements.

Table A-2 shows the measured rock dimensions a , b , and c , the measured mass and volume, and the calculated equivalent sphere diameter d_s $(2\ R_s)$, and rock density. It is seen that the value of the equivalent sphere diameter is somewhere between the rock dimensions a and c . It is also seen that the density varies from rock to rock. This variation is due to variations on the density of the granite itself and to uncertainties in the experimental measurements.

The calculated surface area of the rocks using Eq. A.1 as compared to the actual surface area measurements (paraffin technique) are also

TABLE A-2

Instrumented Rock Parameters

Parameter	1	2	3	4	5	6
Length, a (cm)	25	23	16	19	26	21.5
Breadth, b (cm)	11	21	10	12	18	15
Thickness, c (cm)	10.5	13	7	9.5	13	13
Equivalent Sphere Diameter, d_s (cm)	16.1	19.8	12.2	14.45	21.7	15.3
Mass (kg)	5.6	11.2	2.3	4.2	14.5	5.0
Volume (dm^3)	2.18	4.05	0.95	1.58	5.32	1.86
Density (g/cm^3)	2.57	2.77	2.42	2.66	2.73	2.69
Surface Area (in^2), Eq. A.1	110.1	184.9	58.7	88.3	177.54	132.8
Actual Surface Area (in^2) paraffin technique	137.4	236.3	76.5	109.2	260.6	131.8

shown in Table A-2. It can be observed that the calculated surface area using Eq. A.1 is about 20 percent lower than the actual measurements for rocks 1 to 4, and 32 percent lower for rock number 5. However, for rock number 6, the difference between the calculated and measured surface area is less than one percent. This indicates that Eq. A.1 does not provide an accurate and consistent formula to calculate the surface area of the rock. As it was discussed in Section A.1, it was decided to calculate the Kuo's sphericity directly instead of trying to calculate the surface area to obtain the sphericity. The method utilized is described in Section A.1, and the results are presented in Section 2.

A.3.2 Rock Size and Shape Distribution

Following the sampling procedure described in Section A.2.3., the main

rock geometrical parameters were measured for the 362 rocks required to have a representative sample. These parameters were: the rocks' three orthogonal dimensions, a , b , and c , and the rock weight. The rock volumes and equivalent sphere radius were calculated for each rock from the measured weights and density. Similarly, the pseudo **Kuo's** sphericity and other parameters to characterize the shape of the rocks such as b/a , c/a ratios and Krumbein sphericity were calculated for each rock from the measured rock dimensions. Table 2-2 presents a summary of the mean values and standard deviations of the measured and calculated parameters of the rock collection.

The frequency distribution of the equivalent sphere radius is shown in Figure 2-7. This distribution is approximately exponential. However, the rock orthogonal dimensions were found to be lognormally distributed. This characteristic was reported by Hunsbedt, Kruger, and London (1975b) for previous rock loadings. This distribution of the dimension a is shown in Figure A-5 plotted in a similog paper to illustrate the lognormal distribution.

Figure A-6 shows the frequency distribution of the rock volume. Note that the scale for the frequency is logarithmic. It can be observed that the collection of rocks is heavily concentrated in small rocks. However, when the volumetric fraction of each rock size interval is calculated using Eq. B.17b and Figure A-6, the proportion of the volumetric fraction of large rocks increases significantly, relative to the volumetric fraction of small rocks, as shown in Figure 2-10. In other words, if the collection of rocks contains only a few rocks which volume is significantly larger than the mean value of the rock volume for the collection, the volumetric fraction of these large rocks represents a large

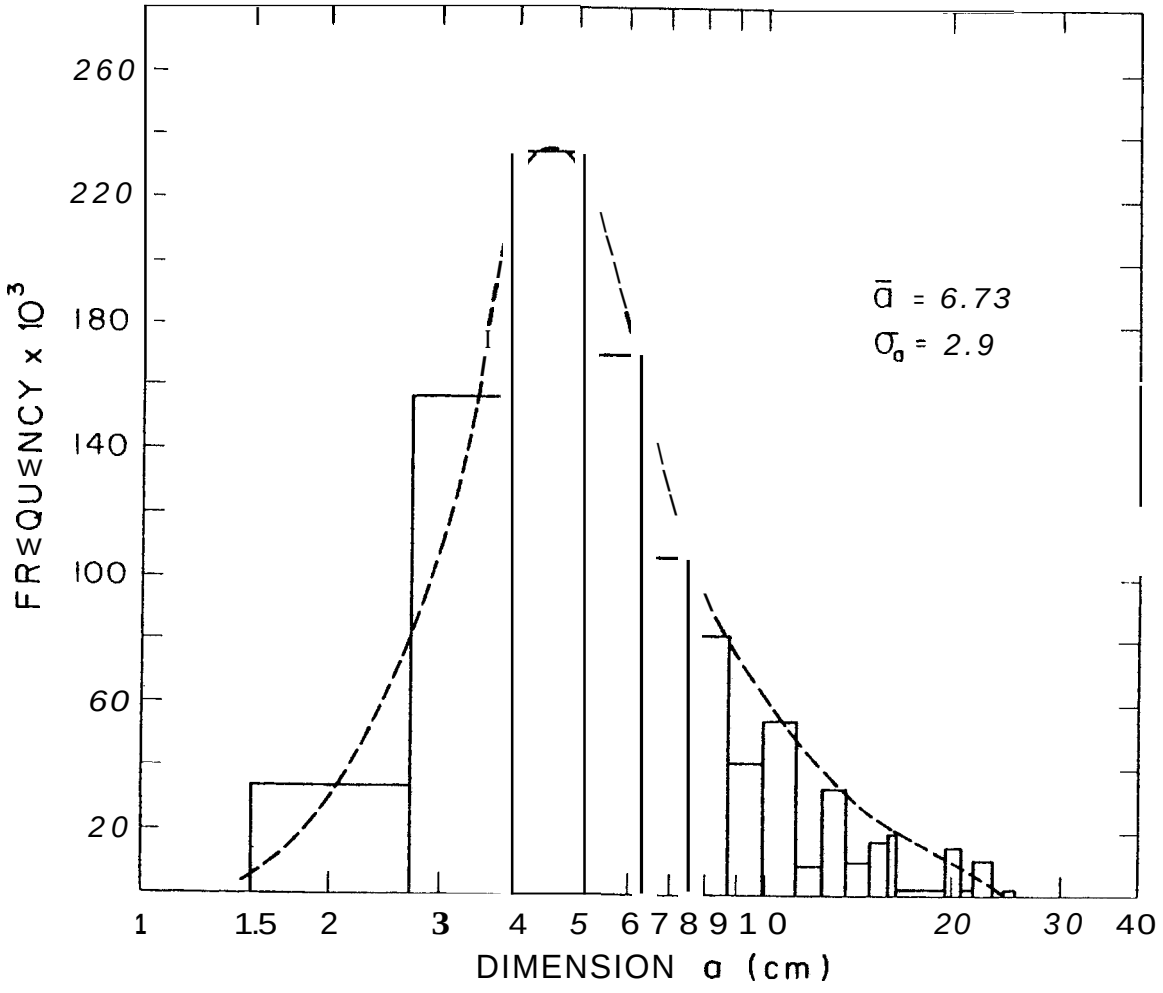

FIGURE **A–5.** Frequency distribution of dimension ***a***

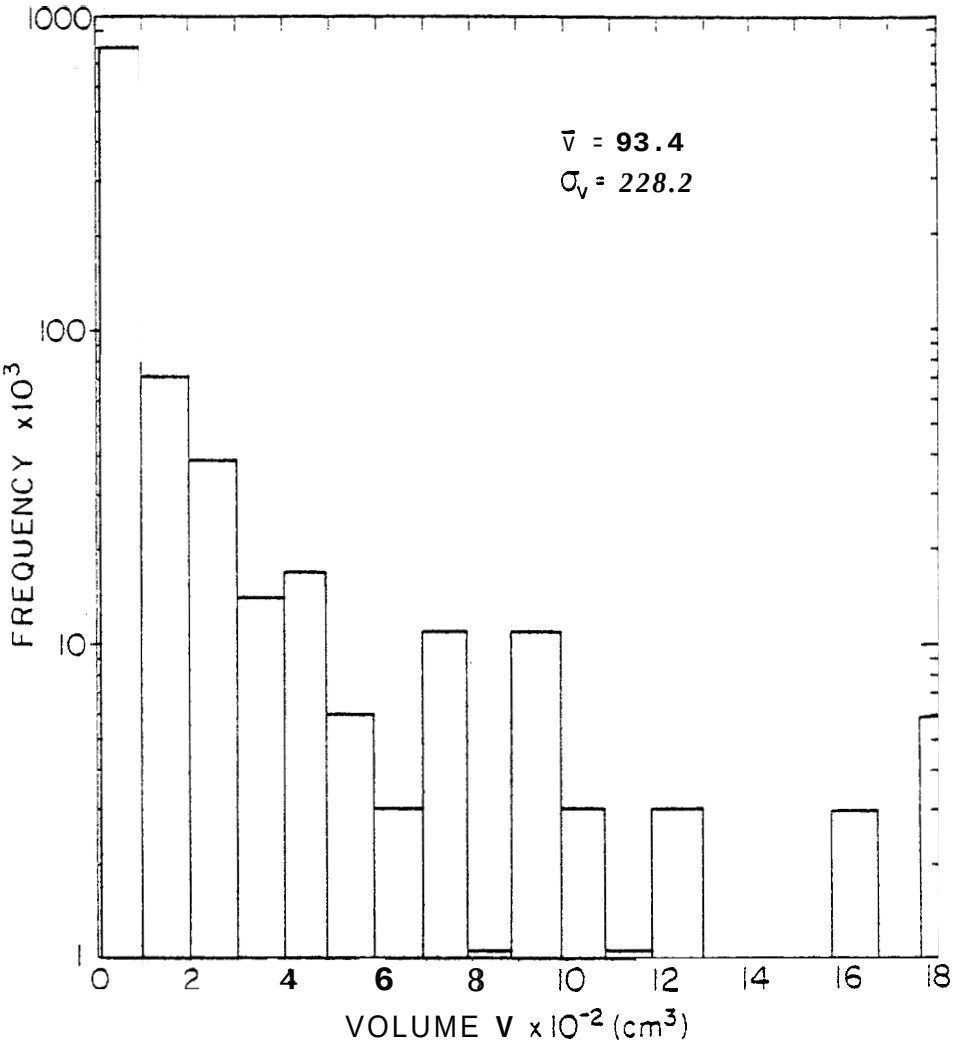

FIGURE A-6. Frequency distribution of the rock volume V

proportion of the total rock volume, and therefore a large proportion of the recoverable energy.

The pseudo Kuo's sphericity frequency distribution is shown in Figure 2–8. The shape of the distribution appears to be that of a normal distribution with the tail end of the high values cutted at a maximum value of 1.0 imposed by definition of the Kuo's sphericity. It was found that the parameters related to the shape of the rock tend to be normally distributed. This characteristic was also reported by Hunsbedt, Kruger, and London (1975b). To illustrate the characteristic, the frequency distribution of the Krumbein distribution and the ratio b/a are shown in Figures A–7 and A–8, respectively,

A statistical analysis was performed to investigate the dependence of the rock shape on the rock size. The BMD-02R package computer program for regression analysis was used to analyze the dependence of the pseudo Kuo's sphericity as a function of the equivalent sphere radius, and the predicted values from the calculated regression equation. It was found that only 1.95 percent of the variations of the pseudo Kuo's sphericity from its mean value were explained from variations on the equivalent sphere radius. Therefore, it was concluded that for practical purposes the pseudo Kuo's sphericity is independent of the rock size, and that its mean value can be used to characterize the shape of a collection of rocks.

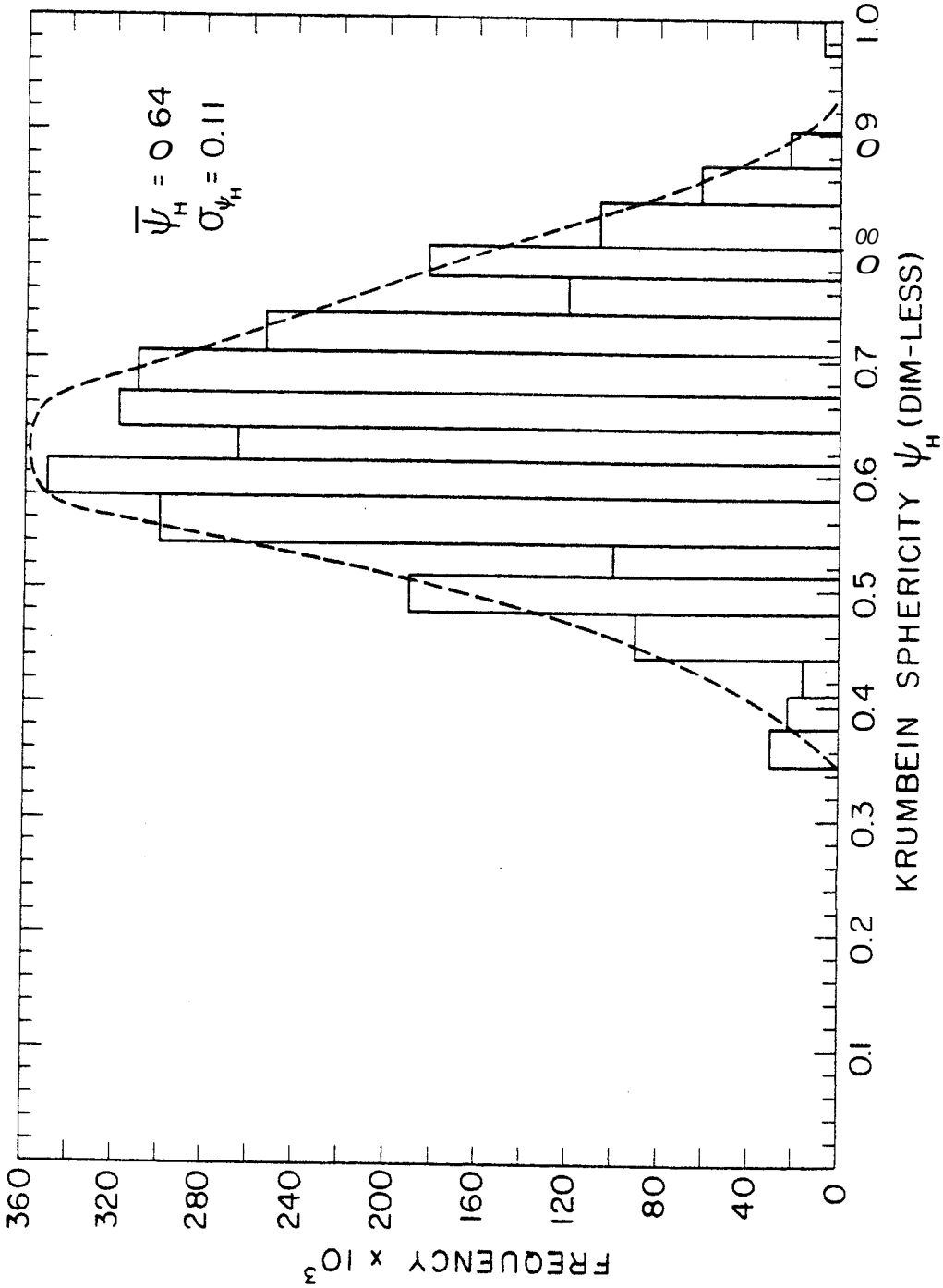

FIGURE A-7. Frequency distribution of Krumbein sphericity ψ

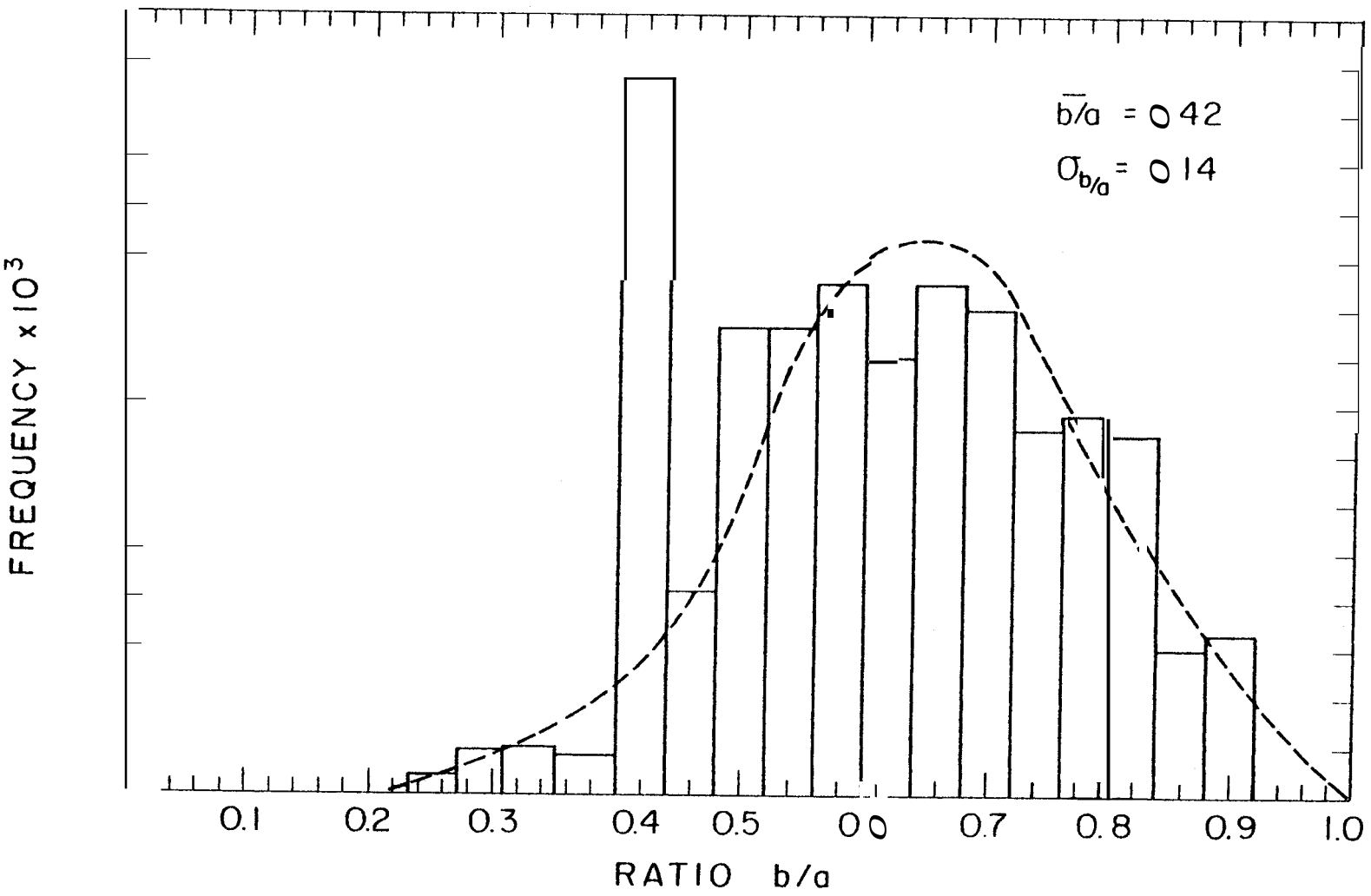

FIGURE 28 Frequency Distribution of ratio b/a

APPENDIX B

DETAILS OF **ANALYSIS**

B.1 Exact Analytical Solution for Spherical Rocks

In Section 3.1.1 the solutions for the temperature transient in spherical rocks is formulated, as a requisite to predict the energy extracted fraction from a single rock. Figure 3-1 describes the physical model of the rock temperature transient for constant fluid cooling rate conditions. If the idealizations listed in Section 3.1.1 are made, from conservation of energy and rate equation considerations a one-dimensional boundary value problem results:

$$\text{PDE:} \quad \frac{\partial T_r}{\partial t} - \frac{\alpha}{r^2}\frac{\partial}{\partial r}\left(r^2 \frac{\partial T_r}{\partial r}\right) = 0$$

$$\text{BC:} \quad \frac{\partial T_r}{\partial r} = 0 \quad \text{at} \quad r = 0$$

$$\frac{\partial T_r}{\partial r} + \frac{h}{k} T_r = -\frac{h}{k}\mu t \quad \text{at} \quad r = R$$

$$\text{IC:} \quad T_r(r,0) = T_1$$

The solution to this problem is given by Hunsbedt, Kruger, and London (1975b) and by Carslaw and Jeager (1957), in non-dimensional form:

$$\frac{T_r(r^*,t) - T_f(t)}{\mu R^2/\alpha} = \frac{(1/2 + 1/N_{Bi}) - r^*/2}{3} - \frac{2N_{Bi}}{r^*} \sum_{n=1}^{\infty} \frac{\sin \beta_n r^* \, e^{-\beta_n^2 N_{Fo}}}{\beta_n^2[\beta_n^2 + N_{Bi}(N_{Bi} - 1)]\sin \beta_n} \tag{B.1a}$$

where the eigenvalues are $\beta_n (n = 1,2...)$ are the roots of the transcendental equation,

$$\beta \cot \beta + (N_{Bi} - 1) = 0 \tag{B.1b}$$

To verify experimentally the temperature transient prediction, the rock center temperature is of particular interest. Finding the limit when $r^* \to 0$ yields, in non-dimensional form,

$$\frac{T_r(0,t) - T_f(t)}{\mu R^2/\alpha} = \frac{(1/2 + 1/N_{Bi})}{3} - \sum_{n=1}^{\infty} \frac{2N_{Bi}\, e^{-\beta_n^2 N_{Fo}}}{\beta_n[\beta_n^2 + N_{Bi}(N_{Bi} - 1)] \sin \beta_n} \quad (B.2)$$

where the non-dimensional variables are defined in the nomenclature. *Also,* the mean temperature of rock defined from the energy storage point of view is of interest to evaluate the energy extracted fraction. Its definition is formulated in Eq. 3.3 as

$$\bar{T}_r \triangleq \frac{\int_V \rho\, c\, T_r(r^*,t)dV}{\rho\, c\, V} \quad (B.3a)$$

or

$$\bar{T}_r = 3 \int_0^1 T_r(r^*,t)\, r^{*2}\, dr^* \quad (B.3b)$$

Substituting Eq. B.1a into B.3b yields

$$\frac{\bar{T}_r(t) - T_f(t)}{\mu R^2/\alpha} = \frac{(1/5 + 1/N_{Bi})}{3} - \sum_{n=1}^{\infty} \frac{6N_{Bi}^2\, e^{-\beta_n^2 N_{Fo}}}{\beta_n^4[\beta_n^2 + N_{Bi}(N_{Bi} - 1)]} \quad (B.4)$$

The solution of Eq. B.1 for $N_{Bi} \to \infty$ is interesting, since the size of the rocks to be considered will usually result in high Biot numbers:

$$\frac{\bar{T}_r(t) - T_f(t)}{\mu R^2/\alpha} = \frac{1}{15} - \sum_{n=1}^{\infty} \frac{6\, e^{-\beta_n^2 N_{Fo}}}{\beta_n^4} \quad (B.5)$$

with

$$\beta_n = (2n-1) \times \pi \ , \quad n = 1,2,\ldots,\infty$$

Finally, the rock surface temperature is needed to experimentally find the convective heat transfer coefficients. Finding the limit when $r^* \to 1$ in Eq. B.1 yields

$$\frac{T_r(r^*=1,t) - T_f(t)}{\mu R^2/\alpha} = \frac{1}{3N_{Bi}} - 2N_{Bi} \sum_{n=1}^{\infty} \frac{e^{-\beta_n^2 N_{Fo}}}{\beta_n^4[\beta_n^2 + N_{Bi}(N_{Bi} - 1)]} \qquad (B.6)$$

Clearly, when $N_{Bi} \to \infty$, the rock surface-fluid temperature difference is zero, since the thermal resistance at the rock surface is negligible.

B.2 One-Lump Parameter Solutions

A complete description of the one-lump solution is given in Section 3.1.2. Figure 3-3 shows the physical model and the corresponding thermal circuit. Solution of the thermal circuit yields

$$\rho V c \frac{dT_r}{dt} = \frac{T(t) - T_r(t)}{R_o} \qquad (B.7)$$

where R_o is given by Eq. 3.8a. Recalling that $T_f(t) = T_1 - \mu t$ results in

$$\frac{dT_r}{dt} + \frac{T_r}{R_o C} = \frac{T_1 - \mu t}{R_o C} \qquad (B.8a)$$

with

$$C \triangleq \rho V c \qquad (B.8b)$$

Multiplying Eq. B.8a by e^{t/R_oC} yields

$$\frac{d}{dt}\left(T_r\, e^{t/R_oC}\right) = \frac{(T_1 - \mu t)\, e^{-t/R_oC}}{R_oC}$$

Integrating and simplifying

$$T_r = T_1 - \mu t - \mu R_o C + I\, e^{-t/R_oC}$$

Applying the initial condition, $T_r = T_1$, at $t = 0$, to find the integration constant I, results in

$$T_r - T_f = \mu R_o C(1 - e^{-t/R_o C}) \qquad (B.9)$$

where the integration constant $I = \mu R_o C$,

B.3 Variable Fluid Cooling Rate Solutions

To model the temperature transient of a rock for variable fluid cooling rate conditions, let the initial temperature of the fluid and rock be T_1 . Let also the fluid temperature start to vary at any arbitrary time $t = 0$, and let it be represented by a series of infinitesimal changes of constant cooling rates, as shown in Figure 3-7a and b. Then the cooling rate will behave as a series of infinitesimal steps, or finite, or both. The rock temperature at any time t can then be determined by summing the contribution of each of the steps, either infinitesimal or finite. For the summarion to be considered, t is the point of time at which it is desired to determine the rock temperature, and thus t is treated as a constant. A dummy time variables ξ , is used to designate the location of each step; ξ thus varies from 0 to t .

Consider now the solution for the rock-fluid temperature difference at a time t resulting from a single step in fluid temperature cooling rate (Eqs. 3.2 and 3.4 or 3.11) and let it be expressed in general form as

$$\Delta T = T_r - T_f = \Delta\mu \times f(\tau, t) \qquad (B.10)$$

Notice that in Eqs. 3.2, 3.4, and 3.11, $\Delta\mu = (\mu - 0) = \mu$, since there is only one step change from a zero initial value to μ .

Now, if the step in fluid cooling rate occurs at ξ the same solution applies but ΔT at time t becomes

$$\Delta T = \Delta\mu \cdot f(\tau, t - \xi)$$

This fact can be well understood by looking at Figure 3-7c. Then,

an infinitesimal change in ξ will also produce an infinitesimal change in ΔT :

$$d(\Delta T) = d\mu \times f(\tau, t - \xi) \tag{B.11}$$

or

$$\frac{d(\Delta T)}{du} = f(\tau, t - \xi)$$

The complete solution for the rock-fluid temperature difference at time t must be simply the summation of the contribution of all the infinitesimal steps in fluid cooling rate (or finite). The linearity and homogeneity of the governing partial differential equation assure that such a sum of solutions still satisfies the differential equation

$$\Delta T(t) = \int_{\mu_o}^{\mu} f(\tau, t - \xi)\, d\mu \tag{B.12}$$

but

$$d\mu = \frac{\partial \mu}{\partial \xi}\, d\xi$$

and

$$\mu_o = 0$$

Then,

$$\Delta T(t) = \int_{0}^{t} f(\tau, t - \xi) \times \frac{\partial \mu}{\partial \xi}\, d\xi \tag{B.13a}$$

or

$$\Delta T(t) = \sum_{i=1}^{n} f(\tau, t - \xi) \times \Delta \mu_i \tag{B.13b}$$

The utilization of Eqs. B.13 is illustrated in Section 4, where the

one-lump solution is used for $f(\tau, t - \xi)$, i.e.,

$$\Delta T(t) = \sum_{i=1}^{n} \tau\left[1 - e^{-(t-\xi)/\tau}\right] \Delta\mu_i \qquad \text{(B. 13c)}$$

Numerical solution of Eqs. B.13 can be readily performed by making use of Figures 3-3 and 3-4 for rock center-fluid temperature differences and mean rock-fluid temperature differences, respectively. A computer program to facilitate its use (Eq. B.13c), when several steps are considered, is shown in Appendix B.4. By inspection of Eq. B.13c, it can be seen how the application of the one-lump solution for this purpose greatly simplifies the analysis compared to the exact analytical solution.

B.4 Computer Program to Predict the Rock Temperature Transient and Energy Extracted Fraction

```
      SWATFIV
      C  SUPERPOCITION OF CONSTANT COOLING RATE
    1       CIMENSICN TR(40),TF(40),Z(40),XT (40),ETA(40),F(40),XMU(40),TD(40)
           1,TDBAR(40),TDA(40),TX(40),YMU(40),XD(40),XDBAR(40),TBAR(40),TRP(40
           2)
    2       READ(5,3)HL,HV
    3     3 FORMAT(2F5.2)
    4       PRINT,HL,HV
    5       READ(5,1)K,N,RE,RF,A,XK,DELC,DELS,XL,XI
    6     1 FORMAT(2I5,6F7.3)
    7       PRINT,J,N,RE,RF,A,XK,DELC,DELS,XL,XI
    9       RF=RF/12.
    9       RE=RB/12.
   10     2 FORMAT(4(6X,F14.7))
   11       READ(5,2)(XT(I),TR(I),TF(I),Z(I),I=1,N)
   12       M=N-1
   13       DO 10 I=1,M
   14       DEXT=XT(I+1)-XT(I)
   15    10 YMU(I+1)=(TF(I)-TF(I+1))/DEXT
   16       YMU(1)=0.0
   17       DO 15 I=1,N
   18    15 TDA(I)=TR(I)-TF(I)
   19       B1=HL*RB/XK
   20       B2=HV*RB/XK
   21       DO 20 I=1,N
   32       Z(I)=50.0*Z(I)
   23    2C CONTINUE
   24       TA=(RF**2)/(3*A)
   25       TAUS2=TA*(DELS+(1/B2))
   26       TAUS1=TA*(DELS+(1/B1))
   27       TAUC2=TA*(DELC+(1/B2))
   28       TAUC1=TA*(DELC+(1/B1))
   29       DO 41 J=1,M
   33    41 XMU(J+1)=YML(J+1)-YML(J)
   31       XMU(1)= 0.0
   32       PRINT,(XMU(I), I=1,N)
   33       DO 51 I=2,N
   34       S=0.0
   35       SBAR=0.0
   3d       DO 50 J=2,I
   37       TX(J)=XT(I)-XT(J-1)
   38       TB=XT(I)-XI
   39       IF(TB.LE.0)GO TO 11
   40       T=TB
   41       XE=XI
   42       GO TO 21
   43    11 XE=TX(J)
   A4       FU=XE/(TA*3)
   45       T=0.
```

```
      21 XD(J)=XMU(J)*TAUC1*(1-EXP(-XE/TAUC1))+XMU(J)*TAUC2*(1-EXP(-T/TAUC2
     C))
         CALL TRAPS(0.1000,1000.1,1)
         PRINT,TAUS1,XE,TAUS2,T,FU
         XDBAR(J)=XMU(J)*TAUS1*(1-EXP(-XE/TAUS1))+XMU(J)*TAUS2*(1-EXP(-T/TA
        CUS2))
         CALL TRAPS(0.1000,1000.1,1)
         S=S+XD(J)
      50 SBAR=SBAR+XDBAR(J)
         TD(1)=0.0
         TDBAR(1)=0.0
         TD(I)=S
         TDBAR(I)=SBAR
         TRP(I)=TD(I)+TF(I)
         TBAR(I)=TDBAR(I)+TF(I)
      51 ETA(I)=(1-(TBAR(I)/TF(1)))/((1-(TF(I)/TF(1)))+0.00001)
         WRITE(6,5)K,RB,RF,A,XK,XL
       5 FORMAT (10X,'ROCK NUMBER=',I2,2X,'BIOT RADIUS=',F5.3,2X,'FURIER
        1RADIUS=',F5.3,2X,'THERMAL DIFF=',F5.3,2X,'THERMAL CONDU=',F5.2,2X,
        2'LEVEL=',F5.2)
         WRITE(6,6)
       6 FORMAT(6X,'TIME',8X,'TR-TF',7X,'(TR-TF)A',4X,'TDBAR-TF',7X,'EFFIC'
        1,6X,'TR',10X,'TF',8X,'LIQU LEV',4X,'TRP')
         WRITE(6,7)(XT(I),TD(I),TDA(I),TDBAR(I),ETA(I),TR(I),TF(I),Z(I),TRP
        1(I),I=1,N)
       7 FORMAT(9(5X,F7.3))
         STOP
         END
```

B.5 Volumetric Fraction as a Function of Size Distribution

When the volumetric fraction of the different rock volumes in a collection of rocks is not known, the frequency distribution can be easily obtained from statistical sampling as described in Appendix A.3. However, the magnitudes of the volumetric fraction are required for the evaluation of the local energy for a collection of rocks.

The volumetric fraction was defined in Eq. 3.29b as

$$\chi_i \triangleq \frac{v_i}{\sum_{i=1}^{N} v_i} \qquad (B.14)$$

Also, the arithmetic mean of the individual rock volume is defined as:

$$\bar{v} \triangleq \frac{\sum_{i=1}^{N} v_i}{N} \qquad (B.15)$$

The total rock volume can then be expressed as

$$\sum_{i=1}^{N} v_i = N \cdot \bar{v} \qquad (B.16)$$

If n_i is the number of rocks with volume v_i, the volumetric fraction of this group of rocks is

$$\chi_i = \frac{n_i v_i}{N \cdot \bar{v}} \tag{B.17a}$$

But the fraction n_i/N is by definition the probability $p(v_i)$ of having a rock with volume v_i in the collection of rocks provided that the sample is sufficiently large. Then the volumetric fraction can be expressed as

$$\chi_i = p(v_i) \times \frac{v_i}{\bar{v}} \tag{B.17b}$$

The volumetric fraction of a group of rocks with a given volume is seen to be proportional to the probability of having a rock with that volume in the rock collection and to the relative size as compared to the mean size.

B.6 Effect of Microfractures on Rock Thermal Properties

To qualitatively analyze the possible effect of microfractures on the rock thermal properties, two different arrangements of the cracks with respect to the direction of the temperature gradient were analyzed: first, when the cracks are perpendicular to the temperature gradient, and second, when the cracks are parallel to them.

B.6.1 Microfractures Perpendicular to the Temperature Gradient

Figure B-la shows the physical model and corresponding thermal circuit for one-dimensional heat transfer in a rectangular bar with a length L, and thickness and width equal to unity. The bar has η cracks of thickness t_c perpendicular to the temperature gradient. Solving the

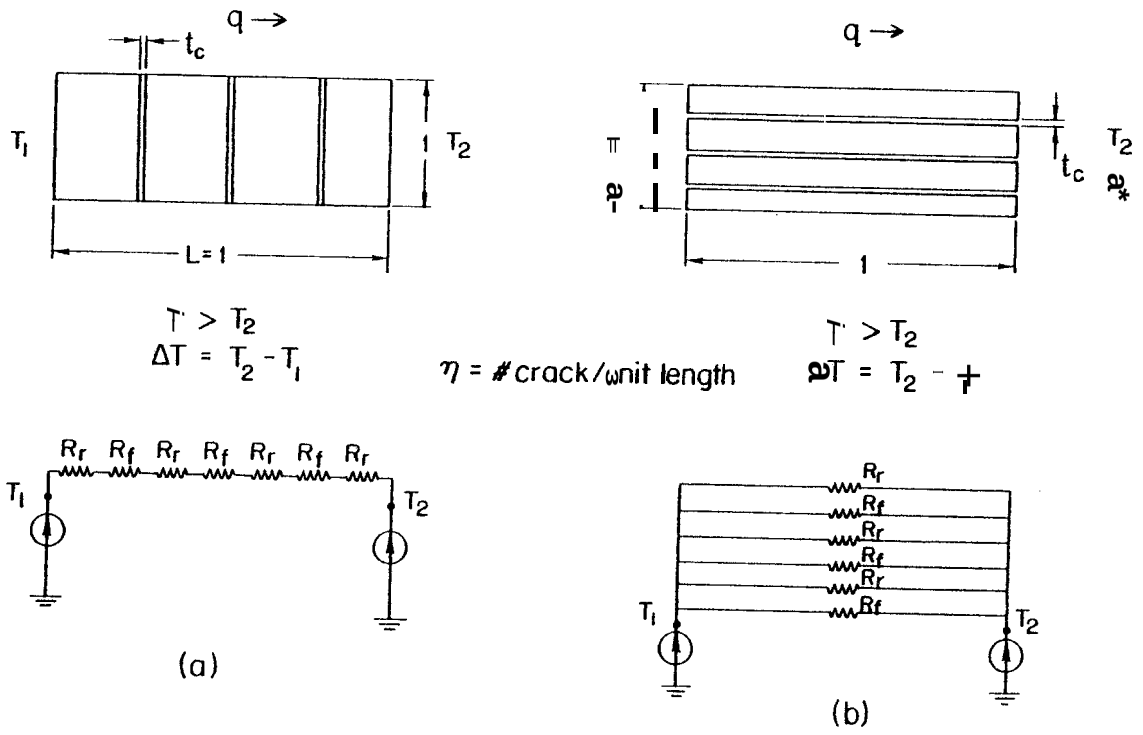

FIGURE B-1. Physical models and thermocircuits to study the effect of microfractures on the thermal properties of the rock. (a) Series model. (b) Parallel model

thermal circuit, the heat transfer per unit area is given by

$$q'' = \frac{\Delta T}{R_T} \tag{B. 18}$$

where R_T is given by

$$R_T = \sum R_r + \sum R_f$$

since the resistances are in series. For the same reason,

$$\sum R_r = \frac{L - \eta t_c}{k_r}$$

$$\sum R_f = \frac{}{k_f}$$

Let $L = 1$ and η the number of cracks per unit length. Then,

$$R_T = \frac{k_f(1 - \eta t_c) + k_r \eta t}{k_r k_f}$$

Simplifying and rearranging,

$$R_T = \frac{1 + \eta t_c \left(\frac{k_r}{k_f} - 1\right)}{k_r} \tag{B.19}$$

If the effective thermal conductivity is defined such that

$$q'' = \frac{\Delta T}{R_T} \quad \text{with} \quad R_T = \frac{1}{k_e} \tag{B. 20}$$

comparison of Eqs. B.20 and B.19 yields

$$k_e = k_r \left\{ \frac{1}{1 + \eta t_c \left(\frac{k_r}{k_f} - 1\right)} \right\} \tag{B. 21}$$

By definition the density is given by

$$\rho_e = \frac{\text{mass}}{\text{vol}} = \frac{\rho_r(1 - \eta t_c) + \rho_f \eta t_c}{1 \times 1 \times 1}$$

or

$$\rho_c = \rho_r \left\{ 1 - \eta t_c \left[1 - \frac{\rho_f}{\rho_r} \right] \right\} \tag{B. 22}$$

Also by definition, the specific heat is

$$c_e = \frac{\rho_r(1 - \eta t_c)c_r + \rho_f \eta t_c c_t}{\rho_r(1 - \eta t_c) + \eta t_c \rho_f}$$

or

$$c_e = c_r \left\{ \frac{1 + \frac{\rho_f c_f}{\rho_r c_r} \left[\frac{\eta t_c}{1 - \eta t_c} \right]}{1 + \frac{\rho_f}{\rho_r} \left[\frac{\eta t_c}{1 - \eta t_c} \right]} \right\} \tag{B. 23}$$

Combining Eqs. B.21, B.22, and B.23, the thermal diffusivity is given by

$$\alpha \triangleq \frac{k_e}{c_e \rho_e} = \alpha_r \left\{ \frac{1}{\left[1 + \eta t_c \left[\frac{k_r}{k_f} - 1 \right] \right] \left[1 - \eta t_c \left[1 - \frac{\rho_f c_t}{\rho_r c_r} \right] \right]} \right\} \tag{B. 24}$$

B.6.2 Microfractures Parallel to the Temperature Gradient

B.6.2.1 Without fluid flow through the cracks: Similarly to the case of perpendicular fractures, Figure B-lb shows the physical model and corresponding thermocircuit for the case of cracks in the same direction as the temperature gradient. Again, solving the thermocircuit yields

$$q'' = \frac{\mathbf{AT}}{R_T} \tag{B. 25a}$$

with

$$\frac{1}{R_T} = \sum \frac{1}{R_r} + \sum \frac{1}{R_f} \qquad \text{(B.26b)}$$

since the resistances are in parallel. For a unit length,

$$\frac{1}{R_T} = \frac{(1 - \eta t_c)}{(1/k_r)} + \frac{\eta t_c}{1/k_f} \qquad \text{(B. 27)}$$

and comparing Eq. B.27 with Eq. B.20,

$$k_e = k_r(1 - \eta t_c) + k_f \eta t_c$$

or

$$k_e = k_r\left\{1 - \eta t_c\left[1 - \frac{k_f}{k_r}\right]\right\} \qquad \text{(B. 28)}$$

The expressions for the specific heat and the density are the same as for the ones for perpendicular cracks. Combining them with B.28 to find the thermal diffusivity,

$$\alpha_e = \alpha_r\left\{\frac{1 - \eta t_c(1 - k_f/k_r)}{1 - \eta t_c\left[1 - \frac{\rho_f c_f}{\rho_r c_r}\right]}\right\} \qquad \text{(B. 29)}$$

A table of the multiplication factors (X_e/X_r) for granite and liquid water at standard conditions, is shown in Section *3.5.4.*

B.6.2.2 With fluid flow through the cracks: If there is sufficient pressure gradient between the two ends of the crack, a very small flow may result. Theenergy transported by the fluid might be significant, considering the rather low thermal conductivity of the rock. For simplicity, it can be assumed that the fluid travels slowly enough to be in thermal equilibrium with the rock surface ($N_{Bi} \approx \infty$). Given this assumption, the effective heat transfer per unit area is given by

$$q'' = \frac{AT}{R_T} + \dot{m}'' \, c_f \, AT$$

where $\dot{m}''$ is the mass flow of fluid per unit area of solid and crack:

$$\dot{m}'' = \rho_f \, \eta t_c \, u$$

where u is the fluid velocity through the cracks. Using Eq. B.27 for R_T:

$$q'' = \Delta T\{k_r(1 - \eta t_c) + k_f \, \eta t_c + \rho_f \, \eta t_c \, c_f \, u\}$$

Simplifying and rearranging,

$$\frac{k_e}{k_r} = 1 - \eta t_c \left(1 - \frac{k_f}{k_r} - \frac{\rho u c_f}{k_r}\right) \qquad \text{(B. 30)}$$

The solution of the correction factor in Eq. B.30 is given in Figure 3-10 for granite and liquid water, and for different flow velocities. Only beyond velocities of 0.002 ft/hr the thermal conductivity is significantly increased. From Poiseuille's law for capillary flow, the flow velocity is given by

$$u = \frac{t_e^2}{12\mu} \times \frac{\partial P}{\partial x} \qquad \text{(B. 31a)}$$

where μ in this case is the viscosity of the fluid. Solving for $\partial P/\partial x$ and rearranging,

$$\frac{\partial P}{\partial x} = \frac{12\mu \, u \, \eta^2}{(\eta t_c)^2} \qquad \text{(B. 31b)}$$

For liquid water, $\eta t_c = 0.01$, and $u = 0.3$ ft/hr, the pressure gradient required for a 10-percent increase in thermal conductivity would be

$$\frac{\partial P}{\partial x} = 3000\ \eta^2 \left[\frac{\text{dynes}}{\text{cm}^3}\right] \quad \text{if } \eta \text{ is } 1/\text{cm}$$

For $\eta = 1/\text{cm}$ ($\eta t_c = 0.01$ cm);

$$\frac{\partial P}{\partial x} = 16.5\ \frac{\text{psi}}{\text{ft}}$$

This kind of pressure gradients are not difficult to find in the vicinity of the well bore. However, in a highly fractured reservoir like the one being considered, thesemagnitudes of pressure gradients might or might not be found apart from the well bore, depending on the fracture permeability, the fluid viscosity, and the production rate. The answer to this question is beyond the scope of this study.

B.7 Energy Balance in a Fractured Stimulated Reservoir

Let us consider the reservoir shown in Figure 3–9 in which fluid is produced at some rate $\dot{m}_p(t)$ with an enthalpy $i_p(t)$. Fluid is injected at a rate $\dot{m}_i(t)$ with an enthalpy $i_i(t)$. Let the reservoir be adiabatic, i.e., there is no heat transfer from the bottom or the surroundings of the reservoir to the fluid or the rock. The reservoir is initially at a uniform temperature T_1 .

If our control volume includes the rock and the 'fluid, energy conservation yields

$$\underbrace{\int_0^t \dot{m}_i\, i_i\, dt}_{\text{Input}} - \underbrace{\int_0^t \dot{m}_p\, i_p\, dt}_{\text{output}} = \underbrace{\int_0^t V_{re}(1-\phi)\rho_r c_r \frac{\partial \bar{T}_r}{\partial t}\, dt + \int_0^t V_{re}\,\phi\,\rho_f c_f \frac{\partial \bar{T}_f}{\partial t}\, dt}_{\text{Increase of Storage}} \qquad \textbf{(B.32)}$$

where $\overline{T}_r$ and $\overline{T}_f$ in this case mean the temperatures of the rock and fluid, respectively, throughout the reservoir volume. If we call the energy produced

$$E_p(t) = \int_0^t \dot{m}_p \, i_p \, dt \qquad \textbf{(B.33)}$$

and the energy injected

$$E_i(t) = \int_0^t \dot{m}_i \, i_i \, dt \qquad \text{(B. 34)}$$

integrating and rearranging yields

$$E_p(t) = V_{re}(1 - \phi)\rho_r c_r(T_1 - \overline{T}_r(t)) + V_{re}\,\phi\,\rho_f c_f(T_1 - \overline{T}_f(t)) + E_i(t) \qquad \text{(B. 35)}$$

From the definition of $\overline{F}_{E,c}$ the first term of the right-hand side of Eq. B.35 can be replaced by

$$V_{re}(1 - \phi)\rho_r c_r \, \overline{F}_{E,c}(T_1 - \overline{T}_f(t)) \qquad \textbf{(B.36)}$$

If the energy produced is expressed as a fraction of the energy that would be extracted, if the reservoir were cooled uniformly to a temperature T_2, i.e.,

$$F_p \triangleq \frac{E_p(t)}{V_{re}(\phi\,\rho_f c_f + (1 - \phi)\rho_r c_r(T_1 - T_2)} \qquad \textbf{(B. 37)}$$

where F_p stands for the "reservoir energy fraction produced."

The degree to which the fluid has been cooled can be characterized by the "reservoir mean temperature drop fraction" defined as

$$\bar{F}_c = \frac{T_1 - \bar{T}_f(t)}{T_1 - T_2} \qquad \text{(B. 38)}$$

Substituting Eqs. B.38, B.37, and B.36 into B.35 yields

$$F_p = \frac{\bar{F}_{E,c} \cdot \bar{F}_c}{(1+\gamma)} + \frac{F_c \cdot \gamma}{(1+\gamma)} + \frac{E_i \cdot \gamma}{(1+\gamma)(T_1 - T_2)\, V_{rc}} \qquad \text{(B. 39a)}$$

where

$$\gamma \triangleq \frac{\phi}{c^*(1-\phi)} \qquad \text{(B. 39b)}$$

and

$$c^* \triangleq \frac{\rho_r c_r}{\rho_f c_f} \qquad \text{(B.39c)}$$

When the reservoir porosity is small enough, the energy storage in the fluid can be neglected, i.e., $\gamma << 1.0$. Besides, if there is no fluid injection, Eq. B.39a becomes

$$F_p = \bar{F}_{E,c} \times \bar{F}_c \qquad \text{(B.40)}$$

Notice that if at the end of the production period the temperature of the fluid is equal to T_2 , the fraction produced is equal to the energy extracted fraction since the fluid has been completely cooled ($\bar{F}_c = 1.0$).

B.8 Alternative Method to Model the Rock Temperature Transient under Variable Fluid Cooling Rate Conditions

In Section 3.1.4 and Appendix B.3, an analytical methodology was derived for the temperature transient of rocks for variable fluids cooling-rate conditions. The validity of this model was verified experimentally and the results are presented in Section 4. However, to model the cold

water sweep process, the coupling of the rock and fluid temperatures makes the solution of the governing equations quite complicated. Then, a simpler form for the rock-fluid temperature difference than the one given by Eq. **3.16** must be derived for this purpose. The superposition of the solution for step changes in fluid temperature provides the simplicity required.

The one-lump solution for step change in fluid temperature from T_1 to T_f is given by

$$\frac{T_r(t) - T_f}{T_1 - T_f} = e^{-t/\tau} \tag{B.41}$$

where τ is given by Eq. 3.10. Similarly to Section ***3.1.4***, if the step change in fluid temperature occurs at a time equal to ξ, the same equation applies but

$$\frac{T_r(t - \xi) - T_f}{T_1 - T_f} = e^{-(t-\xi)/\tau} \tag{B. 42}$$

and for an infinitesimal step change in T_f,

$$\frac{dT_r - dT_f}{-dT_f} = e^{-(t-\xi)/\tau} \tag{B.43a}$$

or

$$dT_r = \left(1 - e^{-(t-\xi)/\tau}\right) dT_f \tag{B.43b}$$

The linearity and homogeneity of the governing partial differential equation assures that the summation of the solutions given by B.43b also satisfy the differential equation. Then,

$$\int_{T_1}^{T_r} dT_r = \int_0^t \left(1 - e^{-(t-\xi)/\tau}\right) dT_f$$

but

$$dT_f = -\frac{\partial T_f}{\partial \xi} d\xi$$

performing the integration,

$$T_r(t) - T_1 = \int_0^t \left(1 - e^{-(t-\xi)/\tau}\right) \frac{\partial T_f}{\partial \xi} d\xi \qquad (B.44)$$

And if we want the solution for the rock-fluid temperature difference, we know that

$$T_f(t) - T_1 = \int_{T_1}^{T_f(t)} dT_f = \int_0^t \frac{\partial T_f}{\partial t} d\xi \qquad (B.453$$

and combining B.45 and B.44 we obtain

$$T_r(t) - T_f(t) = \int_0^t \left(-e^{-(t-\xi)/\tau}\right) \frac{\partial T_f}{\partial \xi} d\xi \qquad (B.46a)$$

or

$$T_r(t) - T_f(t) = \sum_{i=1}^{n} \left(-e^{-(t-\xi)/\tau}\right) \Delta T_{f,i} \qquad (B.46b)$$

Equation B.46a can be tested by deriving the equation for constant cooling rate, i.e.,

$$\frac{\partial T_f}{\partial \xi} = \mu$$

Performing the integration and simplifying yields

$$T_r(t) - T_f(t) = \mu\tau\left(1 - e^{-t/\tau}\right)$$

which is Eq. 3.7.

Clearly, from the mathematical formulation point of view, Eq. B.46 is equivalent to Eq. 3.16 and Eq. B.13. Therefore, as shown in the previous test, both methods should reproduce the same numerical results. However, from the computational point of view, more step changes in temperature are needed to reproduce a given fluid cooldown history than is required, if step changes in constant cooling rate are used. Thus, for a given Biot number more terms are required for Eq. B.46b than for Eq. B.13b to reproduce the same accuracy in the predictions.

B.9 One-Dimensional Heat Transfer Model for the Cold-Water Sweep Process

Let us consider the reservoir shown in Figure B-2. Cold water is being injected at well A and production is done at well B. The rates of injection and production are constant and equal, and the probability of finding any size of rock is the same at any section of the reservoir. Then the bulk-effective radius and time constant given by Eqs. 3.34 and 3.35 are also uniform throughout the reservoir, The net heat transfer q' from the bottom or the surroundings of the reservoir is assumed to be constant. Gravity segregation and natural convection effects are neglected.

If the water and rock are considered in the control volume for our analysis, conservation of energy yields

$$\underbrace{\{v_f \rho_f c_f S(T_f - T_{ref}) + q'\, dx\}}_{\text{Input}} - \underbrace{\left\{v_f c_f v_f S(T_f - T_{ref}) + \rho_f c_f v_f S \frac{\partial \bar{T}_f}{\partial x}\, dx\right\}}_{\text{output}}$$

$$= \underbrace{\phi\, \rho_f c_f\, dx \frac{\partial T_f}{\partial t} + \rho_r c_r (1 - \phi)\, dx \frac{\partial \bar{T}_r}{\partial t}}_{\text{Increase of Storage}}$$

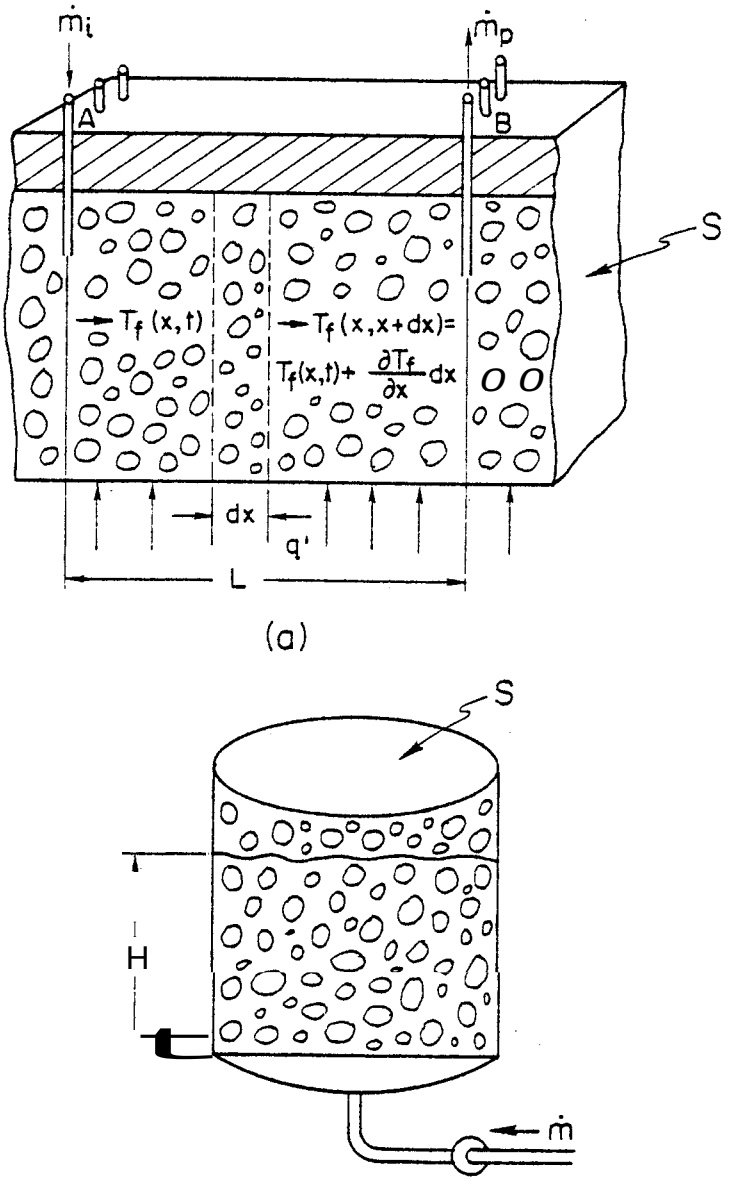

FIGURE B-2. One-dimensional model of a reservoir produced by the cold-water sweep process

where v_f is the Darcy velocity. Simplifying yields

$$\frac{\partial T_f}{\partial x} + \frac{\phi}{v_f}\frac{\partial T_f}{\partial t} + (1-\phi)\frac{\rho_r c_r}{\rho_f c_f}\frac{\partial \bar{T}_r}{\partial t} = \frac{q'}{v_f c_f \rho_f S} \qquad (B.47)$$

Also, from conservation of mass:

$$\dot{m}_p = \dot{m}_i = \dot{m}$$

where $\dot{m}_p$ and $\dot{m}_i$ are the production and recharge rates which can be expressed as a function of the Darcy velocity as

$$\dot{m} = \rho_f v_f S \qquad (B.48)$$

S, being the reservoir cross section. However, the actual velocity w of an element of fluid is different from the Darcy velocity v_f used in Eq. *B.48* which assumes that the total cross sectional area is available for flow. To understand the difference, let us consider the reservoir like the one shown in Figure B-2b full of rocks and with a porosity ϕ. If the pore space is filled with water at a rate $\dot{m}$, the fluid level has reached a height H after some time. Conservation of mass yields

$$\dot{m} \times t = (S\ H\ \phi)\ \rho_f \qquad (B.49)$$

Finding the derivative with respect to time of Eq. *B.49*, we obtain:

$$\dot{m} = \rho_f v_f S = S\ \phi\ \rho_f \frac{dH}{dt}$$

or,

$$w \triangleq \frac{dH}{dt} = \frac{v_f}{\phi} \qquad (B.50)$$

The differential equation for the one-lump parameter solution of a single rock is given by Eq. B.7 as

$$\frac{\partial \bar{T}_r}{\partial t} = \frac{T_f - \bar{T}_r}{\tau} \tag{B.7}$$

If τ is replaced for τ_e to model the collection of rocks with a given size distribution, and Eq. B.46a is used for $T_f - \bar{T}_r$, we obtain

$$\frac{\partial \bar{T}_r}{\partial t} = -\frac{1}{\tau_e} \int_0^t \left[-e^{-(t-\xi)/(\tau_e)}\right] \frac{\partial T_f}{\partial t}\, d\xi \tag{B.51}$$

Substituting B.51 into B.47 yields

$$\frac{\partial T_f}{\partial x} = \frac{\phi}{v_f}\frac{\partial T_f}{\partial t} - \frac{(1-\phi)}{\tau_e}\frac{\rho_r c_r}{v_f c_f \rho_f} \int_0^t \left[-e^{-(t-\xi)/(\tau_e)}\right] \frac{\partial T_f}{\partial t}\, d\xi = \frac{q'}{v_f c_f \rho_f S} \tag{B.52a}$$

This equation is solved for the following conditions:

$$\begin{aligned} &\text{Initial Condition:} \quad T_f(X,0) = \bar{T}_r(X,0) = T_1 \\ &\text{Boundary Condition:} \quad T_f(0,t) = T_{in} \end{aligned} \tag{B.52b}$$

It is convenient now to define the following non-dimensional variables:

For time:

$$t^* \triangleq \frac{v_f t}{\phi L} = \frac{t}{L/W} = \frac{t}{t_{re}} \tag{B.53}$$

where t_{re} is the residence time of the fluid in the reservoir.

For space:

$$x^* \triangleq \frac{x}{L} \tag{B.54}$$

For temperature:

$$T_f^* \triangleq \frac{T_f(x,t) - T_{in}}{T_1 - T_{in}} \tag{B.55}$$

where T_{in} is the fluid inlet temperature to the reservoir.

For the rock effective time constant:

$$N_{tu} \triangleq \frac{t_{re}}{r_e} \tag{B.56}$$

For the external heat transfer:

$$q^* \triangleq \frac{q'L}{\rho_f v_f Sc_f (T_1 - T_{in})} \tag{B.57}$$

For the heat capacities:

$$c^* \triangleq \frac{\rho_r c_r}{\rho_f c_f} \tag{B.58}$$

Substituting Eqs. B.53 through B.57 into B.52a yields:

$$\frac{\partial T_f^*}{\partial x^*} + \frac{\partial T_f^*}{\partial t^*} - N_{tu} c^* \frac{(1-\phi)}{\phi} \int_0^{t^*} \left(-e^{-N_{tu}(t^*-\xi^*)}\right) \frac{\partial T_f^*}{\partial \xi^*} d\xi^* = q^* \tag{B.59a}$$

with the non-dimensional initial condition,

$$T_f^*(X^*, 0) = 1.0 \tag{B.59b}$$

and the boundary condition,

$$T_f^*(0,t) = 0 \tag{B.59c}$$

Equations B.59 can be readily solved if it is transformed to the Laplace space. Using the convolution theorem for the integral term, and standard Laplace transform tables, results in

$$\frac{d\hat{T}_f^*(X^*,S)}{dX^*} + \hat{T}_f^*(X^*,S) \cdot K \cdot S = K + \frac{1}{S} \tag{B.60a}$$

where K is defined as

$$K \triangleq 1 + \frac{1}{\gamma}\left\{\frac{r}{(S/N_{tu})+1}\right\} \qquad \text{(B.60b)}$$

and the boundary condition transforms to

$$\hat{T}_f^*(0,S) = 0 \qquad \text{(B.60c)}$$

This is an ordinary differential equation in X^* which has the solution

$$\hat{T}_f^*(X^*,S) = \left(\frac{1}{S} + \frac{q^*}{S^2K}\right)\left(1 - e^{-K\cdot X^*\cdot S}\right) \qquad \text{(B.61)}$$

Then the solution for the fluid temperature in the real space is obtained by inversion as

$$T_f^*(X^*,t^*) = \mathcal{L}^{-1}[\hat{T}_f^*(X^*,S)] \qquad \text{(B.62)}$$

Attempts to obtain a closed form for the inversion failed. Therefore, the inversion of the Laplace transform was performed numerically using the algorithm given by Stehfest (1970) :

$$T_f^*(X^*,t^*) = \frac{\ln 2}{t^*}\sum_{i=1}^{M} a_i\,\hat{T}\left(X^*,\frac{\ln 2}{t^*}\times i\right) \qquad \text{(B.63a)}$$

with the coefficients given by

$$a_i = (-1)^{M/2+i}\sum_{k=\frac{i+1}{2}}^{\text{Min}(i,M/2)} \frac{k^{(M/2+1)}\,(2k)!}{(\frac{M}{2}-k)!\,k!\,(k-1)!\,(i-k)!\,(2k-i)!} \qquad \text{(B.63b)}$$

It can be seen how the coefficients are independent of time, so that once an M has been selected, only one computation is sufficient for all times. The optimum value of M largely depends on the magnitudes of γ and N_{tu}.

It was found thatavalue between 8 and 10 produced good results. Table B-1 shows these coefficients for several values of M , Given these coefficients, Eq. B.62 can be implemented easily in a programmable calculator.

With the fluid temperature distribution as a function of time, the temperature transient of the "effective" rock can be calculated using Eqs. 3.16 or B.46 for any location in the reservoir and for any time. Also, if the reference temperature for energy fraction calculations is selected to be the temperature of the injecting fluid T_{in} , the reservoir

TABLE B-1

Coefficients for the Inversion of the Laplace Transform

i \ M	Coefficient a_i				
	4	6	8	10	12
1	-2	1.0	-0.333...*	0.0833...	-0.01666...
2	.26	-49	48.333...	-32.0833...	16.0166...
3	-4.8	366	-906	1279.0	-1247.0
4	2.4	-858	5,464.666...	-15,623.666...	27,554.333...
5		810	-14,376.666...	84,244.166...	-263,280.833...
6		-270	18,730.0	-236,957.5	1,324,138.7
7			11,946.666...	375,911.666...	-3,891,705.533..
8			2,986.666...	-340,071.666...	7,053,288.333...
9				164,062.5	-8,005,336.5
10				-32,812.5	5,552,830.5
11					-2,155,507.2
12					359,251.2

* ... means that the figures continue infinitely.
Recommended M = 10 (M must be even).

mean temperature drop fraction as defined in Eq. *3.45* is given by

$$\bar{F}_c = \frac{T_1 - \bar{T}_f(t)}{T_1 - T_{in}} = 1 - \int_0^X \frac{T_f(X,t) - T_{in}}{T_1 - T_{in}} dX = 1 - \int_0^1 T_f^*(X^*,t^*)dX^* \quad (B.64)$$

Similarly, the reservoir energy fraction produced defined in Eq. *3.46* becomes

$$F_p(t) = \frac{\int_0^t \dot{m}c_f(T_f(L,t) - T_{in})\, dt}{V_{re}(\phi\, \rho_f c_f + (1 - \phi)\rho_r c_r)(T_1 - T_{in})}$$

$$= \frac{\int_0^{t^*} T_f^*(1,t^*)\, dt^*}{1 + 1/\gamma} \quad (B.65)$$

where γ is the storage ratio defined in Eq. B.39b.

Finally, from Eq. *3.43* the reservoir rock energy extracted fraction is given by

$$\bar{F}_{E,c} = \frac{F_p}{\bar{F}_c} + \gamma\left(\frac{F_p}{\bar{F}_c} - 1\right) \quad (B.66)$$

An analysis of the effct of the number of transfer units on the energy extraction process is performed in Section *4.4.2.*

APPENDIX C

SAMPLE CALCULATIONS

C.1 Example of a Rock Center Temperature Prediction Under Variable Fluid Cooling Rate

A sample calculation of the superposition methodology described in Section 3.1.4 and applied for the rock center temperature predictions in Section 4.2 is presented to illustrate the simplicity of the technique and to provide physical understanding of the process. Rock number 2 in the cold-water sweep experiment was selected for this purpose. The predicted and actual rock as well as the fluid temperature transients are shown in Figure 4-6.

Let us predict the rock center temperature at the end of the experiment, i.e., at time equal to 7 hours. To do it, the fluid temperature transient is divided into 6 constant cooling rate sections, as shown in Figure 4-6 in dotted lines. Recalling Eq. 3.16 and applying it for the rock center,

$$\Delta T_{rc}(t) = \sum_{i=1}^{n} \tau_{rc}\left(1 - e^{(t-\xi)/\tau_{rc}}\right) \Delta\mu_i$$

where

$$\tau_{rc} = \frac{R_e^2}{3\alpha}\left(\frac{1}{2} + 1/N_{Bi}\right)$$

Recalling also that the equivalent sphere radius of rock number 2 is 3.9 inches and its sphericity 0.8, the shape factor correlation can be applied to find the rock-effective radius:

$$R_e = R_s \cdot \psi_K = 3.9 \times 0.8 = 3.12 \text{ in} = 0.26 \text{ ft}$$

According to experimental data from Kuo, Kruger, and Brigham *(1976)* for granite rock, an average convective heat transfer coefficient of *300* Btu/hr-ft^2-°F can be used. Thus, the Biot number becomes

$$N_{Bi} = h \cdot R_e/k = \frac{300 \times 0.26}{1.4} = 56$$

Then, the time constant for the rock center temperature can be calculated as

$$\tau_{rc} = \frac{0.26^2}{3 \quad 0.039} (0.5 + 1/56) = 0.3 \text{ hr}$$

Table C-1 shows the computational procedure: column **(1)** shows the location in time of the step changes in fluid cooling rate; column *(2)* shows the time during which the step change contributes to the final ΔT_{rc};

TABLE C-1

Calculation of the Rock Center Temperature

(0) i	(1) ξ_i	(2) $(t - \xi_i)$	(3) $T_f(t)$	(4) μ	(5)	(6) $\tau_{rc}\left(1 - e^{-(t-\xi)/\tau_{rc}}\right)\Delta\mu_i$
1	*3.0*	*7.0*	*460*	*0.0*	0.0	-
2	*2.75*	*4.25*	*460*	*40.0*	*40*	11.97
3	*3.0*	*4.0*	*450*	*83.3*	*43.3*	*12.90*
4	*3.6*	*3.4*	*400*	*103.3*	*20.0*	*5.98*
5	*5.1*	1.9	*245*	*78.3*	*-25.0*	*-7.46*
6	*6.25*	0.75	*155*	*46.7*	*-31.6*	*-8.68*
7	7.0	*0*	*120*	-	-	-
						AT_{rc}(7 hr) = 14.71°F

column *(3)* shows the fluid temperature at the beginning and the end of each constant cooling rate interval; and column *(4)* the corresponding cooling rates; column (5) shows the step change in fluid cooling rate that occurs at time ξ and which contributes during $(t-\xi)$ to the final ΔT_{rc} ; it is given by

$$\Delta\mu_{i+1} = \mu_{i+1} - \mu_i \ , \quad i = 1,2,\ldots,7$$

Finally, column (6) shows the contributions of each interval to the final AT_{rc} . The summation of the contributions is shown at the bottom of column (6). Then, the rock center temperature at time equal to 7 hours is

$$T_{rc}\ (7\ \text{hrs}) = T_f\ (7\ \text{hrs}) + \Delta T_{rc}\ (7\ \text{hrs}) = 120 + 14.71$$

$$= 134.71°F$$

In Figure 4-6 it can be seen that the measured rock center temperature was 135°F, i.e., an agreement within less than 1 percent.

C.2 Energy Extracted Fraction Evaluation

In Section 4.3, the effect of the physical parameters on the energy extracted fraction is studied. To perform it, it was necessary to assume some hypothetical rock size distributions, like normal and exponential. This appendix shows the methodology to evaluate the energy extracted fraction for a collection of rocks with a given size distribution.

For simplicity, let us choose a collection of rocks with equivalent sphere radius normally distributed, described by Eq. 3.36 as

$$f(R_s) = \frac{1}{\sigma_{\bar{R}_s}\sqrt{2\pi}}\, e^{-\frac{1}{2}\left[(R_s-\bar{R}_s)/\sigma_{\bar{R}_s}\right]^2} \qquad (3.36)$$

It is convenient to express the radius in normalized form as

$$r_s^* = \frac{R_s - \overline{R}_s}{\sigma_{\overline{R}_s}} \qquad (C.1)$$

If the radius is smaller than the mean, r_s^* is negative, if it is equal to the mean, r_s^* is zero, and if it is larger than the mean, r_s^* is positive. The physical meaning of r_s^* is: how many standard deviations is R_s dispersed from the mean $\overline{R}_s$.

To avoid too many calculations, the normal distribution was divided into five groups of rocks of equal size, as shown in Figure C-1a. If a and b are the limits for one group, the mean size of that group, $\overline{r}_{si}^*$, is given by

$$\int_a^{\overline{r}_{si}^*} \frac{1}{R_s} e^{-\frac{1}{2}r_s^*} r_s^* \, dr_s^* = \int_{\overline{r}_{si}^*}^b \frac{1}{r_s} e^{-\frac{1}{2}r^{*2}} r_s^* \, dr_s^* \qquad (C.2)$$

where the integrals are the areas under the normal distribution curve between a and r_{si}^*, and r_{si}^* and b, respectively. The meaning of Eq. C.2 is that $\overline{r}_{si}^*$ is a value of r_s^* between a and b, such that the area at both sides of the curve between a and b is the same, i.e., $\overline{r}_{si}^*$ is the mean value for the interval [a,b]. The values of $\overline{r}_{si}^*$ can be readily found in statistical tables.

The probability of having a rock of size R_{si} is given by

$$p(\overline{r}_{si}^*) = p(a \leq r_s^* \leq b) = \int_a^b \frac{1}{\sigma_{\overline{R}_s}\sqrt{2\pi}} e^{-\frac{1}{2}r_s^{*2}} dr_s^* \qquad (C.3)$$

where the values of $\overline{r}_{si}^*$ can be found also in statistical tables. If the interval [a,b] is small enough, it can be said with good

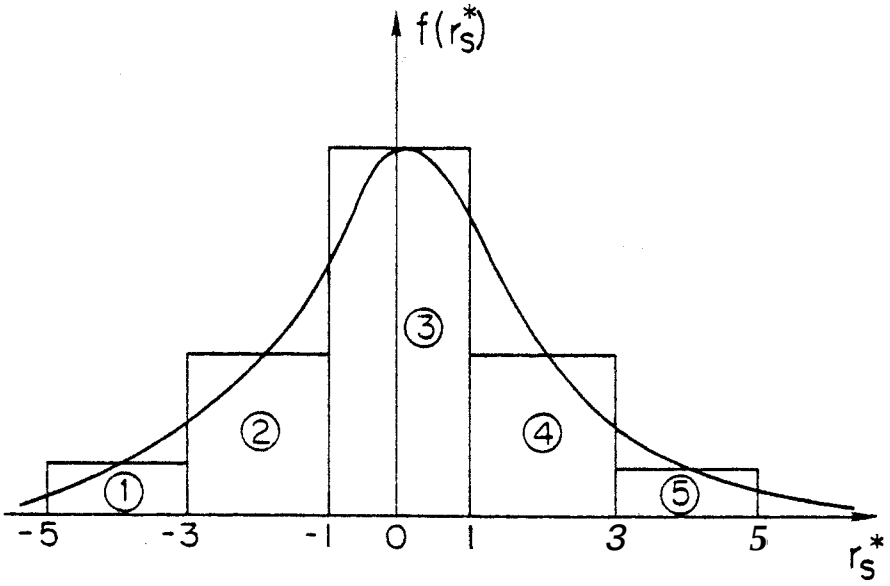

(a) FREQUENCY DISTRIBUTION

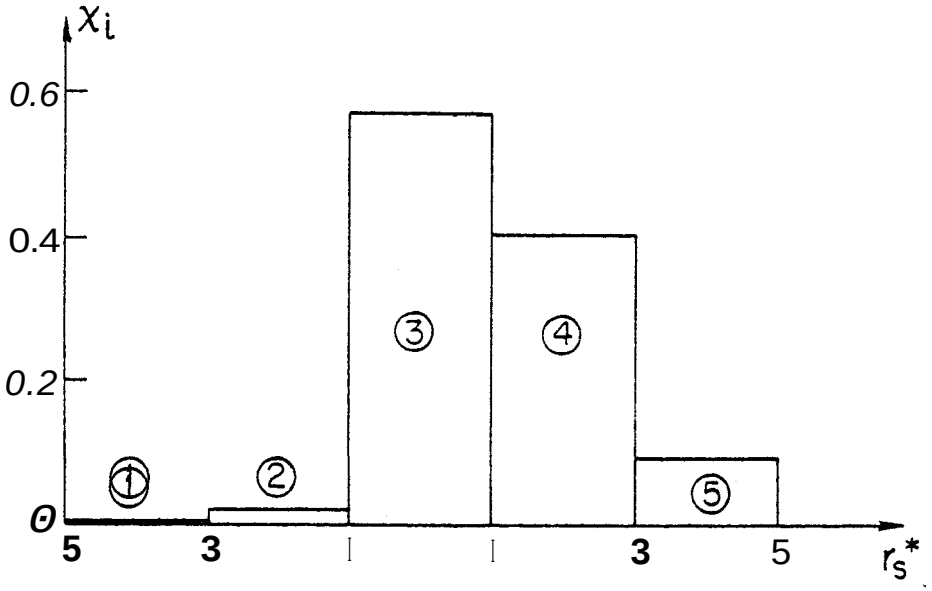

(b) VOLUMETRIC FRACTION DISTRIBUTION

FIGURE C-1. Frequency and volumetric fraction for the sample calculation

approximation that

$$p(\bar{R}_{si}) \approx p(\bar{v}_i) \tag{C.4}$$

where $\bar{v}_i$ is the mean rock volume for each group and it is given by

$$\bar{v}_i \approx \frac{4}{3}\pi \bar{R}_{si}^{3} = \frac{4}{3}\pi(\bar{R}_s + \bar{r}_{si}^{*}\,\sigma_{rs})^3 \tag{C.5}$$

The mean rock volume for the total collection is given by definition as

$$\bar{v} = \sum_{i=1}^{N_L} p(\bar{v}_i) \times \bar{v}_i \tag{C.6}$$

Thus, the volumetric fraction can be found from Eq. 3.30 as

$$X_i = p(v_i) \times \frac{\bar{v}_i}{\bar{v}} \tag{3.4d}$$

For the sample calculation, let the mean equivalent sphere radius $\bar{R}_s$ be 100 ft and the standard deviation $\sigma_{\bar{R}_s}$ equal to 30.7 ft. The value of 30.7 ft for the standard deviation was selected to simulate maximum dispersion (a dispersion of approximately $\pm 3 \times \sigma_{\bar{R}_s}$ covers about 99.9 percent of the population).

Table C-2 shows the mean radius, the mean rock volume, and the volumetric fraction for each one of the groups. Notice that the mean rock volume given by Eq. C.6 is significantly larger than the volume of the mean equivalent sphere radius, $\bar{v}_3$. The same effect can be seen in Figure C-lb for the volumetric fraction X_i with respect to the probability $p(R_{si})$. This is due to the fact that the volume *is* proportional to the third power of the radius, and although the larger rocks can be

TABLE C-2

Calculation of the Collection Parameters

n	r_s^*	$p(\bar{r}_{si}^*)$	$\bar{R}_{si}$ (ft)	$\bar{v}_i$ (ft^3)	X_i
1	-3.25	1.35×10^{-3}	0.23	0.048	1.3×10^{-11}
2	-1.45	0.1574	55.5	715,509	0.022
3	0	0.6826	100.0	4,200,000	0.572
4	1.45	0.1574	144.5	12,638,401	0.397
5	3.25	1.35×10^{-3}	200.0	33,397,351	0.009
				$\bar{v}$ = 5,013,912	

found with the same frequency as the small ones, they have higher volumetric fractions.

The energy extracted fraction can now be evaluated for any fluid cooling rate conditions. For simplicity and to be consistent with Section 4.3.1, let the fluid cooling rate be constant. Then, the energy extracted fractions F_{E_i} for each group can be found as a function of time (Fourier number) in Figure 3-7. Table C-3 shows the energy extracted fraction for the five groups as well as for the toal collection which is calculated from Eq. 3.29a as

$$\bar{F}_{E,c} = \sum_{i=1}^{5} X_i \cdot F_{E_i}$$

It can be observed the rock energy extracted fraction reaches unity in less than half-a-year for the small rocks (group number 1), whereas it takes 30 years to reach a rock energy extracted fraction of 0.7 for the large ones (group number 5). Note also that the rock energy extracted

TABLE C-3

Calculation of the Local Rock Energy Extracted Fraction F_E

Time / i	$F_{E,i}$					
	1 day	0.5 yr	1 yr	3 yr	10 yr	30 yr
1	0.996	1.0	1.0	1.0	1.0	1.0
2	0.002	0.284	0.467	0.77	0.93	0.976
3	0.002	0.103	0.19	0,443	0.773	0.927
4	0.002	0.05	0.097	0.257	0.583	0.843
5	0.002	0.027	0.053	0.147	0.393	0.707
$F_{E,c}$	0.002	0.0853	0.1579	0.374	0.693	0.893

fraction for the collection tends to be some place between that of groups 3 and 4.

C.3 Bulk-Effective Radius for Infinite Number of Equal Rock Size Groups

From Eqs. 3.32 and 3.34 the bulk-effective radius is given by

$$R_{e,c} = \bar{\psi}_K \frac{\sum_{j=1}^{N_L} p(R_{si})\, R_{si}^3}{\sum_{j=1}^{N_L} p(R_{si})\, R_s^2} \qquad (C.7)$$

Recalling the definition of $p(R_{si})$ as

$$p(\bar{R}_{si}) = p(a \leq R_s \leq b) = \int f(R_s)\, dR_s = \frac{1}{N}$$

where a and b are the limits of the size interval i with mean equivalent sphere radius $\bar{R}_{si}$. In the interval there are n_i rocks. If an infinite number of groups are considered, infinitesimal intervals result

and

$$p(\bar{R}_{si}) = \frac{\delta n}{N} = f(\bar{R}_{si}) \tag{C.8}$$

Combining Eqs. C.7 and C.8 the bulk-effective radius is given by

$$R_{e,c} = \bar{\psi}_K \frac{\int_{-\infty}^{\infty} f(R_s) \times R_s^3 \, dR_s}{\int_{-\infty}^{\infty} f(R_s) \, R_s \, dR_s} \tag{C.9}$$

If the distribution is exponential

$$f(R_s) = \frac{1}{\gamma} e^{-R_s/\gamma} \tag{C.10}$$

Combining Eqs. C.9 and C.10 and simplifying,

$$R_{e,c} = \bar{\psi}_K \frac{\int_0^{\infty} R_s^3 \, e^{-R_s/\gamma}}{\int_0^{\infty} R_s^2 \, e^{-R_s/\gamma}} = \frac{\gamma \Gamma(4)}{\Gamma(3)} \times \bar{\psi}_K$$

where Γ is the gama function for which

$$\Gamma(n + 1) = n!$$

Therefore, recalling that for the exponential distribution, $\gamma = \bar{R}_s$,

$$R_{e,c} = 3\gamma \, \bar{\psi}_K = 3\bar{R}_s \times \bar{\psi}_K \tag{C. 11}$$

Performing a similar procedure for a normal distribution, the bulk-effective radius is given by

$$R_e = \bar{R}_s \times \bar{\psi}_K \frac{1 + \frac{3}{2}\sqrt{2\pi}\left(\frac{\sigma_{R_s}}{R_s}\right)^2}{1 + \frac{\sqrt{2\pi}}{2}\left(\frac{\sigma_{R_s}}{R_s}\right)^2} \qquad (C.12)$$

It can be seen in Eq. C.12 how the numerator increases faster than the denominator for a higher size dispersion, which results in a larger bulk-effective radius.

C.4 Reservoir Rock Energy Extracted Fraction. Uncertainty Analysis of Experimental Measurements

Section 4.5 presented the experimental determination of the reservoir rock energy extracted fraction for experiment number 3. It was shown that the uncertainties involved in the experimental measurements were too high to allow a conclusive verification of the analytical model. The procedure followed in evaluating the experimental results and corresponding uncertainties are described in the following.

An energy balance for an adiabatic geothermal reservoir was performed in Appendix B.7. If the reservoir is non-adiabatic as is the case in the SGP laboratory reservoir model, Eq. B.32 becomes

$$\int_0^t \dot{m}_i i_i \, dt + Q_e(t) - \int \dot{m}_p i_p \, dt = \int V_{re}(1-\phi)\rho_r c_r \frac{\partial \bar{T}_r}{\partial t} \, dt + \int_0^t V_{re}\phi\rho_f c_f \frac{\partial \bar{T}_f}{\partial t} \, dt$$

The first term on the right-hand side presents the decrease in energy storage in the rock, and the second term represents the decrease in

energy storage in the fluid. Solving for the energy extracted from the rock yields:

$$Q_r(t) = \int_0^t \dot{m}_p i_p \, dt - V_{re}\, \phi(i_1\rho_1 - i_2\rho_2) - \int_0^t \dot{m}_i i_i \, dt - Q_e(t) \qquad (C.13)$$

where the subindexes 1 and 2 indicate the initial and final conditions respectively. The temperature of the fluid, rock, and vessel wall were uniform throughout the reservoir volume for this experiment. The term Q_e stands for the heat transfer from the surroundings and the procedure to determine its value is described in Appendix C.5. The integration of the energy produced and energy injected were performed by summation of measured flow rates and enthalpies during small time intervals. Recalling the definition of the reservoir rock energy extracted fraction:

$$\overline{F}_{E,c} \triangleq \frac{Qr}{Qmax} = \frac{Qr}{M_r C_r (T_1 - \overline{T}_f)} \qquad (C.14)$$

it can be readily evaluated using Eqs. C.13 and C.14.

For the purpose of evaluating the uncertainty of the reservoir energy extracted fraction the following simplifications were used:

$$\int_0^t \dot{m}_p i_p \, dt \simeq M_P \overline{i}_P \, At \qquad (C.15)$$

$$\int_0^t \dot{m}_i i_i \, dt \simeq M_i \overline{i}_i \, At \qquad (C.16)$$

The heat transfer from the surroundings can be estimated recalling that the temperature of the vessel wall was uniform throughout at a given time, and that there was no electric source in this experiment, as

$$Q_e(t) = M_m c_m (T_1 - T_2) - UA\ \Delta T_{m,1-2} \qquad \text{(C. 17a)}$$

where

$$\Delta T_{m,1-2} = \frac{(T_1 - T_\infty) - (T_2 - T_\infty)}{\ln \dfrac{(T_1 - T_\infty)}{(T_2 - T_\infty)}} \qquad \text{(C.17b)}$$

is the mean temperature difference between the vessel wall and the environment when cooled from the initial temperature T_1 to a given temperature T_2.

These approximations were compared with the actual calculations of the summations as described in Eq. *C.13,* and they were found to be in very good agreement. Note that these approximations are only valid for the particular conditions of the experiment, i.e., uniform temperature throughout.

Substituting Eqs. C.13, C.15, C.16, and C.17 into *C.14,* the first-order replication uncertainty of the reservoir rock energy extracted fraction can be calculated for 95 percent confidence level as:

$$\delta\overline{F}_{E,c} = \left\{ \sum_{i=1}^{N} \left(\frac{\partial F_{E,c}}{\partial X_i}\, \delta X_i \right)^2 \right\}^{1/2} \qquad \text{(C.18)}$$

where X_i are the uncertain variables in Eqs. *C.13,* C.15, C.16, and C.17.

A summary of the relevant uncertainties involved in the determination of the reservoir rock energy extracted fraction is presented in Table *4-3.* It can be observed that the uncertainty on the production and injection enthalpies, and on the rock specific heat have to be significantly reduced to achieve a reasonable uncertainty in the reservoir rock energy extracted fraction.

C.5 Determination of the External Heat Transfer

The heat transfer from the metallic vessel to the fluid was analyzed by Hunsbedt, Kruger, and London (1975a). The value of UA was evaluated to be 32.2 Btu/hr-°F. From an energy balance in the metallic wall of the vessel, the heat transfer to the fluid is given by

$$Q_e = \underbrace{\int_0^t \dot{E}_s \, dt}_{E_s} + \underbrace{M_m c_m \int_{T_2}^{T_1} d\bar{T}_m}_{Q_m} - \underbrace{UA \int_0^t (\bar{T}_m - T_\infty) \, dt}_{Q_L} \qquad \text{(C.19)}$$

or

$$Q_e = E_s + Q_m - Q_L$$

Electric Source — Decrease of Storage in Metal — Heat Losses to Environment

The first term in Eq. C.18 is the energy from the electric tapes. The second term is the energy from the metal that has been cooled from a temperature T_1 to a temperature T_2. The mean temperature of the metal is calculated as

$$\bar{T}_m = \sum_{i=1} X_i T_i$$

where the subindex i indicates the section of the vessel which fraction of the total mass is X_i at a temperature T_i. The mass fractions for each section of the vessel were determined by Hunsbedt, Kruger, and London (1975a). The temperatures T_i are measured by thermocouples 301-306 as shown in Figure 2-5. The third term in Eq. C.19 represents the heat losses to the environment.

C.6 Uncertainty Analysis of Predicted Reservoir Rock Energy Extracted Fraction

The uncertainty in the predictions of the reservoir rock energy extracted fraction is determined by the uncertainty on the mean rock to fluid temperature difference. The reservoir rock energy extracted fraction is given by Eq. 3.43 as

$$\bar{F}_{E,c} = \frac{T_1 - \bar{T}_r(t)}{T_1 - \bar{T}_f(t)} = 1 - \frac{\bar{T}_r - \bar{T}_f}{T_1 - \bar{T}_f} = 1 - \frac{\Delta T_m}{(T_1 - \bar{T}_f)} \qquad (C.20)$$

The first-order replication uncertainty on $\bar{F}_{E,c}$, and for 95 percent confidence level, is given by

$$\delta\bar{F}_{E,c} \simeq \left|\frac{\partial\bar{F}_{E,c}}{\partial\Delta T_m}\right| \times \delta\Delta T_m \qquad (C.21)$$

From Eq. C.20 the partial derivative of $\bar{F}_{E,c}$ with respect to ΔT_m is given by:

$$\frac{\partial\bar{F}_{E,c}}{\partial\Delta T_m} = -\frac{1}{(T_1 - \bar{T}_f(t)} \qquad (C.22)$$

Combining Eqs. C.21 and C.22, and dividing $\delta\bar{F}_{E,c}$ by $\bar{F}_{E,c}$, given by Eq. C.20, to find the percent uncertainty, yields

$$\frac{\delta\bar{F}_{E,c}}{\bar{F}_{E,c}} \simeq \frac{6AT_m}{AT_m} \cdot \frac{(1 - F_{E,c})}{\bar{F}_{E,c}} \qquad (C.23)$$

It can be seen from Eq. C.23 that even if the prediction of ΔT_m is not very certain (the uncertainty in ΔT_m was evaluated in Appendix A.2 to be about ±30 percent), since $\bar{F}_{E,c}$ is some number close to unity, the uncertainty on $\bar{F}_{E,c}$ itself is very low.

C.7 Modification of the Cold-Water Sweep Model to Account for Variable External Heat Transfer

In Section 3.7 a one-dimensional model was developed to predict the fluid temperature transient in the cold-water sweep process. In this analysis it was assumed that the external heat transfer is constant in time and uniform throughout the boundaries of the reservoir. However, in the SGP reservoir model, most of the energy transferred from the boundaries comes from the vessel steel wall, and since there is no temperature difference for heat transfer between the wall and the fluid until the cold fluid front passes through, the external heat transfer parameter varies for different elevations of the reservoir. At a given elevation, the heat transfer from the steel wall also varies with time similarly to the heat transfer from the rock.

The experimental verification of the model derived in Section 3.7 is described in Section 4.6.1. In this experiment, the power input to the electric tapes was set to be approximately equal to the heat losses from the reservoir. Thus, the total energy released as a result of the decrease in steel wall temperature was transferred to the fluid. If the temperature of the steel wall is assumed to respond to fluid temperature changes at approximately the same rate as the rock (time constant for the steel wall $\approx$ 0.01 hr vs 0.058 hr for the rocks), and the mass of the steel vessel is assumed to be uniformly distributed throughout the reservoir volume, the following modifications can be made to the analysis performed in Appendix B.9 to account for the variable external heat transfer.

The mass of steel vessel per unit volume of reservoir is given by

$$M'''_m \triangleq \frac{M_m}{V_{re}} = \frac{3428 \text{ lbm}}{16.57 \text{ ft}^3} = 206.8 \text{ lbm/ft}^3 \qquad \text{(C.24)}$$

If the boundaries of our control volume in Appendix B.9 include the metallic wall, an additional term can be added to the differential equation (B.47) to account for the decrease of storage in the vessel wall:

$$\text{Increase of Storage} = \phi\, \rho_f c_f\, dx\, \frac{\partial T_f}{\partial t} + \rho_r c_r (1 - \phi)\, dx\, \frac{\partial T_r}{\partial t} + M''' c_m\, dx\, \frac{\partial T_r}{\partial t} \qquad (C.25)$$

which in non-dimensional form yields

$$\text{Increase in Storage} = \frac{\partial T_f^*}{\partial t^*} + (c^* + c_m^*)\, \frac{(1 - \phi)}{\phi}\, \frac{\partial T_r^*}{\partial t^*} \qquad (C.26)$$

where

$$c_m^* \triangleq \frac{M_m''' c_m}{\rho_f c_f (1 - \phi)} = \frac{206.8 \times 0.125}{58 \times 1 (1 - 0.42)} = 0.78 \qquad (C.27)$$

Thus, instead of using a $c^* = 0.62$, a modified value equal to $c_{mo}^* = 0.62 + 0.78 = 1.4$ can be used to account for the energy storage in the vessel wall, and the modified storage ratio becomes

$$\gamma_{mo} = \frac{\phi}{c_{mo}^* (1 - \phi)} = \frac{0.42}{1.4(1 - 0.42)} = 0.52 \qquad (C.28)$$

which can be used in Eq. B.60b instead of the calculated value of 1.17 which does not include the energy storage in the vessel wall. A value of the storage ratio equal to 0.52 indicates that the energy stored in the fluid is 52 percent of the energy stored in the rock and steel..

The validity of the foregoing modifications is discussed in detail in Section 4.6.1. Evidently, the large proportion of the energy transferred from the vessel wall to the fluid (56 percent of the rock and steel), produces a two-dimensional effect in the reservoir, and therefore,

temperature variations in the radial direction. Also, the thickness of the vessel steel wall is not uniform throughout the reservoir length, which means that the mass of the vessel is not uniformly distributed throughout the reservoir volume, and γ_{mo} is not a constant for different locations of the reservoir. The rate of heat transfer from the vessel wall to the fluid will be different than the rate of heat transfer from the rock to the fluid depending on the relative magnitudes of the time constant of the steel wall and the rock bulk-effective time constant at different elevations of the reservoir.

REFERENCES

Arihara, Norio. "A Study of Non-Isothermal Single- and Two-Phase Flow Through Consolidated Sandstones," Stanford Geothermal Program Technical Report No. 2, November 1974.

Atkinson, P. G. "Mathematical Modelling of Single-phase Nonisothermal Fluid Flow Through Porous Media," Ph.D. dissertation, Stanford University, May 1976.

Diadkin, Y. D., Y. M. Pariiskii, A. B. Vainblat, and V. A. Romanov. "Research and Development of Efficient Systems of Extraction and Utilization of Heat, Accumulated within Deep Layers of the Earth's Crust in Extreme North and Northeast Regions of the USSR," Izuchenic i Ispol'zovanic Glubinnogo/Templa Zemli, Izdatel'stvo, Nauka Moscow, 1973.

Diadkin, Y. D., and Y. M. Pariiskii, "Theoretical and Experimental Grounds for Utilization of Dry Rock Geothermic Resources in Mining Industry," Proceedings of Second United Nations Symposium on the Development and Use of Geothermal Resources, San Francisco, May 20-29, 1975.

Ewing, A. H. "Stimulation of Geothermal Systems," Chapter 11 in Geothermal Energy, P. Kruger and C. Otte, eds., Stanford University Press, Stanford, CA, 1973.

Gringarten, A. C., and P. A. Witherspoon. "Extraction of Heat from Multiple-Fractured Dry Hot Rock," Geothermics, 2, 119, 1973.

Hunsbedt, A., P. Kruger, and A. L. London. "A Laboratory Model of Stimulated Geothermal Reservoirs," Stanford Geothermal Program. Technical Report No. 7, Report to National Science Foundation, Grant No. GI-34925, February 1975a.

Hunsbedt, A., P. Kruger, and A. L. London, "Laboratory Studies of Stimulated Geothermal Reservoirs," Stanford Geothermal Program. Technical Report No. 11, Report to National Science Foundation, Grant No. NSF-03490, December 1975b.

Hunsbedt, A., P. Kruger, and A. L. London. "Recovery of Energy from Fractured Geothermal Reservoirs," 46th Annual California Regional Meeting of the Society of Petroleum Engineers of AIME, Long Beach, CA, April 8-9, 1976.

Kasameyer, P. W., and R. C. Shroeder. "Thermal Depletion of Liquid Dominated Geothermal Reservoirs with Fracture and Pore Permeability," in Geothermal Reservoir Engineering, Kruger and Ramey, eds., Stanford Geothermal Program Technical Report No. 12, 1975.

Kays, W. M. Convective Heat and Mass Transfer, McGraw-Hill Book Co., New York, 1966.

Kruger, P., and H. J. Ramey. Stimulation of Geothermal Aquifers, Progress Report No. 1. Advanced Technology Dept., RANN, National Science Foundation, Grant No. GI-34925, March 1973.

Kuo, Ming-Ching T., P. Kruger, and W. E. Brigham. "Shape Factors Correlations for Transient Heat Conduction from Irregular Shaped Rock Fragments to Surrounding Fluid," Stanford Geothermal Program Technical Report No. 16, Report to National Science Foundation, Grant No. NSF-03490, August, 1976.

Löf, G. O. G., and R. W. Hawley. "Unsteady State Heat Transfer Between Air and Loose Fluids," Industrial and Engineering Chemistry, 40, No. 6, June 1948.

London, A. L., and W. M. Kays. Compact Heat Exchangers, second edition, McGraw-Hill Book Co., New York, 1964.

London, A. L., and R. K. Shah. "A Short Course in Compact Heat Exchangers," 97th ASME Winter Annual Meeting, New York City, December 9, 1976.

Nathelson, M. "Physical Factors Determining the Fraction of Stored Energy Recoverable from Hydrothermal Convection Systems and Conduction Dominated Areas," U.S. Geological Survey, open file report 75-525, October 1975.

Rabb, D. D. "Particle Size Distribution Study: Piledriver Event," Lawrence Radiation Laboratory, Livermore, CA, UCRL-50489, 1968.

Shockey, D. A., D. R. Curran, L. Seaman, J. T. Rosenberg, and C. F. Petersen. "Fragmentation of Rock under Dynamic Loads," Int. J. Rock Mech. Sci. & Geomech., Abstract Vol. 11, pp. 303-317, Pergamon Press, Great Britain, 1974.

Schumann, T. E. W. "Heat Transfer: A Liquid Flowing Through a Porous Prism," Journal of F.I., September 1929.

Stang, J. H., and J. E. Bush. "The Periodic Method of Testing Compact Heat Exchanger Surfaces," Trans. ASME, Journal of Engineering for Power, 96, Series A, 87-94, 1974.

Stehfest, Herald. "Numerical Inversion of Laplace Transforms. Algorithm No. 368," Communications of the ACM, Vol. 13, November 1, January 1970.

Wheeler, A. J. "Single Blow Transient Testing of Matrix-Type Heat Exchanger Surfaces at Low Values of N_{tu}," Technical Report No. 68, Department of Mechanical Engineering, Stanford University, CA, 1968.

White, D. E., and D. L. Williams, eds., Assessment of Geothermal Resources of the United States--1975, U.S. Geological Survey Circular 726, 1975.